FORMATION OF NANOCRYSTALLINE CELLULOSE BY USING TASK SPECIFIC IONIC LIQUIDS

NURUL ATIKAH BINTI MOHD ISKAK

**INSTITUTE OF GRADUATE STUDIES
UNIVERSITY OF MALAYA
KUALA LUMPUR**

2017

FORMATION OF NANOCRYSTALLINE CELLULOSE BY USING TASK SPECIFIC IONIC LIQUIDS

NURUL ATIKAH BINTI MOHD ISKAK

DISSERTATION SUBMITTED IN FULFILMENT OF THE REQUIREMENTS FOR THE DEGREE OF MASTER OF PHILOSOPHY

INSTITUTE OF GRADUATE STUDIES UNIVERSITY OF MALAYA KUALA LUMPUR

2017

UNIVERSITY OF MALAYA
ORIGINAL LITERARY WORK DECLARATION

Name of Candidate: Nurul Atikah binti Mohd Iskak

Matric No: HGA 140029

Name of Degree:

Title of Thesis ("this Work"): Formation of nanocrystalline cellulose by using task specific ionic liquids

Field of Study: Nanotechnology (Chemistry)

I do solemnly and sincerely declare that:

(1)   I am the sole author/writer of this Work;

(2)   This Work is original;

(3)   Any use of any work in which copyright exists was done by way of fair dealing and for permitted purposes and any excerpt or extract from, or reference to or reproduction of any copyright work has been disclosed expressly and sufficiently and the title of the Work and its authorship have been acknowledged in this Work;

(4)   I do not have any actual knowledge nor do I ought reasonably to know that the making of this work constitutes an infringement of any copyright work;

(5)   I hereby assign all and every rights in the copyright to this Work to the University of Malaya ("UM"), who henceforth shall be owner of the copyright in this Work and that any reproduction or use in any form or by any means whatsoever is prohibited without the written consent of UM having been first had and obtained;

(6)   I am fully aware that if in the course of making this Work I have infringed any copyright whether intentionally or otherwise, I may be subject to legal action or any other action as may be determined by UM.

Candidate's Signature   Date:

Subscribed and solemnly declared before,

Witness's Signature   Date:

Name:

Designation:

ABSTRACT

Nanocrystalline cellulose (NCC) has been classified as a new category of cellulose matter and has been used in various technical extents such as in medicinal and biotechnological areas. The nanocrystalline cellulose is typically constructed by the reaction of condensed and toxic acid on primal cellulose samples at different temperatures to ensure ultrasound breakdown. However, the current method for the formation of nanocrystalline cellulose is neither environmentally friendly nor energy efficient. Therefore, this study made use of ionic liquids, 1-butyl-3-methylimidazolium chloride as an alternative to produce nanocrystalline cellulose. Comprehensive investigations on different parameters, such as ultrasonication time, ultrasonication vibration, temperature, dissolution time and microcrystalline cellulose to ionic liquids ratio were conducted in order to control the specific architecture of nanocrystalline cellulose. This study utilizes 1-butyl-3-methylimidazolium chloride followed by ultrasonication to produce nanocrystalline cellulose with a rod-like structure from microcrystalline cellulose. The crystalline structure was noted as Cellulose I, which is similar to the starting materials. Increasing the vibration amplitude of the ultrasonication increases the yield, crystallinity index, thermal properties and particle size of the NCC. Meanwhile, decreasing the ultrasonication time improved the crystallinity, thermal properties and particle size of the NCC. Increasing the temperature, dissolution time and microcrystalline cellulose to ionic liquids ratio enhance the crystallinity, yield, thermal properties, and also the diameter size of the NCC. Optimized conditions were recorded to be as followings: ultrasonication time (5 minutes), ultrasonication vibration (70%), temperature (100°C), dissolution time (30 minutes) and microcrystalline cellulose to ionic liquids ratio (1:10). In conclusion, 1-butyl-3-methylimidazolium chloride is a suitable alternative to the conventional solvents with the optimized parameters as described above.

ABSTRAK

Selulosa nanohablur adalah kelas baru bahan selulosa yang boleh digunakan untuk aplikasi di dalam pelbagai bidang teknikal, bioteknologi dan perubatan. Selulosa nanohablur selalunya dihasilkan dengan perawatan bahan awal selulosa bersama-sama asid toksik dengan kepekatan dan suhu yang tinggi, diikuti proses hidrolisis menggunakan ultrasonikasi. Malangnya, teknik yang sedia ada untuk penghasilan selulosa nanohablur ini tidak mesra alam sekitar dan kurang berkesan dalam penggunaan tenaga. Maka, di dalam kajian ini, 1-n-butil-3-methylimidazolium klorida ([Bmim]Cl) telah digunakan sebagai bahan ganti asid toksik. Kajian yang menyeluruh pada pelbagai parameter, termasuk tempoh masa ultrasonikasi, getaran, suhu, masa pelarutan and nisbah selulosa mikrohablur kepada cecair ionic dijalankan telah dijalankan untuk mengawal seni bina spesifik selulosa nanohablur. Di dalam kajian ini, selulosa nanohablur dengan bentuk seperti rod telah dihasilkan daripada selulosa mikrohablur menggunakan 1-n-butil-3-methylimidazolium klorida ([Bmim]Cl) dan diiukuti proses ultrasonikasi. Struktur hablur adalah Selulosa I, sama seperti bahan asal. Peningkatan getaran ultrasonikasi telah menyebabkan peningkatan hasil, indeks penghabluran, sifat haba dan saiz zarah selulosa nanohablur. Manakala, penurunan masa ultrasonikasi telah meningkatkan indeks penghabluran, sifat haba dan saiz zarah selulosa nanohablur. Peningkatan suhu, masa pelarutan dan nisbah selulosa mikrohablur kepada cecair ionic telah meningkatkan sifat penghabluran, hasil dan haba selulosa nanohablur selain menghasilan selulosa nanohablur dengan diameter yang lebih besar. Manakala, keadaan yang paling optimum telah direkodkan tempoh masa ultrasonikasi (5 minit), getaran ultrasonikasi (70%), suhu (100 °C), masa pelarutan (30 minit) dan nisbah selulosa mikrohablur kepada cecair ionik (1:10). Kesimpulannya, 1-n-butil-3-methylimidazolium klorida ([Bmim]Cl) adalah bahan ganti yang sesuai untuk pelarut konvensional berdasarkan parameter yang optimum seperti di atas.

ACKNOWLEDGEMENTS

TABLE OF CONTENTS

LIST OF FIGURES

LIST OF TABLES

LIST OF SYMBOLS AND ABBREVIATIONS

[Ac]⁻	:	Acetate ion
AFM	:	Atomic Force Microscopy
AGU	:	Anhydroglucose units
[Amim]⁺	:	1-allyl-3-methylimidazolium
[Amim][Cl]	:	1-allyl-3-methylimidazolium chloride
BC	:	Bacterial cellulose
[BF₄]	:	Tetrafluoroborate,
[Bmim]Br	:	1-N-butyl-3-methylimidazolium bromide
[Bmim]Cl	:	1-butyl-3-methylimidazolium chloride
[Bmim][HSO4]	:	1-butyl-3-methylimidazolium phosphate
[Bmim]SCN	:	1-N-butyl-3-methylimidazolium sulfocyanate
Br	:	Bromide
[(CH₃O)-PO₂]⁻	:	Methyl metaphosphate
Cl⁻	:	Chloride ion
[C₁mim]	:	1,3-dimethylImidazolium
[C₁mim][DMP]	:	1,3-dimethylimidazolium dimethylphosphate
[C₂mim]⁺	:	1-ethyl-3-methyl-imidazolium
[C₂mim]Ac	:	1-ethyl-3-methyl-imidazolium acetate
[C₃mim]⁺	:	1-Propyl-3-MethylImidazolium
[C₄mim]⁺	:	1-n-butyl-3-methylimidazolium
[C₄mim]Cl	:	1-butyl-3-methylimidazolium chloride
[C₄mim][HCOO]	:	1-butyl-3-methylimidazolium formate
[C₆mim]⁺	:	1-hexyl-3-methylimidazolium
[C₆mim]Cl	:	1-hexyl-3-methylimidazolium cation

[C$_8$mim]$^+$	:	1-octyl-3-methylimidazolium
DI	:	Deionized
DLS	:	Dynamic light scattering
DMAc	:	*N,N*-dimethylacetamide
DMI	:	1-3-dimethyl-2-imidazolidinone
DMSO	:	Dimethyl sulfoxide
DP	:	Degree of polymerization
DSC	:	Differential Scanning Calorimetry
EDA	:	Electron donor acceptor
[Emim][Ac]	:	1-ethyl-3-methylimidazolium acetate
[Emim][CH3COO]	:	1-ethyl-3-methylimidazolium acetate
[Emim][Cl]	:	1-ethyl-3-methylimidazolium chloride
FESEM	:	Field emission scanning electron microscopy
FTIR	:	Fourier transform infrared spectroscopy
HCl	:	Hydrochloric acid
HPH	:	High pressure homogenization
ILs	:	Ionic liquids
KBr	:	Potassium bromide
LiCl	:	Lithium chloride
LiClO$_4$.3H$_2$O	:	Lithium Perchlorate Trihydrate
LiSCN.2H$_2$O	:	Lithium Thiocyanate Dihydrate
MCC	:	Microcrystalline cellulose
MD	:	Molecular dynamics
MFC	:	Microfibrillated cellulose
MPa	:	Megapascal
NaOH	:	Sodium hydroxide

NCC	:	Nanocrystalline cellulose
NMMO	:	*N*-methylmorpholine-*N*-oxide
NMP	:	*N*-methyl2-pyrrolidine
NMR	:	Nuclear Magnetic Resonance
OH$^-$	:	Hydroxyl ions
[PF$_6$]	:	Phosphorus Hexafluoride
RTILs	:	Room temperature ionic liquids
[SCN]	:	Thiocyanate
TBAF	:	Tetrabutylammonium fluoride trihydrate
TEM	:	Transmission electron microscopy
TEMPO	:	Tetramethylpiperidine-1-oxyl radical
TGA	:	Thermogravimetric analysis
XRD	:	X-ray Diffractometry

CHAPTER 1: INTRODUCTION

1.1. Introduction

Environmental influence, as well as limited petroleum and varied non-renewable resources, lead researchers to explore the utilization of renewable materials such as cellulose over the past several decades. Being one of the most abundance renewable resources on this planet, cellulose is formed from the repetition of D-glucose units connected via β(1-4)-glycosidic bonds (Isik et al., 2014; Qing et al., 2013). The major factor hampering massive exploitation of cellulose is its low reactivity and resistance to chemical processing owing to the elevated crystallinity of the cellulose fibrils. Conventional chemical methods to modify or derivatize cellulose often involve decomposition under strict and environmentally unsafe circumstances (D'Arrigo, 2014). The demand for utilizing environmentally safe and more effective solvents to break up and treat cellulose had led researchers to venture into the usage of solvents such as ionic liquids (ILs). ILs are considered as green solvents due to its ability to maintain high chemical and thermal constancy, bearing flameproof characteristic and is readily miscible with other solvents (Isik et al., 2014). A combination of the 1-butyl-3-methylimidazolium cation with various anions was being studied to produce nanocrystalline cellulose (NCC). The most potent anion to dissipate cellulose is chloride as it is a better acceptor of hydrogen bond compared to larger non-coordinating anions (Isik et al., 2014). NCC possesses a strong inclination towards forming large structures through clumping and accumulation leading to difficulty in obtaining a homogenously dissolved NCC suspension. Nevertheless, mechanical dispersal or ultrasonication allows uniform distribution of the NCC masses producing a sturdy colloidal suspension (Haafiz, M.K.M. et al., 2014). The gradual disintegration of the microcrystalline cellulose (MCC) into NCC during ultrasonication was due to the process of cavitation,

in which cavities were formed, developed and violently collapsed in the water. The ultrasound energy or sonochemistry delivered to the cellulose chains is approximately 10-100kJ/mol and is still in the hydrogen bond energy range (Chen et al., 2011a).

1.2 Overview of Research Project

Cellulose, which is an innately bountiful polymer, is categorized as a linear homopolysaccharide consisting of β-1,4-linked anhydro-D-glucose units. The monomer comprises of anhydroglucose units (AGU) bearing three hydroxyl groups, which forms the hydrogen bonding network as well as van der Waals connections dictating its robust characteristic (Lavoine et al., 2012; Liu, Y. et al., 2013; Rosa, M. et al., 2010). The most prominent characteristics of NCC extracted from renewable sources are large particular surface area and high aspect ratio, which these characteristics elevated the specific strength and modulus (Azizi Samir et al., 2005). Despite its extensive benefits, the usage of concentrated acid and N-methylmorpholine-N-oxide (NMMO) solution in the preparation of NCC causes detrimental effects to the environment caused by the production of waste acid and released of volatile solvents (Liu, Y. et al., 2013; Rosa, M. F. et al., 2010). Therefore, for obtaining a more effective and environmentally safer method to produce NCC, non-volatile solvents were utilized with the likes of ionic liquids (ILs). ILs and its derivatives such as chloride anions appear to be excellent candidates as compared to the conservative volatile organic solvents in the production of NCC. Moreover, utilization of imidazolium halide salts as the starting material in the anion-exchange reaction proves to be more economical (Zhao, Haibo. et al., 2009). It should be noted that NCC has a high tendency to aggregates, thus ultrasonication technique is added to assist the dispersion of the NCC. Since ILs technology in producing NCC is still new, optimizing the synthesis route is needed to minimize the energy consumption. Thus, three parameters which are dissolution time, temperature,

and MCC/ionic liquids ratio will be considered for optimization of the hydrolysis process of MCC to NCC.

1.3   Problem Statement of Research Project

Due to its natural properties, renewable source and possessing an adequate mechanical feature, NCC is already a favourite choice for the construction of cheaper, lighter but sturdy hybrid compounds for various applications and high aspect ratio. The production of NCC using conventional methods and numerous solvents such as sulphuric acid, hydrochloric acid, and N-methylmorpholine-N-oxide has been discovered in the past. However, these conventional methods have some limitations in terms of high energy consumption and the usage of concentrated acid as the solvent. The usage of high concentrated acid is non-favourable due to the high toxicity and corrosive characteristics of the solvent. Therefore, the major concern in producing NCC is to overcome the high energy consumption process and to convert using a green solvent as an alternative to the conventional solvent. Recently, ILs are referred as "green solvent" in nanocellulose application. It has been used as a catalyst as well as a solvent in chemical reaction and reaction media (Guo, Y. H. et al., 2015). Swatloski and co-workers (2002) reported that imidazole-based ILs containing chloride is more effective in dissolving cellulose most probably via the interaction of hydrogen-bonding between the hydroxyl group of the cellulose and anions of the ILs. The selection of 1-butyl-3-methylimidazolium chloride ([Bmim]Cl) on the other hand, was due to its good dissolution abilities and cellulose loading rates of up to 25% (Jiang, M. et al., 2011). Although there are other ILs exhibit better dissolution abilities as compared to [Bmim]Cl, it is one of the cheapest ILs of choice (Montalbo-Lomboy et al., 2015). Nevertheless, production of NCC using a novel and more efficient ways should be emphasized, especially by using the green methods (Qiu et al., 2012). Thus, the existing

technique should be optimized in accordance with the requirement of low energy production and effective budget reducing measures.

1.4. Research Objective

1) To isolate nanocrystalline cellulose using 1-butyl-3-methylimidazolium chloride ([Bmim]Cl) aided by ultrasonication process

2) To characterize the obtained nanocrystalline cellulose in physical, chemical and surface properties

3) To optimise operating conditions of dissolution and hydrolysis for formation of nanocrystalline cellulose

1.5 Research Hypothesis and Framework

Throughout the reaction procedure, the chloride anion of [Bmim]Cl attacked the free hydroxyl group on the cellulose for protonation process. The breakup of the cellulose is initiated by the interaction of the Bmim+ cation with the hydroxyl oxygen atoms, causing the individual chains to be pushed apart. This reaction causes the hydrogen bond in cellulose to be disrupted and substituted by hydrogen bonding between the cellulose hydroxyls and chloride anion of ILs. The addition of anti-solvent (water) allows the formation of hydrogen bonds between the ions of ILs with water molecules causing them to be transferred into the aqueous phase. The hydrodynamic shells comprise of water molecules built up around the ions of ILs shielded the interaction between ILs and cellulose, which will subsequently cause the cellulose to be expelled. The cellulose then reconstructed its intra and intermolecular hydrogen bonds before finally being precipitated. The precipitated cellulose was separated from the ILs by centrifugation. The research framework has been divided into two major parts as shown in Figure 1.1.

Part 1

```
┌─────────────────────────────────────────────────────────────┐
│                                                             │
│   Microcrystalline cellulose (MCC) will be mixed with 1-    │◄─┐
│   butyl-3-methylimidazolium chloride ([Bmim][Cl]            │  │
│                                                             │  │
└─────────────────────────────────────────────────────────────┘  │
                           │                                      │
                           ▼                                      │
┌─────────────────────────────────────────────────────────────┐  │
│                                                             │  │
│   The mixture will be heated at 40 °C for 30 minutes under  │  │
│   400rpm mechanical stirring                                │  │
│                                                             │  │
└─────────────────────────────────────────────────────────────┘  │
                           │                                      │
                           ▼                                      │
┌─────────────────────────────────────────────────────────────┐  │
│                                                             │  │
│   The reaction process is quenched by adding deionized      │  │
│   water to the mixture                                      │  │
│                                                             │  │
└─────────────────────────────────────────────────────────────┘  │
                           │                                      │
                           ▼                                      │
┌─────────────────────────────────────────────────────────────┐  │
│                                                             │  │
│   The mixture will undergo ultrasonication at different     │  │
│   parameters:                                               │  │
│      1) Ultrasonication time (5,10,15,20 minutes)           │  │
│      2) Vibration amplitude (60, 70, 80, 90%)               │  │
│                                                             │  │
└─────────────────────────────────────────────────────────────┘  │
                           │                                      │
                           ▼                                      │
┌─────────────────────────────────────────────────────────────┐  │
│                                                             │  │
│   The suspension is washed using centrifugation at 7000rpm  │  │
│   for 30 minutes                                            │  │
│                                                             │  │
└─────────────────────────────────────────────────────────────┘  │
                           │                                      │
                           ▼                                      │
┌─────────────────────────────────────────────────────────────┐  │
│                                                             │  │
│   The sediment is freeze-dried for several days             │  │
│                                                             │  │
└─────────────────────────────────────────────────────────────┘  │
                           │                                      │
                           ▼                                      │
┌─────────────────────────────────────────────────────────────┐  │
│                                                             │  │
│   Characterization                                          │  │
│                                                             │  │
└─────────────────────────────────────────────────────────────┘  │
                           │                                      │
                           ▼                                      │
                       ◇ NCC ◇ ──────────────────────►  ┌──────┐ │
                           │                            │  No  │─┘
                           ▼                            └──────┘
                       ┌───────┐
                       │  Yes  │
                       └───────┘
                           │
                           ▼
                    ◇ Optimization ◇
```

Part 2

```
┌─────────────────────────────────────────────────────┐
│ Microcrystalline cellulose (MCC) is mixed with 1-butyl- │◄──┐
│   3-methylimidazolium chloride ([Bmim][Cl])         │   │
└─────────────────────────────────────────────────────┘   │
                        ▼                                   │
┌─────────────────────────────────────────────────────┐   │
│      The mixture is heated under mechanical stirring  │   │
└─────────────────────────────────────────────────────┘   │
                        ▼                                   │
┌─────────────────────────────────────────────────────┐   │
│   The reaction is quenched by adding deionized water  │   │
│                  to the mixture                       │   │
└─────────────────────────────────────────────────────┘   │
                        ▼                                   │
┌─────────────────────────────────────────────────────┐   │
│   The mixture will undergo ultrasonication at defined │   │
│                 optimum conditions                    │   │
└─────────────────────────────────────────────────────┘   │
                        ▼                                   │
┌─────────────────────────────────────────────────────┐   │
│   The suspension is washed using centrifugation at    │   │
│               7000rpm for 30 minutes                  │   │
└─────────────────────────────────────────────────────┘   │
                        ▼                                   │
┌─────────────────────────────────────────────────────┐   │
│      The sediment is freeze-dried for several days    │   │
└─────────────────────────────────────────────────────┘   │
                        ▼                                   │
┌─────────────────────────────────────────────────────┐   │
│                   Characterization                    │   │
└─────────────────────────────────────────────────────┘   │
                        ▼                                   │
                     ◇ NCC ◇                                │
                        ▼                                   │
            ┌──────────┐         ┌──────────┐              │
            │   Yes    │────────►│    No    │──────────────┘
            └──────────┘         └──────────┘
                  ▼
┌─────────────────────────────────────────────────────┐
│ Optimum temperature, dissolution time and MCC/ionic   │
│            liquids' ratio is defined                  │
└─────────────────────────────────────────────────────┘
```

Parameters:

1) Dissolution time
2) Temperature
3) MCC/Ionic Liquids' ratio

Figure 1.1: The framework of research study

1.6. Expected Outcome

As the ultrasonication technique is applied, the regeneration yield of NCC is increased at a higher vibration amplitude and ultrasonication time. Longer ultrasonication time will result in weaker crystalline properties, meanwhile higher vibration amplitude will improve the thermal properties of the NCC. A significant relationship between crystalline and thermal properties is expected from this study. However, aggregation of rod-like NCC might still occur. By using ILs, the crystallinity index and the yield of NCC are expected to be increased. Optimum processing conditions in producing NCC is expected to be at lowest dissolution time and highest reaction temperature as the ultrasonication technique and ILs treatment is combined.

CHAPTER 2: LITERATURE REVIEW

2.1 Introduction

Cellulose, being the most abundant biomaterial on earth composed of homo-polymer of β-D-glucopyranose units. Due to its high tensile strength, chemical inertness, biodegradability, and renewable nature, cellulose is being extensively explored for applications in composite reinforcement, soft-tissue replacement, artificial bones, and food packaging (Chenampulli et al., 2013) in the form of NCC. Various methods exist to produce NCC such as alkali hydrolysis, acid hydrolysis and ball milling, however, the conventional method like acid hydrolysis seems to be a more economical process for the hydrolysis of cellulose. Nevertheless, the method possessed some disadvantages such as tough fractionation of products, risks of corrosion, and environmental pollution (Lai et al., 2011; Wang, Yihong et al., 2013). Over the past decade, ILs have become increasingly recognized as environmentally friendly media, thus the interest in using ILs as dissolution solvent for cellulose also increases (Suzuki et al., 2014). Additionally, a report by Rogers and co-workers in 2002 stated the requirement of moderate heat treatment to dissolve cellulose using 1-butyl-3-methylimidazolium chloride ([Bmim]Cl), while a combination of mechanical, enzymatic, and/or chemical treatments appear to be an attractive approach and are supposedly able to decrease energy consumption (L. Spence et al., 2011). Mechanical treatment through ultrasonication process with high frequency waves (over 20 kHz) has been applied to assist in the production of NCC (Yang, C-Y. et al., 2014). Ultrasonication approach is an effective candidate to disintegrate nanoparticles aggregates connected by hydrogen bonds, hence decreasing the polydispersity and the dimension size of the nanoparticles (Kim et al., 2013b).

2.2 Green Technology

Green technology can be defined as a less harmful energy production to the environment based on its production process or supply chain (Abdul Khalil et al., 2012). Among the principles of "Green Chemistry" is the reduction of harmful synthesis whereby all synthetic practices should be planned to utilize and produce substances with slight or no toxicity threat to mankind and to the environment. Likewise, the dependence of the chemical industry on petroleum-based feedstock should also be monitored. Although the timeline for exhaustion is arguable, long term maintainable substitutes should be recognized (Warner et al., 2004). Thus, application of sustainable materials with less harmful effect has been addressed as one of the principles in green technology prospective.

2.2.1 Sustainable Materials

In view of the current scenario in emphasizing sustainability, industrial ecosystem and green chemistry, the development of NCC have gained international interest. The unique characteristic of the NCC such as being readily available, biodegradable as well as biocompatible, making it a suitable choice of sustainable nanomaterial (Johar et al., 2012; Normand et al., 2014; Wei et al., 2014).

2.2.2 Green Synthesis Process

A few green chemistry methods have been practised worldwide for the isolation of cellulose namely high pressure homogenization, Lyocell process and the use of ILs. High pressure homogenization is a novel green method carried out under the temperate condition without involving the addition of sulphuric acid to the cellulose solution as a pretreatment step. Meanwhile, the Lyocell process makes use a non-

toxic solvent called *N*-methylmorpholine-*N*-oxide (NMMO) to produce cellulose fibres (Wang, Yihong. et al., 2013). Even so, the process involving NMMO is not favourable because of the fibrillating fibre character, side reactions, the by-product of the reaction, and thermal volatility of the cellulose/NMMO solutions (Hao, Yan. et al., 2012). On the contrary, isolation of the NCC using ILs is a chosen method due to its low vapour pressure besides exhibiting reduced risk to the environment (Singh et al., 2013). Furthermore, ILs is a type of direct solvent for cellulose isolation, which does not involve any pretreatment steps (Hao, Yan et al., 2012).

2.3 Cellulose Based Materials

In spite of 700, 000 billion tons global quantity of cellulose available, only 0.1 billion tons found its way into the industry. The application of cellulose in the industry ranges from the manufacturing of textiles, paper, pharmaceutical compounds, fillers, adhesives, parts of electrical devices, foams, aerogels, and biomaterials (Gupta, 2015). The use of NCC as fillers in composites is due to its low gas permeability property as well as stiffness enhancing ability. They can also be used as reinforcement for adhesives, components of electronic devices, biomaterials, foams and aerogels (Morais et al., 2013). Extensive studies have shown that NCC can be used for many applications such as regenerative medicine, optical, and automotive applications (Bai et al., 2009).

2.3.1 Raw Materials

Cellulose fibres as presented in Figure 2.1 are made of microfibrillated cellulose, which starts with 36 separate cellulose molecules consisting of cellulose, hemicellulose and lignin. These starting materials are brought together into bigger

units and are identified as elementary fibrils or microfibrils by biomass. These microfibrils are then packed together into larger units known as microfibrillated cellulose (Habibi et al., 2010).
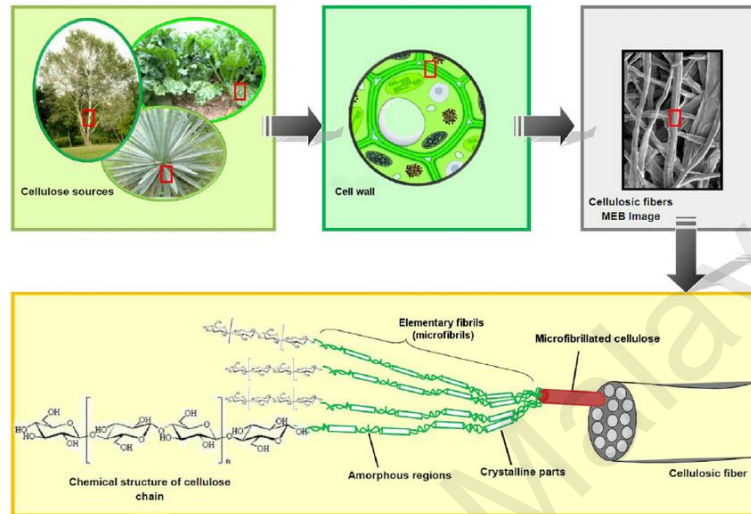
Figure 2.1: From the cellulose sources to the cellulose molecules; details of the cellulosic fiber structure (Lavoine et al., 2012)

Previous studies have focussed on cellulose, accounting for the largest part (40-50%) in biomass (Komanoya et al., 2011). Plants like ramie, flax, cotton, jute and hemp are not the only source of cellulose. Although cellulose is present in the cell walls of plants, other organisms are also able to synthesize it such as bacteria, tunicate, algae and some animals (Abdul Khalil et al., 2012). More details are shown in Table 2.1.

Table 2.1: Various sources of NCC

Sources	Crystallinity index (%)	Particle size (nm)	Synthesis technique	Reference
Wood	-	15	Alkaline extraction + grinding	Abe, Iwamoto, Yano (2007), Chen et al.

Table 2.1, continued

				2011
Cotton	91	AFM:19 ±10 TEM:14±4	Acid hydrolysis + ultrasonication	de Morais Teixeira et al. (2010)
Potato tuber cells	-	5	Alkaline extraction + homogenization	Dufresne et al. 2000
Prickly pear fruits of *Opuntia ficus –indica*	±60	-	Alkaline extraction + homogenization	Habibi, Heux, Mahrouz, and Vignon (2009)
Lemon and maize	Lemon:55, Maize:24	Lemon:3-10 nm, Maize:5-20 nm	Acid hydrolysis	Rondeau-Mouru et al. (2003)
Soybean	-	50-100	Acid hydrolysis + high pressure defibrillation	Wang and Sain (2007a)
Coconut husks	62.2-65.9	5.3-6.6	Acid hydrolysis	Rosa et al. (2010)
Branch-barks of mulberry	73.4	42.4% 25-30 nm	Acid hydrolysis	Li et al. (2009)
Pineapple leaf	73.62	32.5	Acid hydrolysis	Cherian et al. (2010)
Banana rachis	-	5	Alkaline extraction + homogenization	Zuluaga et al.(2009)
Sisal	75 ±1	30.9 ± 12.5	Acid hydrolysis	Moran, Alvarez, Cyras, and Vasquez (2008)
Pea hull	-	7-12	Acid hydrolysis	Chen, Liu, Chang, Cao, and Anderson (2009)
Oil palm empty fruit brunch	58.78 ± 0.70	2.51 ± 1.03	Acid hydrolysis	Fahma, Iwamoto, Hori, Iwata and Takemura (2010)

(Abdul Khalil et al., 2012)

2.3.2 Synthesis Process

The difficulty in processing and isolating lignocellulose is due to the close associated chemical structure of cellulose, hemicellulose and lignin as seen in Figure 2.2. Lignin is covalently bond to hemicellulose and also at the same time cross-linked to microfibrils of cellulose, making it recalcitrant to chemical procedures or biological assault.
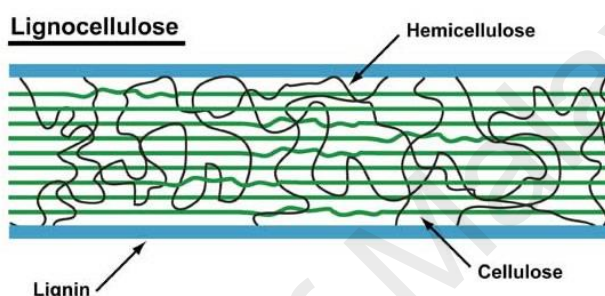
Figure 2.2: Lignocellulose structure of cellulose, hemicellulose and lignins

In order to produce cellulose, delignification is an essential step whereby the linkages between lignin and carbohydrate molecules are cleaved. This step is necessary due to the property of lignin that obstructs the division of natural fibres to its components (Brinchi et al., 2013). Besides the task of removing lignin and hemicellulose by pretreatment of the lignocellulosic complex, the reactivity sites are also shielded by a firmly packed crystalline assembly consisting of intramolecular and intermolecular hydrogen bonds between the cellulose chains. Consequently, pretreatment of lignocellulose to remove lignin and hemicellulose as well as to reduce the crystallinity of cellulose is indeed an essential step (Tan et al., 2012). Pretreatment measures are classified into four groups: (1) physical; (2) chemical; (3) physico-chemical; and (4) biological (FitzPatrick et al., 2010).

2.3.3 Properties and Characteristics

Being a macromolecule, cellulose is made up of the non-branched chain of tightly packed aggregates of long-chain β-1,4 glucan, water-insoluble and also exhibit a robust nature (Abdul Khalil et al., 2012; Tian et al., 2010). Figure 2.3 depicts the chemical structure of cellulose. The length of the β-1,4 glucan chains is dependent upon the origin of the cellulose. A degree of polymerization (DP) of up to 10, 000 exists in the lignocellulosic complex, while its repeating unit is known as cellobiose, a dimer of glucose (Abdul Khalil et al., 2012).
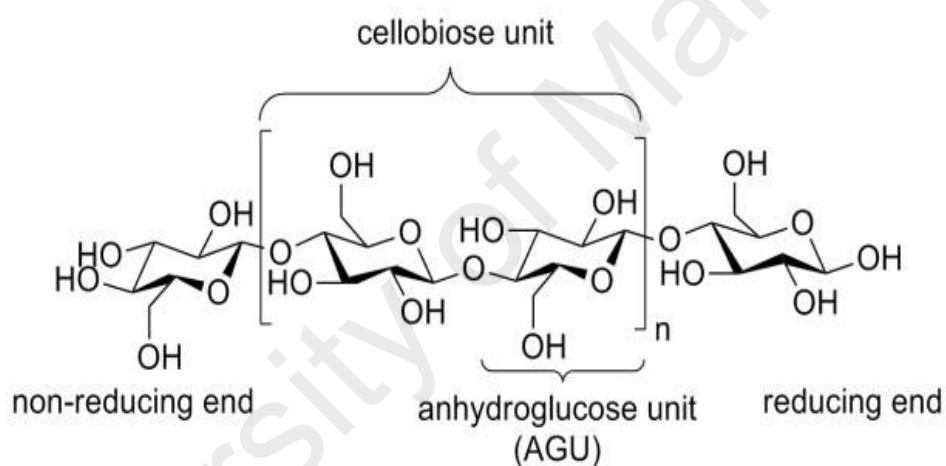
Figure 2.3: Chemical structure of cellulose (Olsson et al., 2013)

The monomer of cellulose, known as an anhydroglucose unit (AGU), consists of three hydroxyl groups (Siró et al., 2010). The three hydroxyl groups are located at positions of C6 (primary hydroxyl groups), C2 and C3 (secondary hydroxyl groups) and are able to form intra- and intermolecular hydrogen bonds, resulting in the conception of a highly ordered, three-dimensional crystal arrangements (Abdul Khalil et al., 2012). However, the stiff molecules resulting from the crystalline structure and close chain packaging via several intermolecular and intramolecular

14

hydrogen bonds dictates the recalcitrant character of the cellulose in water and the usual organic solvents (Zhang, H. et al., 2005). Nageli and Schwendener were the first to identify the presence of crystalline zones interjected in the formless structure of cellulose matter in 1877. This amorphous section is accountable for the crosswise cleavage of the cellulose microfibrils into short monocrystals rendering a structural imperfection (Rosa, M. et al., 2010; Samir et al., 2005). The alternating crystalline and amorphous structure render a very high flexible modulus to cellulose (approximately 134 GPa in crystalline regions of cellulose I) together with high particular strength, making it a perfect candidate to support polymer in the form of NCC (Tingaut, Zimmermann, & Sèbe, 2012).

2.3.4 Limitation

Cellulose is important as the fortification material in the engineering polymer system, however, certain factors hinder the wide usage in the industry. The tendency of cellulose to form aggregates during processing, swelling in water medium, and incompatibility with the hydrophobic polymer substance, particularly in the amorphous regions greatly deter the possibility of original fibres to be utilized as reinforcements in polymers (Brinchi et al., 2013).

2.4 Nanocellulose

"Nanocellulose" mainly refers to the cellulosic matters possessing at least one aspect in the nanometer scale, and it can be categorized into three core subcategories (Table 2.2) based on its functions, dimensions, and methods of preparation (Abdul Khalil et al., 2014).

Table 2.2: Nanocrystalline cellulose (NCC), Microfibrillated cellulose (MFC)

and Bacterial Cellulose (BC)

Types of nanocelluloses	Synonyms	Typical sources	Average size
Nanocrystalline cellulose (NCC)	Cellulose nanocrystal, whiskers, rod like cellulose, microcrystals	Wood, cotton, hemp, flax, wheat straw, rice straw, mulberry bark, ramie, microcrystalline cellulose, Avicel, tunicin, algae, bacteria, etc.	Diameter: 5-70 nm Length: 100-250 nm (from plant); 100 nm-several micrometers (from cellulose of tunicates, algae, bacteria)
Microfibrillated cellulose (MFC)	Nanofibrils, microfibrils, nanofibrillated cellulose, microfibrillated cellulose	Wood, sugar beet, potato tuber, hemp, flax, etc.	Diameter: 5-60 nm Length: several micrometers
Bacterial cellulose (BC)	-	*Acetobacter, Achromobacter, Aerobacter, Agrobacterium, Pseudomonas, Rhizobium, Sarcina, Alcaligenes, Zoogloea*	Diameter: 100 nm Length: 100 µm

(Brinchi et al., 2013)

NCCs are acquired by introducing natural fibres to strong acid hydrolysis prior to sonication treatment in order to gain stiff rod-like nanoparticles (Belbekhouche et al., 2011). The geometrical dimensions of NCCs vary with the width ranging from 5-70 nm and length between 100-250 nm of plant cellulose and 100 nm to several micrometres of tunicates, algae, and bacterial cellulose. The different dimensions are

a result of dependency on the source of the starting cellulose (Brinchi et al., 2013). MFC is composed of crystalline and amorphous domains, having lengths in the micron scale and widths ranging from 5-60 nm (Brinchi et al., 2013). MFC is a result of numerous mechanical disintegration actions on the natural fibres, thus allowing the release of the essential cellulosic microfibrils (Belbekhouche et al., 2011). MFC, which is normally produced by four mechanical methods namely homogenization, microfluidization, microgrinding, and cryocrushing, consists of long, elastic and entrapped cellulose nanofibres. It differs from NCC by containing both amorphous and crystalline phases in its structure (L. Spence et al., 2011; Li, Rongji. et al., 2009; Tingaut, Zimmermann, & Sebe, 2012). Bacterial cellulose (BC) is a kind of cellulose produced by some bacteria and it varies in terms of the possessing higher purity, crystallinity, degree of polymerization and stretchable strength. BC structures, which are formed extracellularly and are excreted in the form of nanofibres, are produced by different kinds of bacterial species including *Acetobacter*, *Rhizobium*, *Agrobacterium* and *Sarcina*. Nanofibres BC has ribbon-like structures with 100 nm in diameter and approximately 100 μm in length. These ribbons are the results of packages of 2-4 nm in diameter of the cellulose microfibrils (G. Torres et al., 2012).

2.4.1 General Properties

As a nanocellulose, NCC possesses few attractive features (Pla, 2013). Among them are increased crystallinity ($> 70\%$), high aspect ratio (~ 70), developed specific surface (~ 150 m^2/g), high tensile strength (7500 MPa), improved dispersal ability, biodegradable, stable towards aggressive medium, increases temperatures of proteolytic enzymes, and adjustable surface properties due to the reactive -OH side groups (Brinchi et al., 2013). NCC is known for two advantages: low cost and

environment friendly. NCC is also known by other nomenclature such as rod-like cellulose crystals, nanowhiskers, and nanorods (Abdul Khalil et al., 2014). Figure 2.4 shows the AFM images of the NCC isolated from switchgrass and cotton. Both NCCs showed a rod-like construct with the length, width, and height dimensions being 148 ± 42.1, 21 ± 4.3, 3.9 ± 1.3 for switchgrass NCC, and 94 ± 31.6, 21 ± 5.5, 7.2 ± 3.0 nm for cotton NCC (G. Torres et al., 2012). As can be seen in Table 2.3, NCC derived from bacterial cellulose and tunicate appear to exhibit larger dimensions as compared to NCC generated from cotton and wood. This may be due to the bacterial cellulose and tunicate properties that possess high crystallinity causing lesser sections of amorphous regions that are needed to be split, hence the larger amount of NCC being produced (Peng et al., 2011).

Table 2.3: Example of length (L) and diameter (d) of NCC from various sources obtained via different techniques

Source	L, nm	d, nm	Technique	References
Bacterial	100-1000	10-50	TEM	(Araki et al., 2001)
Tunicate	1160	16	DLS	(De Souza Lima et al., 2003)
	100-some 1000	15-30	TEM	(Kimura et al., 2005)
Valonia	>1000	10-20	TEM	(Revol, 1982)
MCC	ca. 5000	10	AFM	(Pranger et al., 2008)
Cotton	255	15	DLS	(De Souza Lima et al., 2003)
	100-150	5-10	TEM	(Araki et al., 2001)
Cotton linter	25-320	6-70	TEM	(Elazzouzi-Hafraoui et al., 2008)

	300-500	15	AFM	(Q. Li et al., 2009)
Softwood	100-150	4-5	AFM	(Beck-Candanedo et al., 2005)
Hardwood	140-150	4-5	AFM	(Beck et al., 2013)
Wheat straw	150-300	ca. 5	TEM	(Dufresne et al., 1997)
Rice straw	117 ± 39	8-14	TEM	(Lu et al., 2012)

*TEM: Transmission Electron Microscopy
 AFM: Atomic Force Microscopy
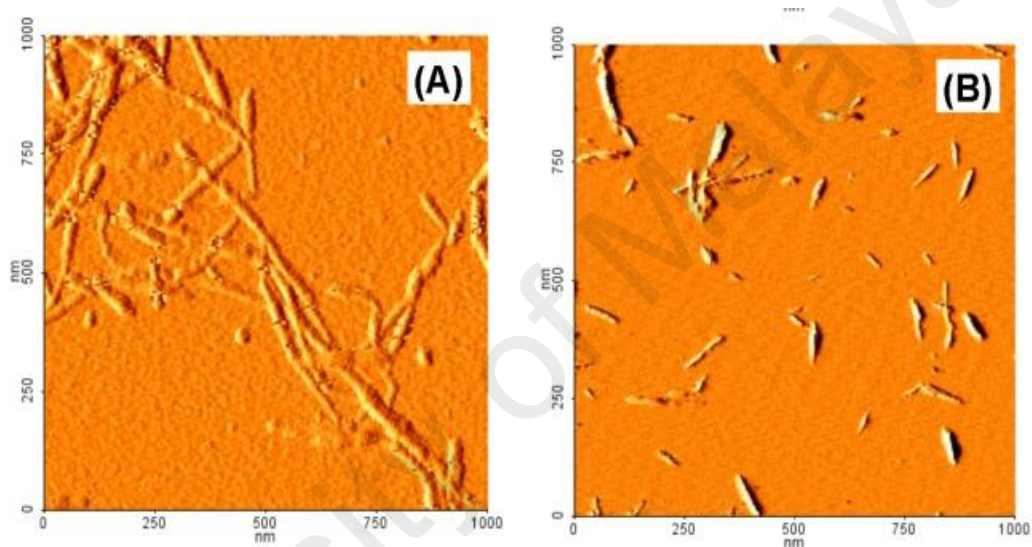
Figure 2.4: AFM images of (A) switchgrass NCC and (B) cotton NCC (Wu et al., 2014)

The crystallinity of the particular plant fibre and the techniques adopted for cellulose extraction dictates the morphological and structural traits of the NCC obtained. The properties include geometrical dispersion and entanglement, and also the product of the extraction process in terms of the quantity of the NCC obtained for a given weight of macrofibre (Fortunati et al., 2013). Identification of the change in crystalline value and the structure of the NCC can be detected via X-ray Diffractometry (XRD) and Differential Scanning Calorimetry (DSC) analysis. These analyses detect the degree of the crystalline structure decomposition based on the

temperature and the quantity of the heat released during the process (Singh et al., 2013). In a previous study, DSC thermograms were utilized to find the augmentation in cellulose crystallinity of polypropylene infused banana fibres (Paul et al., 2010). An increase in the crystalline regions is a concern as it also increases the rigidity of the cellulose and this phenomenon influence the accessibility of the cellulose molecule (Soom et al., 2009). Table 2.4 shows the various degree of crystallinity of the NCC derivatives.

Table 2.4: Crystallinity of NCC derivatives

Particle type	Crystallinity (%)	Reference
Wood and plant pulps	43-65	(Klemm et al., 2005)
MCC	80-85	(Bondeson et al., 2006)
MFC	51-69	(Rondeau-Mouro et al., 2003)
NCC	54-88	(Elazzouzi-Hafraoui et al., 2008; Rondeau-Mouro et al., 2003)
Tunicate NCC	85-100	(Elazzouzi-Hafraoui et al., 2008; Rondeau-Mouro et al., 2003)

2.4.2 Synthesis Process

Naturally, cellulose does not exist as an isolated individual molecule but rather as assemblies of individual cellulose chain-forming fibres. The morphological order starts with elementary fibrils, which then clustered together into larger units called microfibrils, which in turn convened into fibres (Brinchi et al., 2013) as shown in Figure 2.5. The crystalline region consisting of the aggregation of the microfibrils along with the amorphous (disordered) domain forms the core of the cellulose structure. Since the amorphous regions have a lower density as compared to the crystalline regions, the cellulose fibres will break up upon exposure to harsh acid

treatment, thus releasing discrete crystallites resulting in NCC (Abdul Khalil et al., 2014; Peng et al., 2011).
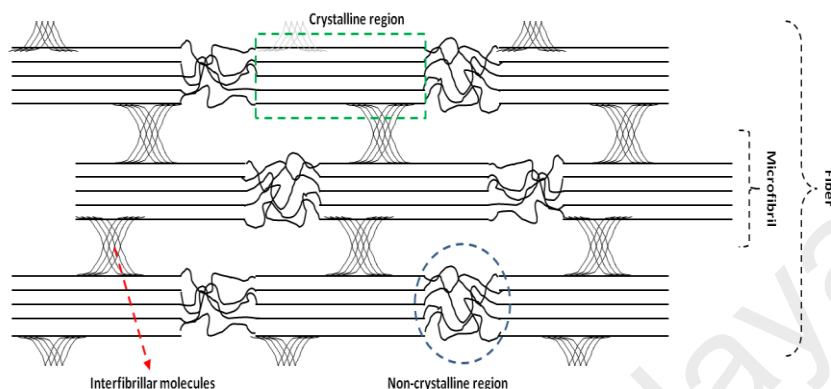
Figure 2.5: Schematic of interaction between cellulose molecular chains within the crystalline region of cellulose microfibrils (Börjesson et al., 2015)

2.4.2.1 Conventional Method

Table 2.5 shows the yield, crystallinity index, diameter and length of the NCC produced by the different synthesis methods.

Table 2.5: Yield, crystallinity index, diameter (d) and length (L) of NCC produced by different synthesis methods.

Sample	Yield (%)	L, nm	d, nm	Crystallinity index (%)	References
NCC prepared by acid hydrolysis	-	400-500	25-30 (42%)	73.4	(Li, Rongji et al., 2009)
NCC prepared by acid hydrolysis	-	-	15-20	59.0	(Johar et al., 2012)
NCC prepared by acid hydrolysis	-	161-193	10-13	90.5	(Morais et al., 2013)

Table 2.5, continued

NCC prepared by acid hydrolysis (HCl)	-	-	-	74.8	(Lamaming et al., 2017)
NCC prepared by acid hydrolysis	16.9	68.6±16.6, 165.6±42.0	2.1±0.7, 6.7±1.8	90.7	(Jiang, F. et al., 2013)
NCC prepared by mechanical defibrillation	12.0	100-200, >10^3	2.7±1.2, 8.5±4.1	81.5	
NCC prepared by TEMPO-mediated oxidation	19.7	10^2-10^3	1.7±0.6	64.4	
NCC prepared by TEMPO-mediated oxidation + ultrasonication	98.4	-	4.7	-	(Mishra, Shree Prakash et al., 2011)
NCC prepared by microwave liquefaction + chemical treatment + ultrasonication	-	-	-	67.4	(Xie et al., 2016)
NCC prepared by ultrasonication	50.7±1.8	-	-	39.8	(Liu et al., 2006)

Most of the NCCs reported in the literature reserve their native cellulose I polymorph following hydrolysis of the amorphous domains. Nevertheless, recent findings showed that NCC with cellulose II structure could also be created during the sulphuric acid process under particular conditions (Tingaut, Zimmermann, & Sèbe, 2012). There are several crystalline cellulose polymorphs exist (I, II, III, and IV) with Cellulose I showed better mechanical properties as compared to the other polymorphs. Cellulose I is the crystalline cellulose that is originally produced by a variety of organisms such as plants, trees, tunicates, algae, and bacteria. It is also

thermodynamically metastable and can be switched to either Cellulose II or III (Abraham et al., 2011; J. Moon et al., 2011). The native state of Cellulose I has been reported to be more recalcitrant than its regenerated forms of Cellulose II, III, and IV (Zhang J. et al., 2014).

2.4.2.2 Catalytic Approach

A more efficient catalytic method is needed, which require low energy, moderate conditions, and the application of green solvents, which are fully biodegradable for the isolation of the cellulose. One promising substitute that could be used is ILs (Zavrel et al., 2009) since it can play a role in the catalytic process as a solvent for the reaction. (Welton, 2004). Although the effect of ILs on the catalytic activity is questionable due to the lack of study in this field, it is known that halide ions are potent converters of the acidity and catalytic activity (Rinaldi et al., 2009). The advantages of ILs usage ranges from acquiring novel catalytic technologies with less energy consumption, enhancing the reaction level to the improvement of the products selectivity. Moreover, the ILs ionic characteristic is able to provide a unique ionic environment to the catalysts that play a positive role in stabilizing the reactive catalytic species or the reaction intermediates, which is deprived in molecular solvents. Therefore, catalysts in ILs exhibit improved catalytic activities over those conducted using conventional solvents. In addition, they are also able to overcome the problems by catalyzing those catalytic reactions that are not possible to be carried out in common organic solvents (Zhang, Q. et al., 2011).

2.4.2.3 Limitation on Synthesis Process of NCC

Over the past decades, numerous solvent systems have been developed for the production of NCC such as lithium chloride (LiCl)/*N,N*-dimethylacetamide (DMAc),

23

LiCl/1-3-dimethyl-2-imidazolidinone (DMI), LiCl/N-methyl2-pyrrolidine (NMP), N-methylmorpholine-N-oxide (NMMO), dimethyl sulfoxide (DMSO)/tetrabuthlammonium fluoride trihydrate (TBAF), DMSO/paraformaldehyde, aqueous solution of NaOH, some molten salt hydrates such as $LiClO_4.3H_2O$ and $LiSCN.2H_2O$, and some aqueous solutions of metal complexes (Rahman et al., 2012). Application of all of the above solvent systems is restricted due to their toxicity, dissolving capability, solvent recovery, high cost, an uncontrollable side reaction, and instability during cellulose processing and/or derivatization (Cao et al., 2009). For example, NCC made from N-methylmorpholine-N-oxide (NMMO) solution competes with the viscose-type NCC. Instead, the NMMO process still cannot substitute the Viscose process till date due to some disadvantages such as the requirement of cellulose activation before dissolution, the demand for high temperature to dissolve the cellulose, the degradation of the cellulose, the side effects of the solvent itself without antioxidants, and it is expensive (Cao et al., 2009). Cryocrushing is another method to produce NCC, which does not involve any solvents. Cellulose is frozen using liquid nitrogen and high shear forces are being applied. Nevertheless, the major obstacle is the high energy consumption in mechanically breaking down the cellulose to NCC (Zhao, Hua. et al., 2009). On the other hand, the use of concentrated mineral acids at high temperature (170-240 °C) was found to be more efficient. However, the disadvantages of this method are risk of corrosion, generation of a large amount of acid wastewater, and difficulty in separating the acids. Enzymatic hydrolysis holds clear disadvantages in isolating the cellulose in which low activity was detected, the high cost of the enzymes, and separation problems due to the solubility of the enzyme in the water. On the contrary, enzymatic hydrolysis is

a cleaner and involves a few discriminating process that takes place at a reasonable pressure and temperatures as compared to the acid hydrolysis. Although acid hydrolysis method portrays advantages such as faster reaction rate and cheaper starting materials as compared to the enzymatic hydrolysis, the use of high temperature, unfortunately, increases the equipment corrosion incidence, hence leads to high maintenance cost (Camacho et al., 1996). Another method for cellulose isolation is the sub- or supercritical water method whereby the reaction occurs in the water medium at a high temperature between 200-400 °C without the presence of the catalysts and are carried out under the pressure of above 20 MPa with low selectivity. However, harsh conditions such as high pressure and temperature are the disadvantages of this method. Therefore, it is vital to find an alternative method that makes use of the green chemistry as well as being economical for the production of the NCC.

2.5 Ionic Liquids as Catalyst

In the view of searching for "greener" alternatives for cellulose production, researchers have to comply with the governmental industries regulations in order to prevent pollution (Zhang, H. et al., 2005). ILs, which refer to an ionic scheme that is in a liquid form at the room temperature or slightly warmer temperature, are also named as room temperature molten salts, room temperature ionic liquids (RTILs), and organic ionic liquids (Feng, Li. et al., 2008). In accordance with the nature of the ILs, it is suitable to be used as a solvent or catalyst (Liu, Yuanyuan. et al., 2013). ILs can act as both solubilizing agents and as catalysts in the process of cellulose hydrolysis, whereby MCC was hydrolysed in 1-butyl-3-methylimidazolium hydrogen sulphate giving NCC yield with high crystallinity. Nonetheless, this NCC displayed low thermal stability (Brinchi et al., 2013). Therefore, attentions have been

25

directed towards developing multifunctional ILs using cooperative "chemical" properties (Olivier-Bourbigou et al., 2010).

2.5.1 Derivatives and General Properties

ILs are a class of highly polar solvents that are entirely constitute of ions (Cheng et al., 2006). The evident characteristics that differentiate ILs from the conventional solvents are the wide range of melting temperature (-40 °C – 400 °C), high thermal stability (up to 400 °C), high conductivity (both ionic and thermal), low flammability, weakly coordinating properties, broad electrochemical potential window (-4V to 4V), and low vapour pressure. All these characteristics prove to be an advantage to the workforces due to its minimal emission of volatile fumes as experienced with other chemical pretreatments (Gupta et al., 2015; Montalbo-Lomboy et al., 2015). Besides that, ILs are categorized as a class of highly polar solvents entirely constitutes of ions (Cheng et al., 2006). Notably, ILs are recyclable, hence promising a reduction of the cost and waste generation throughout the overall procedures (Montalbo-Lomboy et al., 2015). Furthermore, the chemical and physical properties are adjustable by the variation of the cations and anions, a condition that is considered impossible with conventional solvents (Gupta et al., 2015). Naturally, most of the cations in ILs possess particular characteristics such as bulkiness, asymmetric, and organic. Among the cations are imidazolium, pyrrolidinium, ammonium, piperidinium, pyridinium, thiazolium, pyrazolium, sulfonium, and phosphonium (Gupta et al., 2015). To date, alkylimidazolium salts are the most extensively studied and the best characterized ILs (Cheng et al., 2006). Research was mainly focussed on the 1-alkyl-3-methylimidazolium type of ILs, in order to reach the optimum solubilisation of cellulose in high concentrations (Wendler et al., 2012).

Table 2.6 shows the different solubility of the cellulose in several types of ILs, whereby 1-butyl-3-methylimidazolium chloride ([Bmim][Cl]) has the highest rate of solubility.

Table 2.6: Solubility rate of cellulose in different types of ILs

ILs	Temp (°C)	Solubility (wt%)	Type of cellulose	Reference
1-ethyl-3-methylimidazolium chloride ([Emim][Cl])	90	5	MCC Avicel	(Zavrel et al., 2009)
1-ethyl-3-methylimidazolium acetate ([Emim][Ac])	90	16	MCC Avicel	(Zavrel et al., 2009)
	85	13.5	Eucalyptus pulp	(Kosan et al., 2007)
	110	15	MCC Avicel	(Zhao, H. et al., 2008)
1-allyl-3-methylimidazolium chloride ([Amim][Cl])	90	5	MCC Avicel	(Hao Zhang et al., 2005)
	100	10	MCC (DP:250)	(Fukaya et al., 2006)
	100-130	5-14.5	Pulp cotton linter	(Hao Zhang et al., 2005)
1-butyl-3-methylimidazolium chloride ([Bmim]Cl)	90	<5	MCC Avicel	(Zavrel et al., 2009)
	100	10	Dissolving pulp	(Swatloski et al., 2002)
	110	10	MCC Avicel	(Zhao, H. et al., 2008)
	83	18	MCC Avicel	(Heinze et al., 2005)
	83	13	Suprice sulfite pulp	(Heinze et al., 2005)
	83	10	Cotton linters	(Heinze et al., 2005)
	100	20	MCC (DP:250)	(Fukaya et al., 2006)
	100	20	MCC Avicel	(Vitz et al., 2009)

Table 2.6, continued

	85	13.6	-	(Kosan et al., 2007)
1-butyl-3-methylimidazolium formate ([C4mim][HCOO])	110	8	MCC Avicel	(Zhao, H. et al., 2008)

In another study, attempts were made on cellulose hydrolysis using ILs, since cellulose has good solubility in chloride and acetate anion ILs (Guo, H. et al., 2012). Some study also showed the ability of the hydrophilic ILs named as 1-allyl-3methylimidazolium chloride ([Amim]Cl) and 1-butyl-3-methylimidazolium chloride ([Bmim]Cl) in the dissolution of the cellulose (Zhu et al., 2006). The effectiveness of ([Amim]Cl) is supported by other study using wood chips as the starting material in which, the 1-ethyl-3methylimidazolium chloride ([Emim]Cl) is proven as a good dissolving capability for cellulose. The leading interaction was reported to be between the hydroxyl group of the cellulose and the chloride anion. Chromatographic analysis depicted that chloride anion exhibits strong hydrogen-bonding basic property, while a combination of [Bmim] with a succession of anions was reported to display weak hydrogen-bonding basicity. The anions of Br, [PF6], [SCN], and [BF4] were found to be unfit to be used to dissolve the cellulose (Ohno et al., 2009). This was supported by Swatloski et al. (2002) that showed the solubility of cellulose in 1-N-butyl-3-methylimidazolium sulfocyanate ([Bmim]SCN) and 1-N-butyl-3-methylimidazolium bromide ([Bmim]Br) was reduced to half as compared to [Bmim]Cl (Cao et al., 2009). More detailed study on the impressions of the anionic structure for ILs having various anions but the similar cationic structure ([C2mim]$^+$) was also reported. The relation between cellulose and anions were found to be decreased as follows; Cl$^-$ > [Ac]$^-$ > [(CH3O)-PO2]$^-$ > [SCN]$^-$ > [PF6]$^-$ (Gupta et al., 2015). Figure 2.6 shows 1-alkyl-3-methylimidazolium cations with its chemical

structures. The solubility of cellulose increased with the reduction of the alkyl group length ($[C_8mim]^+$ to $[C_4mim]^+$), which is being replaced at the imidazolium ring for the interaction between alkylimidazolium chlorides with cations (Cao, 2009).

R=CH$_3$	:	[C$_1$mim]
R=CH$_3$CH$_2$	:	[C$_2$mim]$^+$
R=CH$_3$CH$_2$CH$_2$	:	[C$_3$mim]$^+$
R=(CH$_3$)$_2$CH$_2$	:	[C$_3$mim]$^+$
R=CH$_3$CH$_2$CH$_2$CH$_2$	:	[C$_4$mim]$^+$
R=CH$_3$CH$_2$CH$_2$CH$_2$ CH$_2$CH$_2$	:	[C$_6$mim]$^+$
R=CH$_3$CH$_2$CH$_2$CH$_2$CH$_2$CH$_2$ CH$_2$CH$_2$	:	[C$_8$mim]$^+$
R=CH$_2$= CHCH$_2$	:	[Amim]$^+$

Figure 2.6: Formula of 1-alkyl-3-methylimidazolium cations (Cao et al., 2009)

Other reports are also in agreement with the findings that the longer the chain that replaced the imidazolium cations joined with chloride salts (1-hexyl-3-methylimidazolium cation ($[C_6mim]Cl$)), the lower the efficiency of the cellulose dissolution. For example, ($[C_6mim]Cl$) dissolves 5wt % of cellulose at 100 °C, whereas it is up to 10wt % in ($[C_4mim]Cl$) (Ohno et al., 2009).

2.5.2 Catalytic and Dissolution Properties

Cellulose breakup mechanism starts with the formation of the electron donor-electron acceptor (EDA) complexes via the interaction of oxygen and hydrogen atoms of cellulose-OH. The EDA complex will then interact with the ILs, where the cellulose atoms function as the electron pair donor while the role of the hydrogen atoms is to act as an electron acceptor. Comparatively, the cations in ILs solvents

serve as the electron acceptor centre while anion acts as the electron-donor centre. The location of these two centres should be adequately near to each other to allow the interaction to occur as well as to permit the formation of the EDA complexes. The oxygen and hydrogen atoms from hydroxyl groups are separated upon interaction of the cellulose-OH and the ILs, causing the opening of the hydrogen bonds between the molecular chains of the cellulose and eventually dissolves the cellulose (Feng, Li. et al., 2008). A review by Feng and Chen (2008) stated that the cation with its electron rich aromatic л system only inadequately interacts with the hydroxyl oxygen atom through the nonbonding actions of the л electrons, whereas anions were hydrogen-bonded to the hydroxyl proton of the cellulose. Remsing et al. (2006) carried out a relaxation study, which showed that the hydrogen bonds present in between the ILs anion and the hydrogen molecule are at a stoichiometric ratio of 1:1. The disruption of the intramolecular and intermolecular hydrogen bonds found in cellulose is caused by the separation of the oxygen and hydrogen atoms, thus leading to the dissolution of the cellulose. Figure 2.7 demonstrates the dissociation mechanism of the cellulose in ILs [Bmim]Cl as suggested by Feng and Chen (Feng, Li et al., 2008; Tan, H. T. et al., 2012).
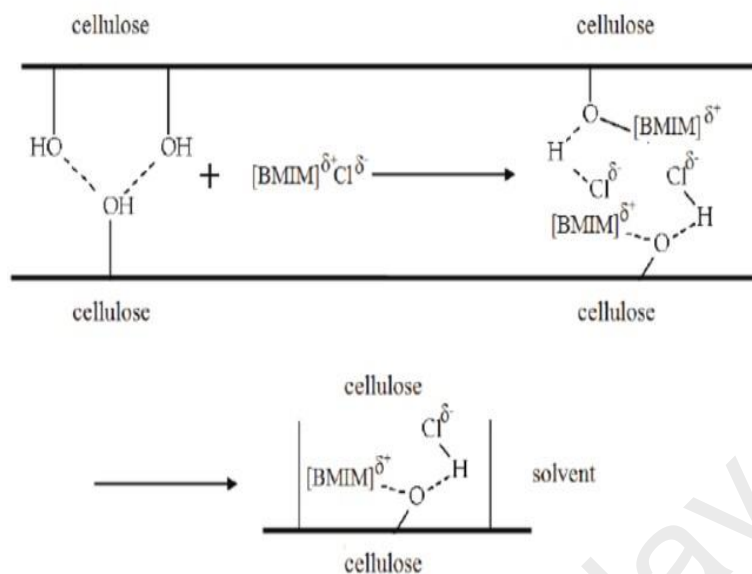
Figure 2.7: Dissolution mechanism of cellulose in [Bmim]Cl (Feng et al., 2008b)

The cleavage mechanism of the cellulose fibres with I_α and I_β structures was explored using all-atom molecular dynamics (MD) simulation study. By using three different ILs [C_1mim][DMP], [C_2mim]Ac, and [C_4mim]Cl, the breakup of the cellulose bundles was observed. As cellulose bundles were mixed with the ILs, the anions were strongly bonded to the -OH groups of the cellulose. The negatively charged complex was then formed weakening the intra H-bonds and decreases the strand stringency. The association of the cations with the complex will push to incapacitate the individual chains apart, thus initiating the breakup. [C_2mim]Ac was the only ILs detected to possess the ability to strip individual strands from the core bundle. Besides the intra H-bond breakage which plays an important role in stripping off the individual chains as compared to the inter H-bonds breakage, cations were also postulated to play a significant role in the preliminary breakup of the cellulose bundle during dissolution (Gupta et al., 2015). Nuclear Magnetic Resonance (NMR) spectroscopy was being employed to study the solubilizing mechanism of the cellulose in ILs. The study of the relaxation times as a function of rising the

31

cellobiose concentration disclosed that although the reaction between [Bmim] cation

and the sugar unit is insignificant, the reaction with chloride anion was found to be

very strong. This discrepancy is due to the hydrogen bonding of chloride anion to the

OH groups of the sugar unit. Despite the strong interaction between glucose and the

anion, the glucose penta-acetate structure had almost no influence on the relaxation

rate of the ^{35}Cl. Earlier studies reported that the interaction between D-glucose

(model compound) and [Bmim]Cl are due to the molecular dynamic simulation.

Meanwhile, the cations were also reported to interact weakly with the sugar (Ohno et

al., 2009). Albeit some experiments suggest that the governing reactions in cellulose

dissolution are related to the anions, other studies revealed that cations are the major

role player. Thirteen types of ILs with various cations but identical anion [Ac]⁻ have

been recorded to date concluding that cation does influence cellulose dissolution

(Gupta et al., 2015).

2.5.3 Application of Ionic Liquids in NCC Production

Despite earlier attempts by the researchers to dissolve cellulose, the significance

of ILs was not appreciated only until recently (Gupta et al., 2015). For instance,

cellulose dissolution in N-ethylpyridinium chloride in the existence of N-containing

bases was carried out back in 1934. Table 2.7 shows the different types of ILs used

in producing the NCC.

Table 2.7: Different types of ILs used in producing NCC and the results

Type of ILs	Temp (°C)	Time (h)	CrI (%)	Diameter (nm)	Length (nm)	Reference
[Emim][CH₃COO]	50	-	57	-	-	(Lee et al., 2009)
	70	-	52	-	-	
	90	-	47	-	-	

Table 2.7, continued   32

	110	-	38	-	-	
	130	-	30	-	-	
	-	0.5	56	-	-	
	-	1.5	47	-	-	
	-	5.0	43	-	-	
	-	8.0	40	-	-	
	-	14	42	-	-	
	-	19	46	-	-	
	-	32	41	-	-	
	-	42	43	-	-	
	-	70	38	-	-	
[EMIM] AC	60	-	42.8	-	-	(Xin et al., 2016)
	75	-	38.7	-	-	
	50	10	34.9	-	-	(Bian, 2014)
[Bmim][HSO$_4$]	70	1	82.4	14-22	50-300	(Man, Z. et al., 2011)
	80		88.1			
	90		91.2			
	120	24	-	-	-	(Mao et al., 2015)
	100	12	82±1	5±2	146±36	
[Bmim][Cl]	70	1.5	84	15-20	75-80	(Tan, X. Y. et al., 2015)
	80		82			
	90		96			
	100		96			
[Bmim][Cl]/H$_2$SO$_4$	80	2	93	20±5	260±82	(Lazko et al., 2014)
		5	93		208±79	
		16			213±85	

[Bmim]Cl is one type of protic ILs, which is developed through direct proton swap from a Brønsted acid to a Brønsted base. Since the formation of [Bmim]Cl does not involve any remaining by-products formation, it offers the benefits of being cost effective and the ease of method preparation. Solubilisation of cellulose by ([Bmim]Cl) is best under conventional heating. This was supported by the formation

of clear solutions with 3 and 10wt % of cellulose (DP≈1000) acquired from simple mixing at 70 and 100 °C, respectively (Ohno et al., 2009). Liquid crystalline solutions of cellulose are formed when high concentrations of cellulose (>10 wt %) are dissolved in ([Bmim]Cl). These crystalline solutions are visually anisotropic between the crossed polarizing filters and displays birefringence (Zhu et al., 2006). Compared to the microwave heating, it can be noted that the rate of degradation under conventional heating is lower than under the microwave irradiation, thus giving an exceptionally big advantage to the conventional heating method (Olivier-Bourbigou et al., 2010). In another experiment, up to 10wt % of cotton linter was dissolved, with slightly degraded DP from 1198 to 812, probably due to the mechanical shearing during stirring (Cao et al., 2009). Extreme degradation of cellulose was observed when the cellulose was dissolved in [Bmim]Cl at a high temperature (100 °C) as depicted by the molar mass distribution of the cellulose. However, degradation of the cellulose in [Bmim]Cl was absent at ~80 °C suggesting that the [Bmim]Cl is a non-derivatizing solvent (Zhao, Hua. et al., 2009). Therefore, based on previous studies, [Bmim]Cl was the best cellulose solvent at that time for two main reasons: (1) low or almost no degradation of cellulose with DP (290-1200) after the dissolution; (2) able to dissolve cellulose up to very high concentrations (25wt %) (Cao et al., 2009). As presented in Table 2.8, good dissolution of the cellulose was obtained by using [Bmim]Cl. Halide based ILs, especially chloride anion was known for its ability to dissolve cellulose. As a study pointed out that higher anion concentration leads to better cellulose solubilisation, therefore, chloride anion is clearly beneficial due to its minute size and strong electronegativity. Anion-exchange reactions with imidazolium halide salts as starting materials produce

expensive ionic liquids as compared to the chloride-based ILs (Olivier-Bourbigou et al., 2010).

Table 2.8: Solubility and DP of cellulose samples in ILs ([Bmim]Cl)

Substrate	DP	Solubility (wt%)	Temp. (°C)	Reference
Cellulose	286	18	83	(Heinze et al., 2005)
	593	13	83	(Heinze et al., 2005)
	~1000	3	70	(Swatloski et al., 2002)
	~1000	10	100	
	~1000	25	110	
	1198	10	83	(Heinze et al., 2005)
	6500	6	80	(Schlufter et al., 2006)
	250	4.5	110	

In 2006, Remsing and co-workers (Remsing et al., 2006) investigated the solvation of cellulose in an imidazolium-based ILs bearing a chloride counter-anion. Due to their high nucleophilic capacity, chloride ions are able to interact with the hydroxyl protons of the carbohydrates to break down the hydrogen-bonding network to promote dissolution (Hernoux-Villière et al., 2014). The first attempt to combine pretreatment by the ILs 1-butyl-3-methylimidazolium chloride ([Bmim]Cl) with high pressure homogenization (HPH) was carried out by Li et al. (2012) from sugarcane bagasse for the isolation of the nanofibrillated cellulose (NFC). The ILs dissolved cellulose can easily pass through the homogenizer without clogging. Next, the

cellulose was precipitated by the addition of water and redeveloped by subjecting to freeze drying process (Cao et al., 2009).

Figure 2.8 shows the FTIR spectra of the [Bmim]Cl. The peaks with the 2973 cm^{-1} and 2870 cm^{-1} wave numbers are the results of the aliphatic asymmetric and symmetric (C-H) stretching vibrations due to the presence of the methyl groups. A broad peak in the 3330-3450 cm^{-1} range is due to the formation of the quaternary amine salt with chlorine. Peak at 840 cm^{-1} wave number is due to the C-N stretching vibration, while the characteristic band of chloride can be observed between 1630-1635 cm^{-1} wave number (Dharaskar et al., 2013) (Yassin et al., 2015).
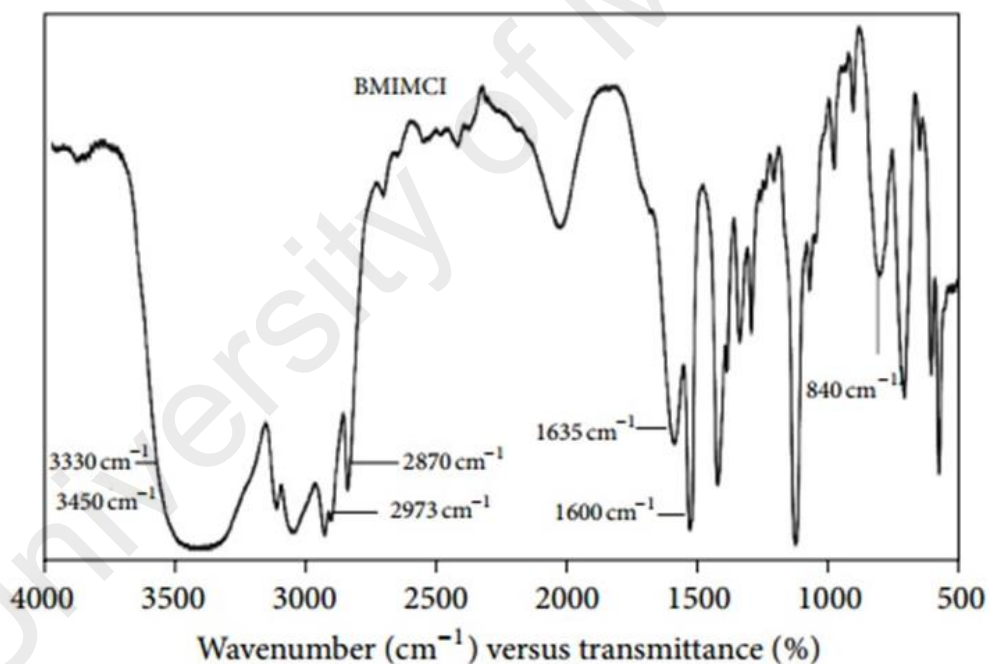
Figure 2.8: FTIR spectra of BmimCl (Dharaskar et al., 2013)

2.6 Ultrasonication Treatment

The disadvantages of using NCC in any applications are that the crystallites have to be isolated from the crystalline bundles, amorphous cellulose, hemicellulose, and

lignin. Besides that, controlling the dispersion level during incorporations of the NCC in a matrix is also a challenge (Bondeson et al., 2006). In nature, NCC is always in polar and hydrophilic form. This specific characteristic of NCC points to the different kinds of agglomeration. The first accumulation of the NCC takes place during incorporation of the NCC with a polar and hydrophobic matrix. Next, the irreversible accumulation of the NCC happened during the drying process (Abdul Khalil et al., 2014). During the agglomeration or aggregation, a uniform and dispersed structure of the NCC will be difficult to obtain. The microscopic images show that NCC has a strong tendency in forming larger and agglomerated structure. However, when subjected to mechanical dispersion or ultrasonication, it permits the dispersion of the NCC aggregates, resulting in the production of stable colloidal suspensions (Haafiz, M. K. Mohamad. et al., 2014).

2.6.1 Basic Principle of Ultrasonication Process

Ultrasonication has been extensively utilized for catalysing the chemical reactions containing carbohydrate compounds such as the hydrolysis and depolymerisation of starch, dextran, and other di- and polysaccharides, which also includes cellulose derivatives (Mishra, S.P. et al., 2011). Besides it is known for the dispersion and disaggregation process, ultrasonication is also widely used in catalysis, homogenization, scission, and emulsification. Briefly, ultrasonication is a part of the sound spectrum within the range of 20kHz -10MHz generated by a transducer that converts mechanical or electrical energy into a high frequency acoustical energy (Wang et al., 2009). Ultrasonication induces cavitation and acoustic streaming in materials once a high power (~10W/cm^2) wave spread throughout a liquid medium such as water. Cavitation, which is the development, growth, and implosive collapse

of the microbubbles produced during the ultrasonication causes the rigid cellulose structure to breakdown. However, increased solvent vapour pressure during the ultrasonication can slow down the cavitation collapse. Since ILs is known for its negligible vapour pressure characteristic, this makes ILs an ideal solvent for ultrasonication (Montalbo-Lomboy, 2015). The efficiency of ultrasonication in cellulose dissolution can be justified by the energy provided during the ultrasonication, which is approximately 10-100 kJ/mol. This range is within the hydrogen bond energy scale, thus showing that ultrasonication impact can gradually disintegrate the MCC into NCC.

2.6.2 Application of Ultrasonication Treatment in NCC Production

In 2009, Mikkola et al (2009) showed 2 minutes complete dissolution of cellulose in ILs as compared to the heat treatment which took a couple of hours to complete (Montalbo-Lomboy et al., 2015). In another study, acid hydrolysis process of NCC from MCC, recycled pulp, and Avicel, assisted by high intensity ultrasonication (1050 W) have been examined (Tang et al., 2013). Meanwhile, Yang et al. (2010) have improved the enzymatic hydrolysis of the cellulose in ILs by using ultrasonication pretreatment methods (Montalbo-Lomboy et al., 2015). Chen et al. (2011) studied the isolation of NCC from poplar wood using high-intensity ultrasonication (400-1200W) joined with chemical treatment, and in 2013, they described the disintegration of the NCC through the chemical pretreatment and high-intensity ultrasonication (1200 W). The group also studied the dynamic rheological behaviour of the nanocrystalline cellulose suspensions (Tang et al., 2014). Despite the growing interest in ultrasonication technique to dissolve cellulose, a study by Ninomiya et al., in 2012 showed that cellulose materials treated using conventional

heating exhibited higher crystallinity as compared to the ultrasonically treated kenaf powder (Montalbo-Lomboy et al., 2015). In addition, NCC obtained by ultrasonication technique aggregated in a wide distribution width due to the complicated multi-layered structure of the cellulose and interfibrillar hydrogen bonds. Despite the disadvantages, previous study has shown no chemical changes were observed on the cellulose chains due to the ultrasonication treatment (Mishra, S.P. et al., 2011). In 2013, Chen et al., studied the disintegration of the NCC through chemical pretreatment and high-intensity ultrasonication (1200 W) and the dynamic rheological behaviour of the nanocrystalline cellulose suspensions (Tang et al., 2014). Overall, ultrasonication has been applied to assist in the pretreatment of lignocellulosic biomass with different reaction solutions. For example, previous research has investigated the potential of ultrasonication to treat rice hull as the fermentation substrate for the production of oligosaccharides. In addition, ultrasonication pretreatment of sugarcane bagasse, buckwheat hulls, wheat straw, kenaf powder, and rice hulls also has been reported (Yang, C-Y. et al., 2014). Table 2.9 summarizes different studies on ultrasonication technique in producing NCC.

Table 2.9: Different studies on ultrasonication technique in producing NCC

Initial source	Time (min)	Vibration amplitude (%)	Output power (W)	d, (nm)	L, (nm)	Yield (%)	CrI (%)	References
Oil palm trunk	5	-		3.58	82.8	-	74.8	(Lamaming et al., 2017)
Corncob	10	-		4.0± 1.1	195.9± 45.9	46	78	(Silvério, 2013)

Table 2.9, continued

Table 2.9, continued

Spruce bark	10	27		2.8 ±0.8	175.3± 61.8	-	84	(Normand et al., 2014)
Switchgrass	15					80		(Montalbo-Lomboy et al., 2015)
	120					50		
	4	160				53		
	3	90				90		
Mengkuang leaves	30			5-25	200	28	-	(Sheltami, 2012)
Wood, bamboo, wheat straw, flax fibers			40	62% d<20 , 38% d>20			69.70	(Chen et al., 2011b)
			800	77% d,20, 23% d>20			68.6	
			1000	13.0			68.7	
			1200	12.8			69.7	

CHAPTER 3 :MATERIALS AND METHODOLOGY

3.1 Introduction

In this chapter, the experimental setup used to produce nanocrystalline cellulose (NCC) and optimization of operating conditions are briefly presented. Next, the characterization techniques of each set up are explained in details. The results must be reproducible and they are dependent on the experimental procedures and materials employed during the course of the study. Synthesis of the NCC using ionic liquids assisted by ultrasonication and optimization of the operating conditions (dissolution time, temperature and MCC/ionic liquids ratio) were reported. Each of these experimental steps has their own standard procedure and characterization method to accumulate data and subsequently to investigate their properties. Various kinds of parameters including ultrasonication time and vibration amplitude, reaction temperature, dissolution time, and MCC/ ionic liquids ratio were utilized in order to achieve the optimum results. All the results recorded in this project are reproducible within the given experimental limitation. The maximum care is taken in conducting the experiments and collecting data and whenever necessary, some experiments were repeated. The following materials and methods are adopted in the present investigation.

3.2 Materials

Chemicals used in this project are listed in Table 3.1. These chemicals were purchased from Merck Millipore and Friendemann Schmidt. In this work, deionized water (DI) (182 MΩ-cm) at 25 °C was used to prepare all solutions.

Table 3.1 Chemical list

Chemicals	Molecular Formula	Supplier	Purity
Microcrystalline cellulose (MCC)	$(C_6H_{10}O_5)n$	Friendemann Schmidt	99.0%
1-butyl-3-methylimidazolium chloride ([Bmim] Cl)	$C_8H_{15}ClN_2$	Merck Millipore	99.0%

3.2.1 Microcrystalline Cellulose (MCC)

MCC (Friendemann Schmidt) with an average particle diameter of 2-20μm was purchased. The MCC was confirmed to be cellulose I by X-ray diffraction patterns and the crystallinity index was 60% calculated by Segal method (Segal et al., 1959).

3.2.2 1-Butyl-3-Methylimidazolium Chloride

1-butyl-3-methylimidazolium chloride ([Bmim] Cl) of analytical grade (purity = 99%, melting point = 60 °C) was purchased from Merck and used without further purification.

3.3 Synthesis of NCC with ILs

[Bmim]Cl is heated at 60 °C since it is in solid form. As the [Bmim]Cl is melted, temperature is controlled until it reached ~40 °C before mixing the MCC with [Bmim] Cl at 1:10 ratio in a round bottom flask. Beforehand, MCC is added with 10 mL of deionized water. The mixture was heated at 40 °C for 30 minutes and 400 rpm mechanical stirring. After 30 minutes, the reaction was quenched by the addition of 10 mL deionized water.

3.4 Synthesis of NCC with ILs Assisted Ultrasonication

The suspension (NCC and ionic liquids) was sonicated at different vibration amplitude (60, 70, 80, 90%) and time (5,10,15 and 20 minutes). The suspensions

were then washed repeatedly with DI water by using centrifuge (15 minutes, 2000 rpm). The supernatant was discarded and replaced with new deionized water and centrifuged further at 7000 rpm for 30 minutes to isolate the NCC particles. The centrifugation process was stopped once the supernatant became turbid. The NCC samples were then subjected to freeze-drying for two days before further characterization were performed.

3.5 Characterization of NCC

Characterization of NCC can be divided into three parts: 1) physical characterization 2) chemical properties and 3) surface analysis.

3.5.1 Physical Characterization

3.5.1.1 Total Yield

NCC's yield was gravimetrically determined in following step. After separation of the NCC using a centrifuge at 7000 rpm for 30 minutes, the NCC was dried and weighed. The NCC yield was decided as a percentage of dry weight of the "starting" material. Total yield (Y) of NCC was calculated as follows (Equation 1):

$$Y, \% = 100\,(\,W / W_0\,),$$
(Equation 1)

where W_0 is the initial dry weight of the sample and W is the weight of dried sediment

3.5.1.2 Fourier Transform Infrared Spectroscopy (FTIR)

Fourier Transform Infrared Spectroscopy (FTIR) spectroscopy was employed to study the changes in the chemical conformation of NCC after treatment. Infrared spectra were measured with diffuse reflectance (Bruker – IFS 66) between 4000-400

cm^{-1}, with a resolution of 4 cm^{-1} and 16 times of scans. Samples were dried, ground and pelletized using KBr.

3.5.1.3 X-ray Diffraction (XRD) Analysis

X-Ray diffraction measurements were carried out to examine the crystallinity index (CrI), which is changes in the crystalline structure of the samples using D8 Advance, Bruker AXS model system equipped with Cu Kα radiation (λ = 0.154 nm) at 40 kV and 40 mA in range of 5° - 40° at 0.01° interval with fixed time method. The CrI was calculated using Segal's method (Segal et al., 1959) as follows:

$$\text{CrI (\%)} = \frac{I_{200} - I_{AM}}{I_{200}} \times 100\% \qquad \text{(Equation 2)}$$

where I_{200} is the height of the 200 peak, which represents both crystalline and amorphous material; I_{AM} is the lowest height between the 200 and 110 peaks, which represents amorphous material only.

3.5.2 Chemical Properties

3.5.2.1 Thermogravimetric (TGA) Analysis

Thermogravimetric analysis (TGA) could stipulate detailed information on the change of mass of a sample as a function of temperature, whereby in the presence of inert gases, the loss of mass was credited to the loss of volatile matter and decomposition as a function of temperature. Information of separate constituents within the lignocellulosic biomass based on their temperature response and rate of volatilization/decomposition was obtainable from the TGA. The thermal stability of the NCC was characterized using thermogravimetric analysis (TGA) (Mettler Toledo, TGA/SDTA 851) model. Approximately 5 mg of each sample was heated

from room temperature to 700 °C at a heating rate of 10°C /min under nitrogen atmosphere.

3.5.2.2 Differential Scanning Calorimetry (DSC) Analysis

Differential Scanning Calorimetry (DSC) was used to measure heat conveyed or heat needed by a material to undergo various conversions at different temperatures. DSC is usually combined with TGA to analyse the thermal changes of different materials as a function of temperature. DSC measurements were carried out on a Differential Scanning Calorimetry (DSC) analysis, Mettler Toledo (HPDSC 822$_e$). Dynamic DSC scans were conducted in a temperature range from 25 °C to 700 °C, at a constant heating rate of 10 °C/min. The experiments were carried out under nitrogen atmosphere, at a flow rate of 60 ml/min.

3.5.3 Surface Analysis

3.5.3.1 Field Emission Scanning Electron Microscopy (FESEM)

The freeze-dried samples were mounted onto aluminum specimen stubs by using double sided adhesive carbon tape. Specimens were sputter-coated with 5 nm gold-palladium. Images were viewed and photographed using field emission scanning electron microscopy (FESEM; FEI Quanta 200F, USA) at 2 kV.

3.5.3.2 Atomic Force Microscopy (AFM)

In order to determine NCC's length, diameter and aspect ratio (length-to-diameter) and to indicate the accumulation state of the NCC, highly diluted samples of the hydrolysed suspension were analysed by AFM. Samples were prepared by dispersing NCC in distilled water in an ultrasonic bath at room temperature for 1 hour, in order to loosen up the cellulose particles. A droplet of the resulting solution

was cast onto cleaved mica and dried under ambient conditions. The samples were then analysed with a scanning probe microscope by using Nanoscope Analysis 1.5 software. At least 50 measurements for each condition were used to determine average and standard deviation values.

3.5.3.3 Dynamic Light Scattering (DLS)

The size of particle was measured by laser diffractometry using a Nano Size Particle Analyzer (ZEN 1600 MALVERN USA) under the following conditions: particle refractive index 1.59, particle absorption coefficient 0.01, water refractive index 1.33, viscosity 0.8872 cP, temperature 25 °C and general calculation model for irregular particles. The NCC was diluted in water with ultrasound for 30 minutes. All measurements were conducted at room temperature. The data reported are means of three replicates.

3.6 Optimization of NCC

Hydrolysis was carried out using [Bmim]Cl solvent at three different parameters: 1) reaction temperature (40, 60, 80, 100 °C) 2) dissolution time (30, 60, 90, 120 minutes) 3) MCC/ionic liquids' ratio (1:4, 1:6, 1:8, 1:10) under 400 rpm mechanical stirring. The reaction was quenched by adding 10 mL DI water. The resulting suspensions was sonicated for 5 minutes at 70% vibration amplitude. The hydrolysed sample was washed by repeated centrifugation (2000 rpm, 15 minutes) to remove excess of ILs. Then, the sediment was mixed with DI water before further centrifuge at 7000 rpm for 30 minutes until the sediment become turbid, to isolate the NCC particle. The sediment was freeze-dried for several days. Optimum operating conditions were determined based on the value of aspect ratio. Meanwhile, the

absence of ionic liquids from the final product of NCC was confirmed by using FTIR spectra.

CHAPTER 4: RESULT AND DISCUSSIONS

4.1 Introduction

After hydrolysis, a clear, dark amber solution was acquired and the precipitate was washed several times with deionized water by centrifugation at 2000 rpm for 30 minutes to ensure the residue was eliminated. Repeated washing and FTIR study were employed to ensure that the residue was fully eliminated. Since the recovered NCC is expected to be in the nano region size (<100 nm), therefore, it is not practical to recover the final product using filtration method. Thus, the centrifugation technique was applied to further separate the individual nanocellulose fibre in this study. The appearance of white precipitate that was acquired in this step is an indication that the cellulose is the main component. No further analysis was done on the liquid after the washing steps. This study has shown that ILs is an efficient cellulose solvent due to its ability to dissolve cellulose up to 10wt % and at the same time it is an environment friendly process with minimum waste. Although many studies have successfully engaged heat treatment and ultrasonication for the formation of the NCC, there are limited findings on the regeneration yield of the NCC. The physical, chemical and surface properties of the NCC was analysed and the aspect ratio of the NCC was calculated for the optimization process.

4.2 Isolation of NCC

4.2.1 Yield

Recently, NCC samples from various sources of cellulose have been prepared by using high-intensity ultrasonication combined with ILs hydrolysis (Yang, Chun-Yao et al., 2014). However, there are limited studies on the NCC yield by using

ultrasonication treatment. The effect of ultrasonication time on the NCC yield was preliminarily studied at 40 °C heating temperature, 1:10 MCC/ionic liquids ratio and 30 minutes dissolution time. Later, the cellulose suspension undergoes mechanical disintegration by ultrasonication at 70% vibration amplitude and different ultrasonication time at 5, 10, 15 and 20 minutes. The total yield produced from each of the ultrasonication treatment is presented in Table 4.1.

Table 4.1: Yield of NCC at increasing ultrasonication time (U5=5 minutes, U6=10 minutes, U7=15 minutes and U8=20 minutes)[1]

Sample	Yield (%)
U5	83
U6	84
U7	86
U8	87

The NCC yield derived from ILs hydrolysis at 5 minutes of ultrasonication treatment was 83%. Interestingly, increasing the ultrasonication treatment to 10, 15, and 20 minutes resulted in 84, 86, and 87% of the NCC yield (Table 4.1), respectively, which showed a percentage increase of 1, 2 and 1%. The similar trend was observed by Frone et al., 2011. In the study, the yield of the cellulose fibres increased from 7.8, 14.3, 17, 7, and 27.6%, respectively. In another study, further ultrasonication treatment at 20 and 30 minutes resulted in 35% and 40.4% of the NCC yield, which showed a percentage increase of 22.4% (Tang et al., 2014). The

---

[1] Reaction condition: U5=5 minutes, U6=10 minutes, U7=15 minutes, U8=20 miutes ultrasonication time. Meanwhile, U4=60%, U8=70%, U12=80% and U16=100%) vibration amplitude.

above results indicated that the ultrasonication treatment had a noticeable influence on the NCC yield. This phenomenon is brought together by the effect of acoustic cavitation. The release of heat and excited species via the cavitation effect loosen the MCC surface and leads to glycosidic bond rupture, particularly in the lattice defects of the MCC (Tang et al., 2014). Thus, the use of ultrasonication treatment can assist the interaction between single fibre and micro bubbles produced by the ultrasonicator, which then further split the micro-sized cellulose into nano size.

The effect of the vibration amplitude on the NCC yield was preliminary studied at 40 °C, 1:10 MCC/ionic liquids ratio and 30 minutes dissolution time. The cellulose suspension was then undergone mechanical disintegration by ultrasonication at 20 minutes and different vibration amplitude at 60, 70, 80, and 90%. The results are presented in Table 4.2. The NCC yield increased from 82, 87, 88 to 89% at higher vibration amplitude. The results are coherent with a previous study by Frone et al., 2011. In the study, the yield of the cellulose fibres increased from samples U4 to U16 at greater ultrasonication treatments indicating the effectiveness of increasing the vibration amplitude of the ultrasonication.

Table 4.2: Yield of NCC at increasing vibration amplitude (U4=60%, U8=70%, U12=80% and U16=90%)

Sample	Yield
U4	82
U8	87
U12	88
U16	90

Another study reported that the NCC yield increased at higher values of ultrasonication vibration (Liu, L. et al., 2013). At higher vibration amplitude, the solubility of the MCC in ILs improved since ultrasonication treatment can facilitate the penetration and diffusion of the ILs in the entire structure of the sample, thus increasing the regeneration rate of the NCC. The above results signified that the ultrasonication treatment has an apparent impact on the NCC yield.

4.3 Characterization of NCC

4.3.1 Fourier Transform Infrared Spectroscopy (FTIR)

The FTIR spectroscopy was used to determine the chemical assembly by recognizing the functional groups present in each sample. The main chemical bond vibrations of NCC are detected in the region of 4000-400 cm^{-1}. Figure 4.1 shows the FTIR spectra of the MCC and NCC. The broad absorption at 3345-3346 cm^{-1} and was attributed to the stretching of H-bonded OH groups and FTIR band at 2900-2903 cm^{-1} and 2400 cm^{-1} are related to the C-H stretching. As shown in Figure 4.1, the peak at 3345-3346 cm^{-1} became sharper as the ultrasonication time extended, indicating that the increasing intensity of hydrogen bonding. This provides significant morphological structural changes of the NNC. The band at 1640-1646 cm^{-1} was accredited to the bending mode of the absorbed water. According to the previous studies, this band is connected to the bending modes of the water molecules due to a strong interaction between cellulose and water (Abnisa et al., 2013). The band at 1433 cm^{-1} and 1237 cm^{-1} in the spectrum were assigned to the symmetric CH$_2$ bending and wagging. The C-H bending occurred at 1369 cm^{-1}. A small peak at 665-667 cm^{-1} corresponded to the out-of-plane bending of C-O-H. The FTIR spectra profiles were very similar before and after the treatment, whereas the intensity of the

peaks was different to some extent. The absorbency around 3400 cm^{-1} weakly shifted to the lower wave number, indicating the increase of the hydrogen bonds. Cellulose characteristic bands in the region of 1250-850 cm^{-1} such as 1164, 1114 and 1059 cm^{-1} could be mainly observed in a FTIR spectrum of cellulose. The band at 1163-1164 cm^{-1} arose from C-O-C stretching at the β-(1,4)-glycosidic linkages. Meanwhile, the in-plane stretching gave a shoulder at 1114-1115 cm^{-1}. The strong peak at 1058-1059 cm^{-1} was an indicative of C-O stretching at C-3 and C-C stretching. Figure 4.1 shows the FTIR spectra of the MCC and NCC synthesized at a different ultrasonication time.
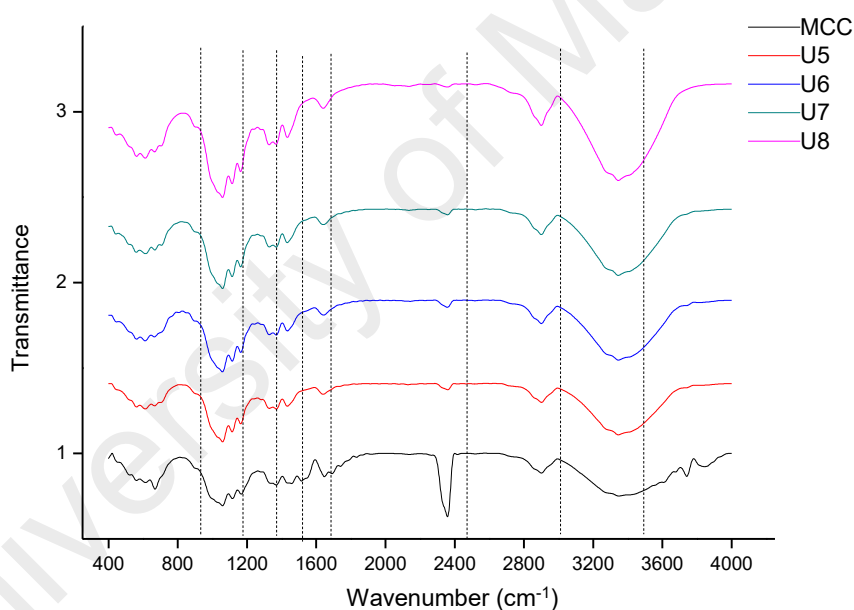

Figure 4.1: FTIR spectra of NCC at increasing ultrasonication time (U5=5 minutes, U6=10 minutes, U7=15 minutes and U8=20 minutes)[2]

---

[2] Reaction condition: U5=5 minutes, U6=10 minutes, U7=15 minutes, U8=20 miutes ultrasonication time. Meanwhile, U4=60%, U8=70%, U12=80% and U16=100%) vibration amplitude.

Figure 4.2 shows the FTIR spectra of the MCC and NCC synthesized at increasing vibration amplitude. As shown in Figure 4.2, the top band in the O-H stretching region for NCC shifted to lower wave numbers (from 3347 to 3345 cm^{-1}) indicating an average increase in hydrogen bond strength (Le Normand et al., 2014). During the hydrolysis, amorphous cellulose was removed from the surface, exposing more C-OH, C-O-C, and C-C bonds, resulting in the increase of the stretching absorbency (Jahan et al., 2011). C-H bending vibration appears in between 1350-1370 cm^{-1}, while the deformation, wagging and twisting modes of the anhydroglucopyranose vibration are shown in between 600 to 1800 cm^{-1}. More importantly, the intensity of most of the peaks was found to be significantly increases as vibration amplitude increases, such as the peaks at 3346, 2900, 1115 and 1058 cm^{-1}. The increase in absorbance peak at 3346 cm^{-1} was evidently due to the increasing hydroxyl groups of the NCC after hydrolysis, as supported by previous studies (Chang, 2010; Tang et al., 2013). Significantly, there was no difference between the spectrum of the MCC and NCC. The results indicated that there was no other derivational reaction occurred during the dissolution process.
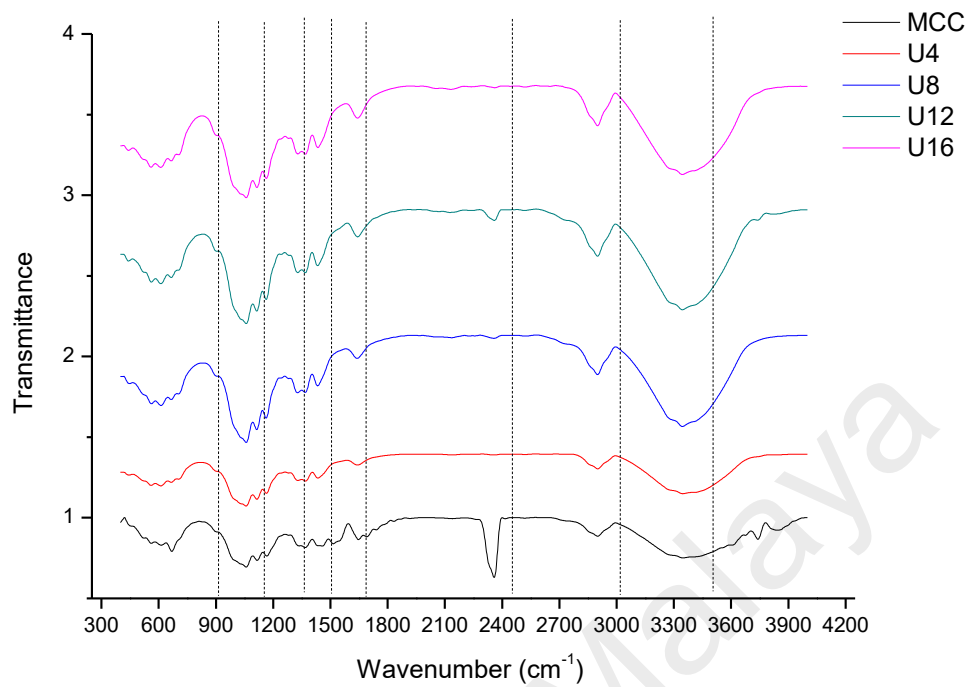
Figure 4.2: FTIR spectra of NCC at increasing vibration amplitude (U4=60%, U8=70%, U12=80% and U16=90%)

In addition, the signals presence at 1433-1434, 1163-1165 and 1114-1115 cm^{-1} indicated that the NCC are primarily in the form of Cellulose I, ratifying the result from XRD analysis, which supported the study from other group (Fortunati et al., 2013).

4.3.2 X-ray Diffractometry (XRD)

The crystallinity of the NCC is the main indicator in determining the thermal and mechanical properties. To analyse the crystalline properties of the NCC, X-ray diffractometry (XRD) studies were conducted. Figure 4.3 shows the diffraction patterns obtained for MCC, U5, U6, U7, and U8. They consist of the typical cellulose I with three well-defined crystalline peaks around 2Θ = 14.0, 16.0 and

22.0°. No changes in the crystal structure of the NCC happened during the chemical and ultrasonication treatment as justified by the peaks shown in Figure 4.3.
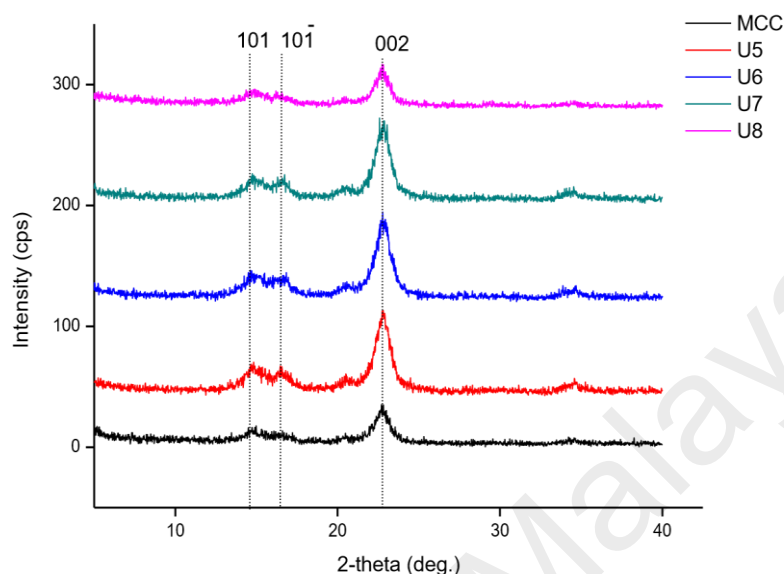
Figure 4.3: Diffractograms of NCC at increasing ultrasonication time (MCC, U5=5 minutes, U6=10 minutes, U7=15 minutes, U8=20 minutes)[3]

These results are strongly supported by the data from the previous study (Mohamad Haafiz et al., 2013). In the study, the cellulose I structure was maintained after chemical hydrolysis. In addition, the narrow and sharp peaks of the NCC can also be interpreted as the higher crystalline value of the respected NCC. The XRD of U5 exhibited the most intense 002 peak and most resolved 101 and 10ī, indicating highest crystallinity among all other samples. Meanwhile, U8 had the broadest and least defined XRD peaks, a clear sign of lower crystallinity. The crystallinity index (CrI) was determined for various samples and the results are summarized in Table 4.3.

---

[3] Reaction condition: U5=5 minutes, U6=10 minutes, U7=15 minutes, U8=20 miutes ultrasonication time. Meanwhile, U4=60%, U8=70%, U12=80% and U16=100%) vibration amplitude.

Table 4.3: Crystallinity index of NCC at increasing ultrasonication time (U5=5 minutes, U6=10 minutes, U7=15 minutes and U8=20 minutes). [4]

Sample	Crystallinity index (%)	Crystallite size (nm)
MCC	60 ± 0.2	12.5
U5	73 ± 0.1	9.9
U6	70 ± 1.3	5.8
U7	68 ± 0.2	5.4
U8	65 ± 0.1	4.5

A significant increase of CrI from 60% to 73% was observed as the MCC was hydrolysed at 5 minutes ultrasonication time. The increased crystallinity of U5 as compared to the MCC was attributed to the progressive elimination of the amorphous materials. A continuous decrease of the CrI value was detected upon the successive ultrasonication treatment at 10, 15 and 20 minutes due to the breakage of the crystal structure at longer ultrasonication time. These data were shown to be corresponding proportionally to the sharpness of the peaks in the diffractograms (Figure 4.3). Aside from the calculated data, the previous study also supports these results (Silvério, 2013). The crystallite size decreased from 9.9 nm to 5.8, 5.4, and 4.5 nm for U5, U6, U7, and U8, respectively. However, there was no significant relationship between crystallite size and crystallinity index of the NCC since crystallite size basically about the grain size of the NCC particle, meanwhile

---

[4] Reaction condition: U5=5 minutes, U6=10 minutes, U7=15 minutes, U8=20 miutes ultrasonication time. Meanwhile, U4=60%, U8=70%, U12=80% and U16=100%) vibration amplitude.

crystallinity index is about the intensity of the crystalline structure in NCC. At minimum ultrasonication time (5 minutes), the amorphous region was effectively removed by the ultrasonication treatment causing increased of the CrI. However, as the ultrasonication time increases, the ultrasonication treatment became non-selective, thus removing both the amorphous and crystalline regions decreases the CrI. Another reason was probably due to the breakage of the intermolecular hydrogen bonds of the NCC, causing the collapse of the crystal structure of the NCC. As the ultrasonication time increases, more crystal structure would collapse, thus reducing the CrI. Overall, longer ultrasonication time would result in weaker crystalline properties, as supported by previous study (Kim et al., 2013a).

The X-ray diffractograms of the cellulose samples MCC, U4, U8, U12, and U16 are shown in Figure 4.4. They consist of the typical cellulose I with three well defined crystalline peaks around 2Θ= 14.0, 16.0 and 22.0°.
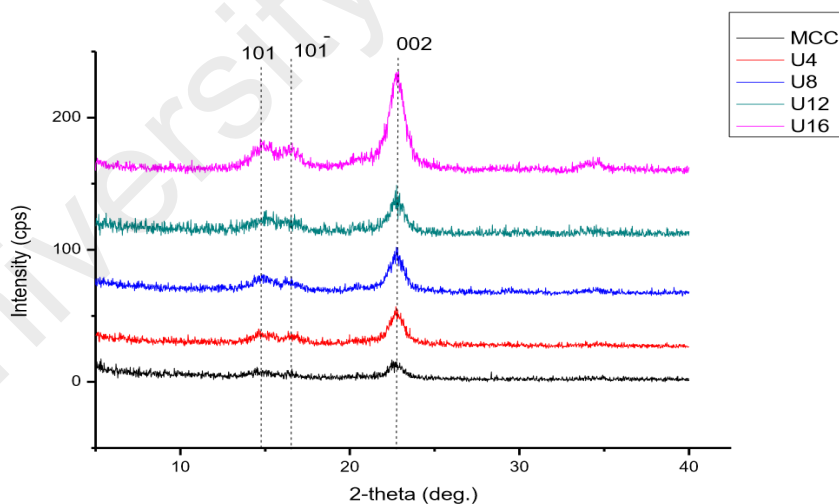

Figure 4.4: XRD diffractograms of NCC at increasing vibration amplitude (U4=60%, U8=70%, U12=80% and U16=90%) [5]

---

[5] Reaction condition: U5=5 minutes, U6=10 minutes, U7=15 minutes, U8=20 miutes ultrasonication time. Meanwhile, U4=60%, U8=70%, U12=80% and U16=100%) vibration amplitude.

As hypothesized, the ILs molecules will slowly diffuse into the cellulose, as the vibration amplitude is exerted. For untreated and treated cellulose, the (002) peak position and peak width remains essentially the same. The crystalline region is considered to be responsible for producing a sharp X-ray diffraction pattern at 22.8°. After the hydrolysis, the 22.8° plane peak (002) of the NCC becomes sharper, representing the higher perfection of the crystal lattice in the (002) plane than the original cellulose. In other words, the CrI of this NCC was higher than the initial materials (MCC). The peak for the (10ī) plane (2Θ=14.7°) also become more intense and separated from the 101 (2Θ=16.4) peak for the NCC. The CrI was determined for all the samples and the results are summarized in Table 4.4. The XRD results together with the FTIR data confirm that the NCC retained the Cellulose I crystalline structure following the hydrolysis and ultrasonication process while becoming more crystalline as the vibration amplitude increases. In the hydrolysis process, the crystalline region of the Cellulose I tend to increase so that the CrI of NCC becomes higher than the raw material (MCC).

Table 4.4: Crystallinity index of NCC at increasing vibration amplitude

(U4=60%, U8=70%, U12=80% and U16=90%)

Sample	Crystallinity index (%)	Crystallite size (nm)
MCC	60 ± 0. 2	12.5
U4	63 ± 0.1	5.0
U8	65 ± 0.1	4.5
U12	67 ± 0.1	10.9
U16	70 ± 0. 2	6.0

A significant increase of CrI from 60% to 63% was observed as the MCC was hydrolysed at 60% vibration amplitude. The increased CrI of U4 as compared to the MCC was attributed to the progressive elimination of the amorphous materials. A continuous increase of the CrI was observed upon the successive ultrasonication treatment at 70, 80, and 90%. These data were shown to be corresponding proportionally to the sharpness of the peaks in the diffractograms as shown in Figure 4.4. As the vibration amplitude increased from 60 to 70, 80, and 90%, respectively, a greater impact was shown by the implosive cavitation collapse which will gradually disintegrate the initial cellulose materials (MCC). With the enhanced disintegration process of the initial cellulose materials (MCC), the cleavage of the amorphous and crystalline regions could easily occur. The growth and rearrangement of the monocrystals may also occur in parallel and thus can improve the crystallinity of the cellulose. This occurrence could explain the tapering of the diffraction peaks. This result was also supported by the previous literature, which stated the same increasing crystallinity trend of the NCC produced by the ultrasonication treatment. In some cases, the application of the ultrasonic treatment alone or with other treatments lead to an increase in the cellulose crystallinity. Cheng et al. (2010) reported that in the case of untreated Lyocell fibres, the NCF crystallinity increases from 35% 43-44% (ultrasonicated fibres) (Frone et al., 2011). An increase in the CrI is related to the increases in the rigidity of the cellulose structure, which can lead to a higher tensile strength of the fibres (Mohamad Haafiz et al., 2013).

4.3.3 Differential Scanning Calorimetry (DSC)

Differential Scanning Calorimetry (DSC) technique was applied to compare the thermal properties of the NCC at different ultrasonication time (Figure 4.5 and Table 4.5).

Table 4.5: Thermal stability of NCC at increasing ultrasonication time (U5=5 minutes, U6=10 minutes, U7=15 minutes and U8=20 minutes).

Sample	Onset (°C)	Max (°C)	Enthalpy (kJ/mol)
U5	34	76	103
	328	350	267
U6	35	74	102
	325	350	270
U7	45	82	96
	325	350	250
U8	40	87	99
	322	348	257

Meanwhile, the DSC diagrams shown in Figure 4.5 exhibited two endothermic peaks within 25 °C to 700 °C. Most of the studies connecting the disintegration of the lignocellulosic materials were found in the specific literature. For example, Yang et al. (2007) showed that in the thermal analysis, cellulose disintegration started at 315 °C and was persevered until 400 °C (Morán et al., 2008). In this study, the initial endotherm occurred between 34 °C to 45 °C, which means that the loss of the moisture was due to the evaporation. Polymers with hydrophilic groups such as cellulose absorb water easily, therefore, some of the water will associate with the cellulose powder inevitably even in the dry state. A previous study has examined that the dehydration of the cellulose usually takes place in the temperature ranging from 10-90 °C (Zhang, J. et al., 2014).
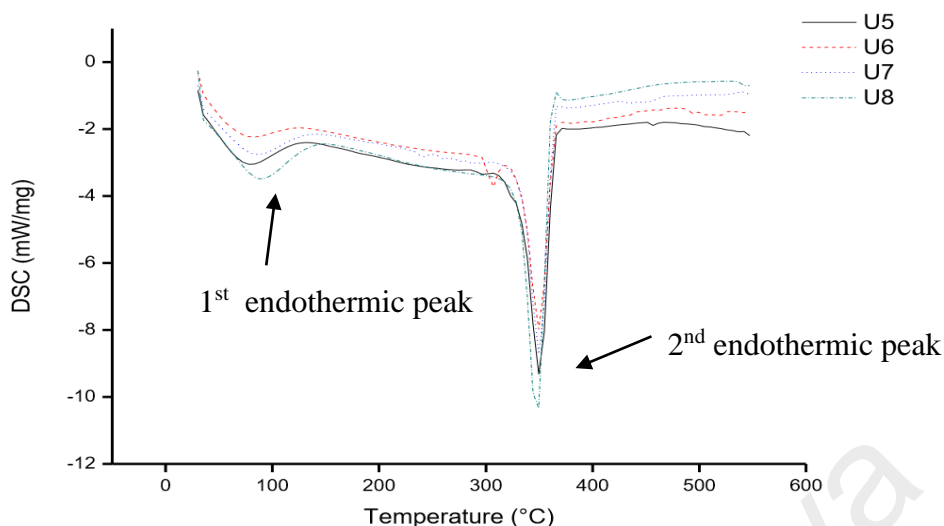
Figure 4.5: Thermograms of NCC at increasing ultrasonication time (U5=5 minutes, U6=10 minutes, U7=15 minutes and U8=20 minutes)

Generally, the second endothermic peaks of the NCC indicated the course of the fusion or melting, which provides an overview of the NCC decomposition magnitude, the extent of which decomposition temperature was gradually decreased with the increase of ultrasonication time from 5, 10, 15 and 20 minutes. In the thermal analysis for U5, U6, U7, and U8, NCC decomposition started at 328, 325, 325, and 322 °C. Ultrasonication treatment at 5 minutes probably caused the solution to lose a considerable proportion of the amorphous regions and in this process the rearrangement of the cellulose crystallites took place leading to a denser crystal structure. Besides causing higher CrI as shown in Table 4.3, this would also cause a higher onset of the decomposition temperature and narrow endotherm width, which is supported by the previous finding (Mandal et al., 2011). However, as the ultrasonication time extended, the de-structuring process of the NCC took place, thus decreasing the CrI of the NCC. This would facilitate the degradation of the NCC, therefore cause decreased value of the NCC decomposition temperature. The previous study also mentioned that a shift of the maximum temperature of the dehydration process to lower values may be observed with the decrease of the CrI

61

(Ibrahim et al., 2013). However, the enthalpy value obtained (267, 270, 250, 257 kJ/mol) for U5, U6, U7, and U8 shows no significant relationship with the decomposition temperature.

Table 4.6 shows the thermal stability of the NCC at different vibration amplitude and the initial endotherm occurs between 34-40 °C, which indicates moisture removal due to evaporation. As for the second endotherm, the decomposition temperature gradually increased from 308 to 322, 327 and 330 °C at higher vibration amplitude.

Table 4.6: Thermal stability of NCC at increasing vibration amplitude

(U4=60%, U8=70%, U12=80% and U16=90%)

Sample	Onset (°C)	Maximum (°C)	Enthalpy (kJ/mol)
U4	34	68	127
	308	330	235
U8	40	87	99
	322	348	257
U12	35	77	35
	327	349	254
U16	34	77	109
	330	350	333

The heating DSC curves were conveyed in terms of the heat flow (Figure 4.6). All DSC thermograms displayed two clear endothermic changes within the range of the studied temperature.
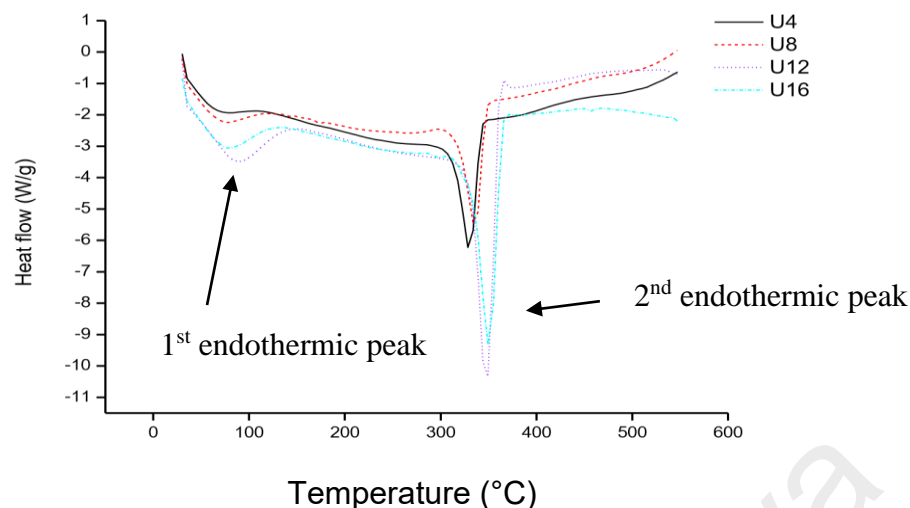
Figure 4.6: Thermograms of NCC at increasing vibration amplitude (U4=60%, U8=70%, U12=80% and U16=90%)[6]

A greater crystalline structure required a greater disintegration temperature since the rigidity of the crystalline structure permits the NCC to withstand radical heat and processing conditions. As the vibration amplitude increases, the rearrangement process of the cellulose crystallite takes place, thus increasing the CrI of the NCC, which would increase the value of the NCC decomposition temperature. The enthalpy values associated with the moisture desorption and cellulose decomposition is shown in Table 4.6. The increased CrI of the cellulose and the increased H-bonding between the closely packed cellulose chains during each treatment tend to stabilize the structure and increase the enthalpy values. Similar results were observed in the previous study (Mohamad Haafiz et al., 2013). The DSC results showed that due to the improved thermal properties, the developed NCC demonstrated less inclination to degradation, thus allowing it to be administered at higher temperatures as compared to their non-treated counterparts.

---

[6] Reaction condition: U5=5 minutes, U6=10 minutes, U7=15 minutes, U8=20 miutes ultrasonication time. Meanwhile, U4=60%, U8=70%, U12=80% and U16=100%) vibration amplitude.

4.3.4 Atomic Force Microscopy (AFM)

The size distribution of NCC was analysed by AFM and are shown in Table 4.8. Measurements were carried out on 50 NCC randomly selected from Figure 4.6. The sample with the smallest particle size of the NCC aggregates was derived from U5 which was obtained from the lowest ultrasonication time. The method used to chemically characterize the samples was accurately and precisely chosen and executed as shown by the low standard deviation achieved.

Table 4.7: Diameter (nm), Length (nm) and aspect ratio of NCC synthesized at increasing ultrasonication time (U5=5 minutes, U6=10 minutes, U7=15 minutes, U8=20 minutes)[7]

Sample	Diameter (nm)	Length (nm)	Aspect ratio
U5	9 ± 0.3	155 ± 0.8	17
U6	11 ± 0.6	136 ± 0.3	12
U7	15 ± 0.7	126 ± 0.5	8
U8	16 ± 0.4	143 ± 0.4	9

In this study, the diameter of the NCC was found to be between 9-16 nm. The diameter size of each sample increased proportionally with the ultrasonication time. Meanwhile, the length of the NCC was between 143-155 nm. Table 4.8 shows the comparative study of previous AFM data.

---

[7] Reaction condition: U5=5 minutes, U6=10 minutes, U7=15 minutes, U8=20 miutes ultrasonication time. Meanwhile, U4=60%, U8=70%, U12=80% and U16=100%) vibration amplitude.

Table 4.8: Summary of AFM data from previous studies

Cellulose feedstock	Diameter (nm)	Length (nm)	Aspect ratio	Reference
Sisal fibers	(30.9 nm ± 12.5 nm)	-	-	Moran et al. (2008)
Mengkuang leaves	5-25 nm	50 to 400 nm	9-17	Sheltami et al. (2012)
Sisal cellulose whiskers	3.6 ± 1 nm	211 ± 106 nm	60	Garcia de Rodriguez et al. 2006
Alfa	10 ± 2 nm	200 ± 20 nm	20	Ben Elmabrouk et al., 2009
Flax	21 ± 7 nm	327 ± 108 nm	16	Cao, Dong, & Li, 2007

The NCC diameter measured was lower than those acquired in a study by Moran et al. (2008) on sisal fibres (30.9 nm ± 12.5 nm) demonstrating the effectiveness of the experimental conditions in this study, henceforth confirming the presence of individualized NCC in the aqueous suspension. Another study reported that although NCC extracted from *Mengkuang* leaves yield varies length ranging from 50 to 400 nm, with an average value around 200 nm and diameter in the range of 5-25 nm, the aspect ratio was in the range of 9-17, which is quite low when compared to the value

of 60 reported for sisal cellulose whiskers (Garcia de Rodriguez et al. 2006; (Sheltami, 2012). Nevertheless, the value detected here is comparable to the aspect ratio values reported from NCC extracted from cotton (Ebeling et al., 1999), alfa (Ben Elmabrouk et al., 2009), flax (Cao, Dong, & Li, 2007; (Sheltami, 2012), and Curaúa (Corrêa et al 2010). During the hydrolysis process, NCC was continuously produced in parallel with the fragmentation of the MCC by ILs. However, the resulting NCC tends to agglomerate and form deposits as microparticles. To hinder the agglomeration and/or dissociate of the NCC, ultrasonication treatment was subjected to the NCC dispersions at four different parameters namely 5, 10, 15 and 20 minutes. The high frequency (20-25 kHz) ultrasonication effect causes acoustic cavitation, which involves the formation, expansion, and implosion of microbubbles in aqueous solution, thus singularly isolating the NCC. Micro jets and shock waves were induced on the surfaces of the synthesized cellulose caused by the violent collapse. This, in turn, causes erosion on the fibre surfaces initiating them to split along the axial direction. The impact of the ultrasonication is able to break the fragile interfaces bonded mainly by hydrogen bonds between NCC. To confirm the separation of the individual crystallites and to investigate the effect of ultrasonication time on the morphology of the NCC, diluted suspensions obtained after various ultrasonication time were observed by AFM. Aside from the rod-like structure seen in the micrographs, some aggregations of the NCC were also observed probably due to the moisture evaporation during sample preparation. Figure 4.7 shows the AFM images of U5, U6, U7, and U8.
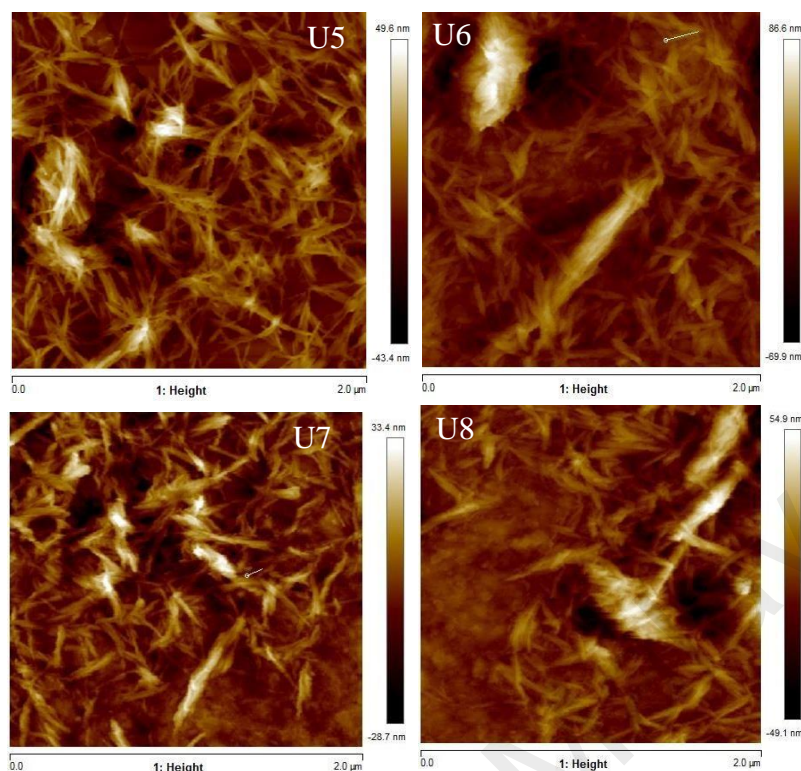
Figure 4.7: AFM images of NCC at increasing ultrasonication time (U5=5 minutes, U6=10 minutes, U7=15 minutes and U8=20 minutes)

The increased intensity of the agglomeration can be caused by the increased strength of the hydrogen bonding established between the NCC, which also have been reported in the previous study (Normand et al., 2014). In this study, this statement is further justified by the FTIR spectra in Figure 4.1, whereby the spectrum shows an increasing intensity of the band representing the hydrogen bond with maximum ultrasonication time (20 minutes) and maximum aggregations. In addition, the attachment of smaller bundles or partly individualized NCC with the large aggregates was also observed. In contrast, the number of the individualized NCC increased with the minimum ultrasonication time applied (5 minutes). Despite the presence of few NCC bundles in the suspension, small openings between the un-individualized NCC could be observed in the NCC aggregates. This is an indication that the hydrogen bonding between the NCC was low at minimum ultrasonication

time. Based on the interpretation concluded rom the effect of the minimum ultrasonication time on the morphological properties of the NCC, it can be assumed that the extreme ultrasonication treatment causes conflicting results to the morphological properties of the NCC. Excessive ultrasonication times probably induced accumulation through the secondary interactions between the individual NCC. Kim et al. (2008) showed parallel findings from waxy rice starches hydrolysed to α-amylase (Kim et al., 2013a). To confirm the separation of the individual crystallites and to investigate the effect of the vibration amplitude on the morphology of the NCC, diluted suspensions obtained after various ultrasonication vibrations were observed by AFM (Figure 4.8). Aside from the rod-like structure seen in the micrographs, some aggregations of the NCC were also observed probably due to the moisture evaporation during sample preparation.
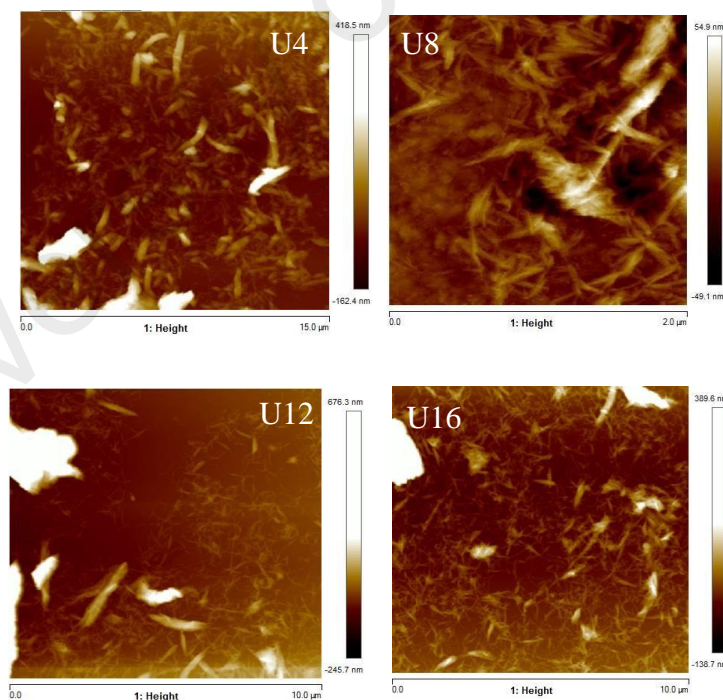

Figure 4.8: AFM images of NCC at increasing vibration amplitude (U4=60%, U8=70%, U12=80% and U16=90%)

Table 4.9 depicts the ultrasonication effect on the diameter, length and aspect ratio of NCC at different vibration amplitude (60, 70,80 and 90%).

Table 4.9: Diameter (nm), Length (nm) and aspect ratio of NCC at increasing vibration amplitude (U4=60%, U8=70%, U12=80% and U16=90%) [8]

Sample	Diameter (nm)	Length (nm)	Aspect ratio
U4	21 ± 0.1	200 ± 1.2	10
U8	16 ± 0.4	143 ± 0.4	9
U12	34 ± 1.2	400 ± 0.6	12
U16	39 ± 0.3	574 ± 0.3	15

As the vibration amplitude increases from 60 to 70%, the diameter of the NCC decreased from 21 to 16 nm. The length and aspect ratio of the NCC also decreases from 200 to 143 nm and 10 to 9, respectively. These results demonstrate the efficiency of the ultrasonication vibration at 70% vibration amplitude. However, NCC exhibited increase widths (34, 39 nm), length (400, 574 nm), and aspect ratio (12, 15) with increasing vibration amplitude (80, 90%). It can be concluded that excessive ultrasonication treatment resulted in opposite effect on the morphological properties of the NCC. Excessive ultrasonication vibration probably has induced aggregation through the secondary interactions between the individual NCC. A similar result was reported by Kim et al(2008) from waxy rice starches hydrolysed to α-amylase (Kim et al., 2013a).

---

[8] Reaction condition: U5=5 minutes, U6=10 minutes, U7=15 minutes, U8=20 miutes ultrasonication time. Meanwhile, U4=60%, U8=70%, U12=80% and U16=100%) vibration amplitude.

4.3.5 Field Emission Scanning Electron Microscopy (FESEM)

Besides AFM, the surface morphology of the NCC sample has been analysed using Field Emission Scanning Electron Microscopy (FESEM). The micrograph of treated cellulose shows defibrillation, which takes place during the hydrolysis process. Figure 4.9(a) shows the optical micrograph of MCC, U5, U6, U7, and U8 obtained after the chemical treatment and ultrasonication. Under controlled conditions, the chemical treatment and ultrasonication were predicted to cleave the amorphous sections of the cellulose while diagonally keeping the straight crystalline domains undamaged. Furthermore, the treatment should also be able to decrease the size of the fibres from micron to nanometre scale. It also showed that the NCC slightly aggregate with other particles clustering to each other. The length and diameter of the NCC were not measured because it is hard to distinguish the individual NCC from the agglomerated structures. Figure 4.9(b) is a comparison of FESEM images of NCC at four different vibration amplitude conditions which are 60, 70, 80, and 90%. The micrograph in Figure 4.9(b) shows the agglomeration of the NCC structure. This was probably due to the sample preparation method, whereby the NCC suspensions were dry out before analysis. Besides the formation of the agglomerates, water removal causes the NCC bundles and aggregates to come closer to each other. General conclusions can be deduced from these observations despite the extent of fibre agglomeration masking the differences effects of the treatment process. It is clear, that chemical treatment and ultrasonication gave significantly finer NCC with less intensity of agglomeration as compared to the MCC.
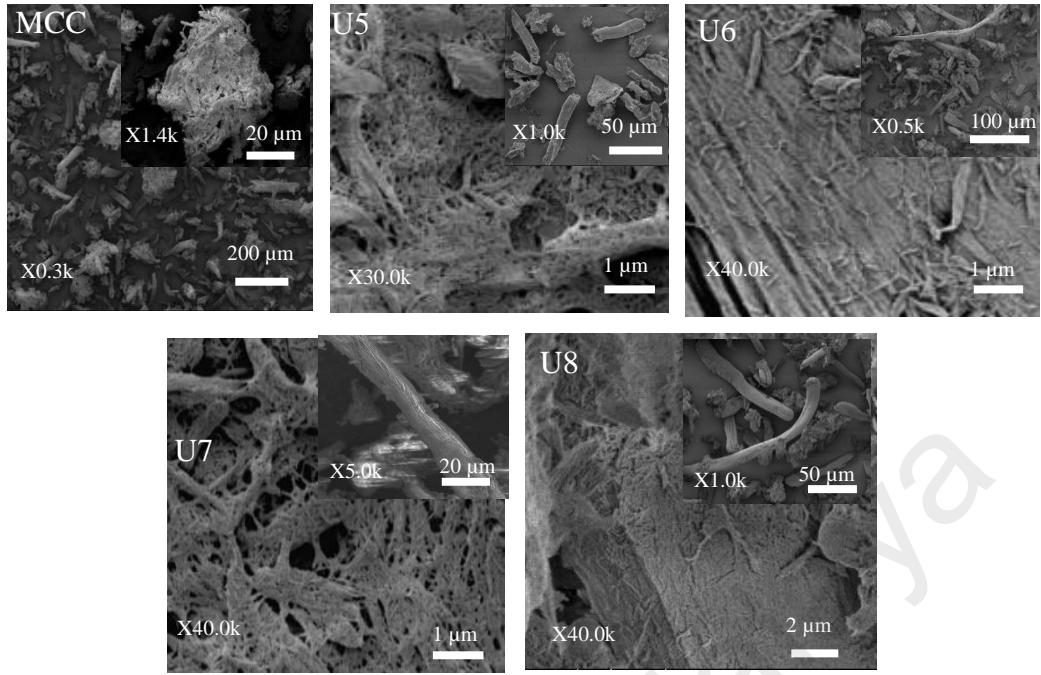
Figure 4.9(a): FESEM images of MCC and NCC at increasing ultrasonication time (U5=5 minutes, U6=10 minutes, U7=15 minutes and U8=20 minutes)
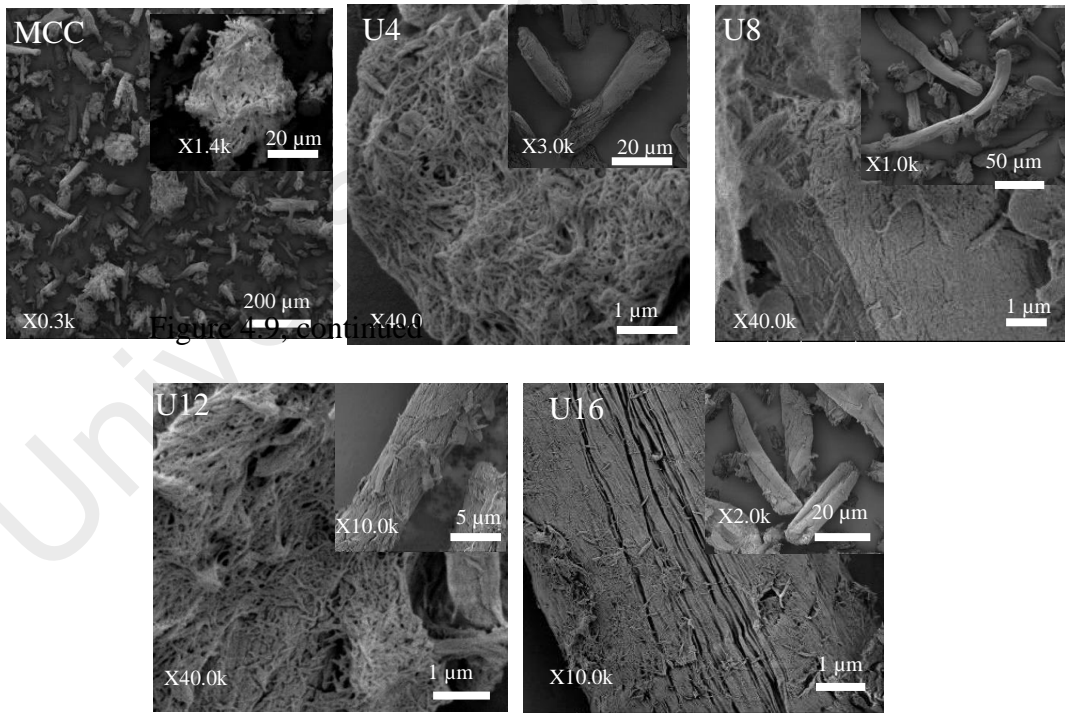

Figure 4.9, continued

Figure 4.9(b): FESEM images of MCC and NCC at increasing vibration amplitude (U4=60%, U8=70%, U12=80% and U16=90%)

FESEM and AFM images verified the effectiveness of the ultrasonication treatment, ratifying that aqueous suspension containing NCC mostly comprises of the individual crystals and some aggregates.

4.3.6 Dynamic Light Scattering (DLS)

DLS analysis results portrayed various sizes of NCC groups detected by light scattering for different ultrasonication treatments being applied (Table 4.10).

Table 4.10: Particle distribution size of NCC at increasing vibration amplitude (U4=60%, U8=70%, U12=80% and U16=90%)

Sample	Particle distribution size (nm)
U4	56
U8	36
U12	55
U16	57

As the vibration amplitude increases from 60 to 70%, the size peak of the NCC shifted towards the smaller range of the NCC size. The dissociation of the nanoparticles clusters became more efficient due to the increased intensity of the bubble collapse caused by the higher vibration amplitude. Chen et al. (2011) reported similar findings stating that the degree of the nanofibrillation rely on the output power of the ultrasonic treatment, meanwhile Kim et al. (2013a) verified that a more uniform and slender NCC was observed with increased intensity of ultrasonication.

Figure 4.10 shows the particle distribution size of the NCC at increasing vibration amplitude.
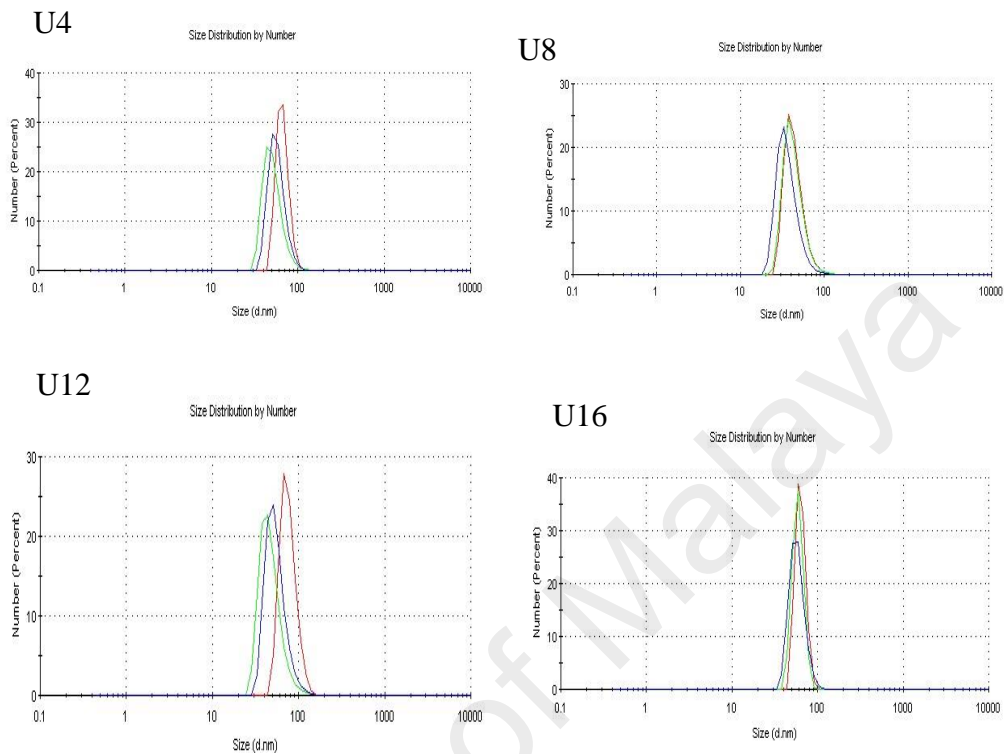

Figure 4.10: Particle distribution profile NCC at increasing vibration amplitude (U4=60%, U8=70%, U12=80% and U16=90%)[9]

However, not every extent of the size decrease was comparative to the levels of the amplitudes applied. The existence of very large bubbles due to higher vibration amplitude may reduce the tendency of cluster breakage since they do not have sufficient time to collapse in the adjacent rarefaction cycle. From Table 4.9, the size peak of the NCC shifted towards the bigger size range as the vibration amplitude increased to 80 and 90% probably due to the re-aggregation of the NCC. Higher vibration amplitude might induce the growth of bubbles to become so large that the time available in the adjacent rarefaction cycle became insufficient for them to

---

[9] Reaction condition: U5=5 minutes, U6=10 minutes, U7=15 minutes, U8=20 miutes ultrasonication time. Meanwhile, U4=60%, U8=70%, U12=80% and U16=100%) vibration amplitude.

collapse reducing the tendency of the cluster breakage. A similar trend was also observed in the previous study (Kim et al., 2013a). Overall, ultrasonication treatment at 70% vibration amplitude was justified to be most effective to produce NCC based on the ability in preventing aggregation of the NCC. Figure 4.11 shows the particle distribution size of the NCC at increasing ultrasonication time.
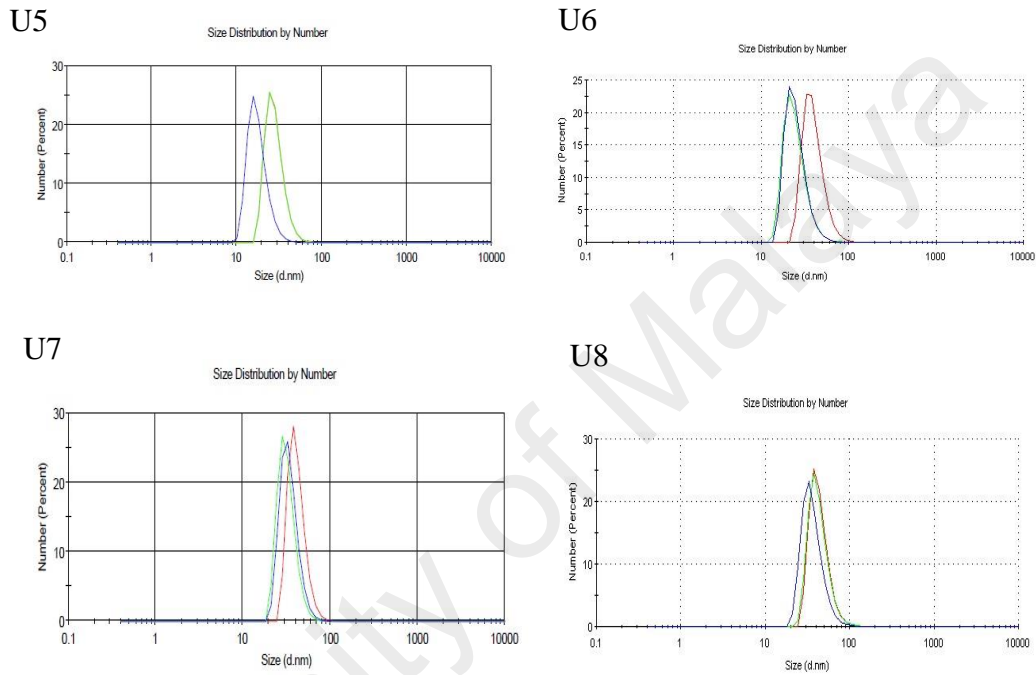

Figure 4.11: Size distribution profile of NCC at increasing ultrasonication time (U5=5 minutes, U6=10 minutes, U7=15 minutes and U8=20 minutes)

Table 4.11 shows the particle distribution size of NCC at increasing ultrasonication time. The particle distribution size (PSD) of U5, U6, U7, and U8 are 18, 25, 34, and 36 nm, respectively. It can be seen from the table that the particle size of NCC increased at longer ultrasonication time probably due to the re-aggregation of the NCC. This result was strongly supported by AFM data obtained in Table 4.7.

Table 4.11: Particle distribution size of NCC at increasing ultrasonication time (U5=5 minutes, U6=10 minutes, U7=15 minutes and U8=20 minutes)[10]

Sample	Particle distribution size (nm)
U5	18
U6	25
U7	34
U8	36

DLS measurements are strongly affected by various issues. Firstly, since DLS measures the hydrodynamic radius of spherical particles, which is determined from the Einsten-Stokes relation, the rod-like fibres of NCC are regarded as spherical units, which is absolutely untrue. For particles to be evaluated via the DLS, the size of the particle should be bigger than the real dimensions. However, the size acquired most probably varied from those measured by the image analysis. This phenomenon arises because the measurement principles of DLS are based on the scattered light intensity caused by the Brownian motion of particles in the solvent with the absence of an electric field. This poses a problem when measuring particles with a high aspect ratio because the length determined is affected by the diameter of the NCC. Further challenges arise where while the extent of particle-particle interactions in an aqueous suspension controls the hydrodynamic radiuses of the 'spherical' particles, other factors also greatly dictate the size of the NCC. Particle concentrations in the system, the formation of hydration shells, and the potential effects of modification of

---

[10] Reaction condition: U5=5 minutes, U6=10 minutes, U7=15 minutes, U8=20 miutes ultrasonication time. Meanwhile, U4=60%, U8=70%, U12=80% and U16=100%) vibration amplitude.

the fibre on their surface chemistry are among the key factors that regulate the size of the NCC. Therefore, as a precaution, data from DLS are not true indicators of the NCC size. However, they still allow comparison between the samples made under varying processing conditions (Qua et al., 2011). Based on the value of the aspect ratio, the following optimal conditions of mechanical disintegration (ultrasonication) were recorded at 5 minutes of ultrasonication time and 70 % of vibration amplitude. Further study was then conducted to determine the optimum temperature, dissolution time, and MCC/ionic liquids ratio.

4.4 Optimization of Operating Conditions

4.4.1 Yield

The effect of the dissolution time on the structure and size of NCC was preliminarily studied using 1:10 MCC/ionic liquids ratio, 40 °C heating temperature, and different dissolution time at 30, 60, 90 and 120 minutes. Then the cellulose suspension undergoes mechanical disintegration by ultrasonication at 70% vibration amplitude for 5 minutes. The MCC was subjected to hydrolysis at different time periods, 30, 60, 90 and 120 minutes. Table 4.11 shows the NCC yield at increased dissolution time.

Table 4.12: Yield of NCC at increased dissolution time (NCC-1=30 minutes, NCC-2=60 minutes, NCC-3=90 minutes and NCC-4=120 minutes)[11]

Sample	Yield (%)
NCC-1	83
NCC-2	86
NCC-3	88
NCC-4	89

The NCC yields were 83, 86, 88, and 89% (NCC-1, NCC-2, NCC-3 and NCC-4) from ILs hydrolysis for 30, 60, 90, and 120 minutes, respectively. The yields increased considerably by 3, 2 and 1% with additional times validating the effectiveness of longer dissolution time. This was probably due to the formation of total reducing sugars (TRS) or glucose at shorter reaction time. As mentioned in the previous study, longer reaction time yields neither TRS nor glucose formation at a higher temperature such as 170 °C and 180 °C, whereas more TRS and glucose were produced in shorter reaction time (Tian et al., 2010). Since a low temperature was used (40 °C), a longer time is required for the reaction process to achieve optimum yield. The 89% yield of NCC-4 shows that the ILs hydrolysis at 120 minutes is optimum in releasing NCC from MCC. In the previous study, the longer the hydrolysis time, the amount of dispersed NCC increased and reaching almost 92% within 90 minutes of dissolution time (Fahma et al., 2010).

---

[11] Reaction condition 1: NCC-1=30 minutes, NCC-2=60 minutes, NCC-3=90 minutes, NCC-4=120 minutes reaction time 2: NCC-1=40 ℃, NCC-5=60 ℃, NCC-9=80 ℃ and NCC-13=100 ℃, 3: NCC-9C=1:4, NCC-9B=1:6, NCC-9A=1:8 and NCC-9=1:10 MCC/ionic liquids' ratio.

The effect of temperature on structure and size of the NCC was initially studied at 1:10 cellulose/ionic liquids ratio, 30 minutes dissolution time and at different heating temperatures (40, 60, 80, and 100 °C). Then, the cellulose suspension undergoes mechanical disintegration by ultrasonication at 70% vibration amplitude for 5 minutes. The strategy of adapting heat to further enhance the dissolution of cellulose in ILs is in parallel with the previous studies that utilized assisted treatment with one of the most commonly practised assisted treatment is heat, ranging from 45 °C up to 160 °C (Montalbo-Lomboy et al., 2015). To minimize the energy consumption and to avoid cellulose degradation, this study narrows down the temperature range between 40 °C to 100 °C., The maximum yield of NCC for all cellulose treatment has always been a critical challenge. The result after hydrolysis at the different temperatures of 40, 60, 80, and 100 °C are presented in Table 4.12.

Table 4.13: Yield of NCC at increasing temperature (NCC-1=40 °C, NCC-5=60 °C, NCC-9=80 °C and NCC-13=100 °C)[12]

Sample	Yield (%)
NCC-1	83
NCC-5	84
NCC-9	86
NCC-13	90

[12] Reaction condition 1: NCC-1=30 minutes, NCC-2=60 minutes, NCC-3=90 minutes, NCC-4=120 minutes reaction time 2: NCC-1=40 ℃, NCC-5=60 ℃, NCC-9=80 ℃ and NCC-13=100 ℃, 3: NCC-9C=1:4, NCC-9B=1:6, NCC-9A=1:8 and NCC-9=1:10 MCC/ionic liquids' ratio.

The NCC yields were 83, 84, 86, and 90% (NCC-1, NCC-5, NCC-9 and NCC-13) from ILs hydrolysis at 40, 60, 80, and 100 °C, respectively. The yields increased expressively by 1, 2 and 4 % with the increasing temperature verifying the effectiveness at a higher temperature. Generally, when the reaction temperature increased, the reaction rate improved (Tan, H. T. et al., 2012). From Table 4.12, when the heating temperature increases, the NCC yield also increases with the highest yield achieved was at 100 °C. As reported by Remsing, et al (2006), cellulose was dissolved into ILs because the chloride ions in ILs could go into the interspaces of 1,4-linked β-D-glucose units and disrupt the intermolecular hydrogen bonds between the units (Hu et al., 2013). Increasing the temperature allegedly makes the [Bmim]Cl less viscous due to the increased movement rate of the chloride ions, which in turn will hasten the dissolution of the cellulose and improve the NCC yield. However, contrary to the previous research, more cellulose was regained at 90 °C as compared to 120 °C which was probably related to the different viscosity of the ILs used. In contrast with the conventional method, using ILs was proven to be more efficient in producing a high yield of cellulose as only 21-38% of NCC can be recovered at the 65 °C by using sulphuric acid (Brinchi et al., 2013).

The effect of MCC/ionic liquids ratio on the structure and size of the NCC was initially studied at 80 °C heating temperature, 30 minutes dissolution time and at different MCC/ionic liquids ratio (1:10, 1:8, 1:6, and 1:4). The higher temperature was used to improve the reaction rate. Then the cellulose suspension undergoes mechanical disintegration by ultrasonication at 70% vibration amplitude for 5 minutes. The NCC formation at varying ratio was investigated. Table 4.13 shows the yield of NCC at increasing cellulose/ionic liquids ratio.

Table 4.14: Yield of NCC at increasing MCC/ionic liquids' ratio (NCC9C=1;4, NCC-9B=1:6, NCC-9A=1:8 and NCC-9=1:10) [13]

Sample	Yield (%)
NCC-9C	85
NCC-9B	72
NCC-9A	79
NCC-9	86

From Table 4.13, the NCC yield at 1:6 cellulose to ILs ratio (72%) was found to be lower than the yield at 1:4 cellulose to ILs ratio (85%). This means that increasing the MCC/ ionic liquids ratio enhances the dissociation of cellulose which also intensified the cellulose degradation and cellulose loss in anti-solvent (water), thus resulting in reduce regenerated NCC yield, as supported by the previous study (Tan, H. T. et al., 2012). However, the NCC yield was gradually increased at higher MCC/ionic liquids ratio of 1:8 and 1:10 (79 and 86%). According to the previous study, the NCC yield should decrease with increased MCC/ ionic liquids ratio due to the better dissolution that enhanced the mass loss of the NCC. Better dissolution of NCC at higher MCC/ ionic liquids ratio was attributed to the frequent interaction and collision between the cellulose particles in high MCC/ ionic liquids ratio (Tan, H. T. et al., 2012). In contrast with the previous study mentioned, this current study was able to overcome the undesirable lower yield trend as can be seen in Table 4.13 probably via the assisted ultrasonication technique.

---

[13] Reaction condition 1: NCC-1=30 minutes, NCC-2=60 minutes, NCC-3=90 minutes, NCC-4=120 minutes reaction time 2: NCC-1=40 ºC, NCC-5=60 ºC, NCC-9=80 ºC and NCC-13=100 ºC, 3: NCC-9C=1:4, NCC-9B=1:6, NCC-9A=1:8 and NCC-9=1:10 MCC/ionic liquids' ratio.

4.4.2 Fourier Transform Infrared Spectroscopy (FTIR)

FTIR spectroscopy portrays a comparatively simple method of acquiring direct information on chemical changes occur during various chemical treatments, hence the extensive use in the cellulose research (Mandal et al., 2011). The efficiency of each chemical treatment was confirmed by FTIR. Figure 4.10 (a, b and c) shows the FTIR spectra recorded after hydrolysis with different dissolution time, temperature, and MCC/ionic liquids ratio.
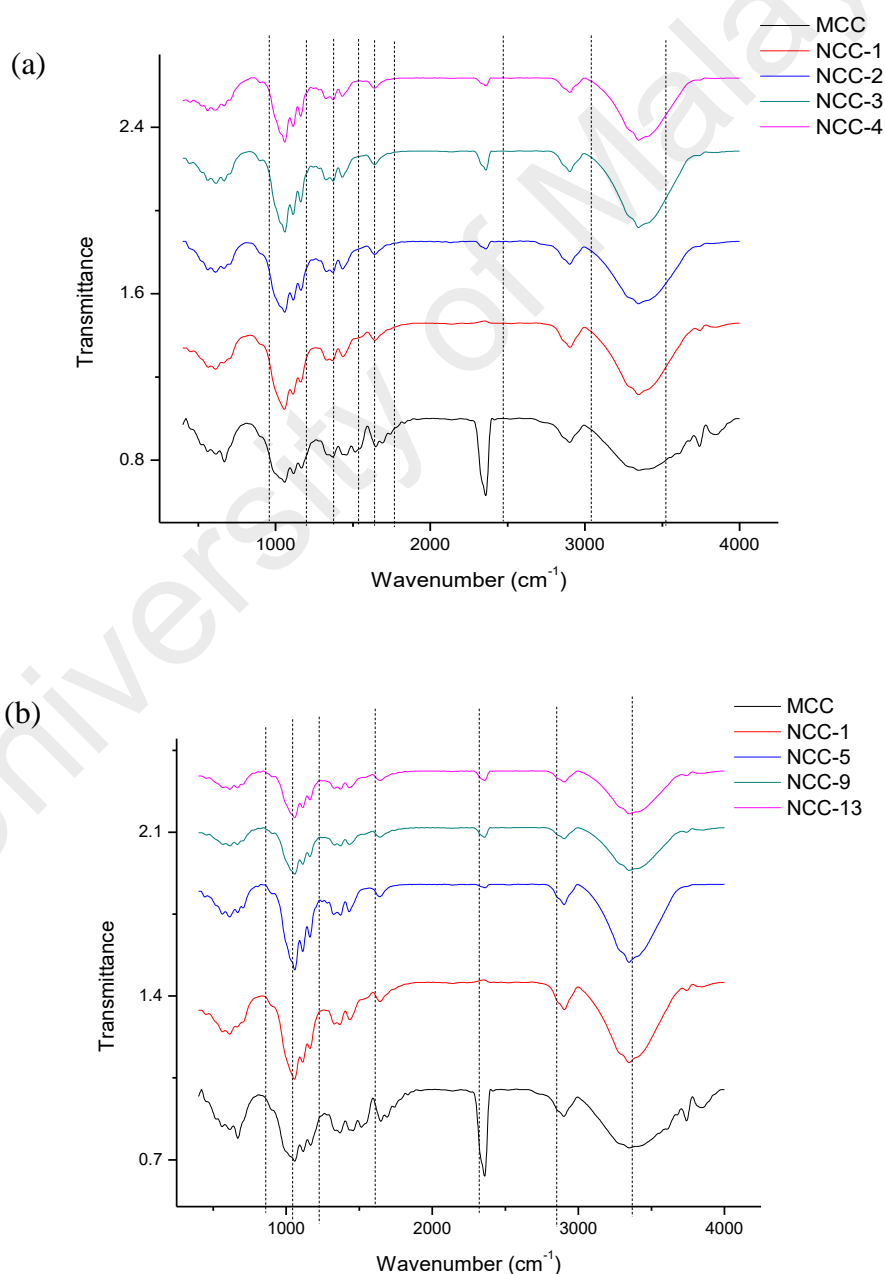

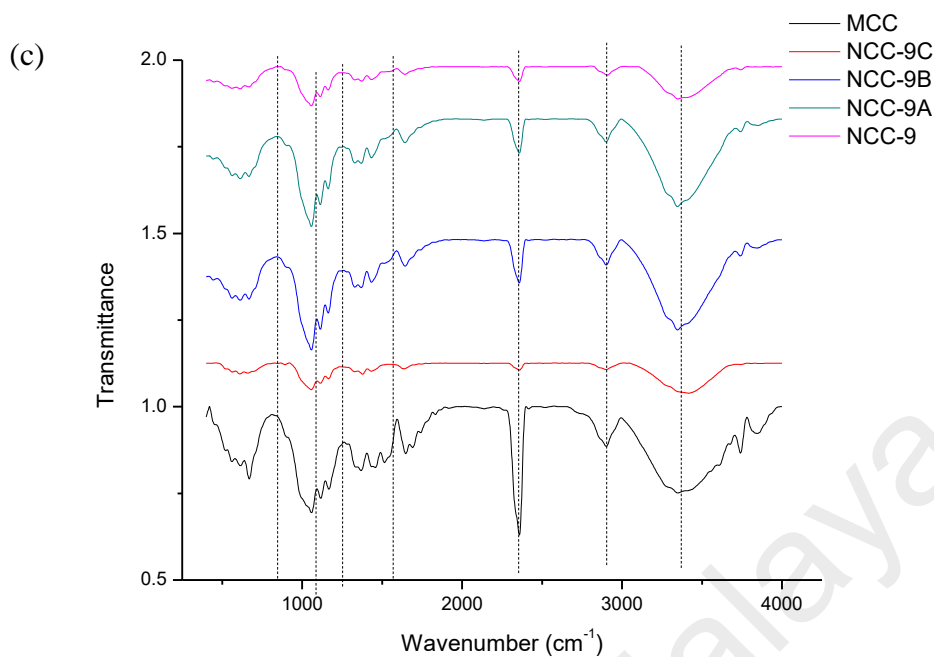Figure 4.12, continued

Figure 4.12, continued

Figure 4.12: FTIR spectra of NCC at (a) increasing dissolution time (NCC-1=30 minutes, NCC-2=60 minutes, NCC-3=90 minutes and NCC-4=120 minutes), (b) increasing temperature (NCC-1=40 °C, NCC-5=60 °C, NCC-9=80 °C and NCC-13=100 °C) and (c) MCC/ionic liquids' ratio (NCC-9C=1;4, NCC-9B=1:6, NCC-9A=1:8 and NCC-9=1:10)

All spectra were characterized by the dominant O-H stretch band (3345-3348 cm^{-1}), C-H stretch band (2903-2906 cm^{-1}, and 2400 cm^{-1}) corresponding to the aliphatic moieties in polysaccharides. The band at 1639-1643 cm^{-1} was accredited to the bending mode of the absorbed water. The bands at 1431-1433 cm^{-1} in the spectrum were assigned to the symmetric CH$_2$ bending, while the C-H bending occurred at 1371-1372 cm^{-1}. The absorption band at 1158 cm^{-1} denotes C-O-C stretching at the β-(1,4) -glycosidic linkages. The in-plane ring stretching gave a shoulder at 1113-1115 cm^{-1}. The strong peak at 1058-1059 cm^{-1} was an indicative of C-O stretching at C-3. A small peak at 667-668 cm^{-1} corresponded to the out-of-plane bending of C-O-H. As the MCC/ionic liquids ratio varied, the characteristics of the intermolecular

82

and intramolecular O-H stretching vibration band of the NCC spectrum in the range of 3346 cm^{-1} appeared broader when the ratio decreased to 1:6 and 1:8. According to the previous results, this indicated a stronger intermolecular hydrogen bonding and the breakdown of the crystalline structure during hydrolysis. The increase in the intermolecular hydrogen bond happens when the structure loosened and the surface is increases. This enables the surface energy to become larger, making the cellulose bundled comes together, thus, decreasing the surface free energy (Sun et al., 2008). However, the relationship between the crystalline structure and the hydrogen bonding could not be observed as mentioned in the previous literature. A medium peak at 2900-2906 cm^{-1} was due to the C-H stretching. A band in the range within 1643-1646 cm^{-1} is associated with the adsorbed water. The bands at 1329-1330 cm^{-1} and 1431-1433 cm^{-1} were assigned to C-C/C-O skeletal vibrations and CH$_2$ symmetric bending, respectively. The sharp bend at 1369-1378 cm^{-1} reflects the C-H asymmetric deformation of the cellulose. The absorption band at 1163 cm^{-1} corresponds to the C-O antisymmetric bridge stretching of the cellulose. The absorption bands at 1113-1115 cm^{-1} and 1057-1058 cm^{-1} correspond to the C-O-C pyranose ring skeletal vibration of the cellulose. The absorption band at 894 cm^{-1} corresponds to the C-H rocking vibrations of the cellulose. FTIR analysis showed that both untreated MCC and NCC obtained after treatment with [Bmim][Cl] have the same basic structure as shown in Figure 4.10. Meanwhile, the lack of ILs peaks in the spectra indicated that the ILs has been completely eliminated during washing.

4.4.3 X-ray Diffractometry (XRD)

To give more detailed information about the effect of the chemical hydrolysis of the MCC with different dissolution time (30, 60, 90, and 120 minutes), an X-ray diffractometry (XRD) analysis was used to verify the CrI obtained from NCC.

Figure 4.11 shows the diffraction patterns obtained for NCC-1, NCC-2, NCC-3, and NCC-4. They are distinctive cellulose I with four well-defined crystalline peaks around 2Ө=14.0, 16.0, 22.0 and 34.0°.
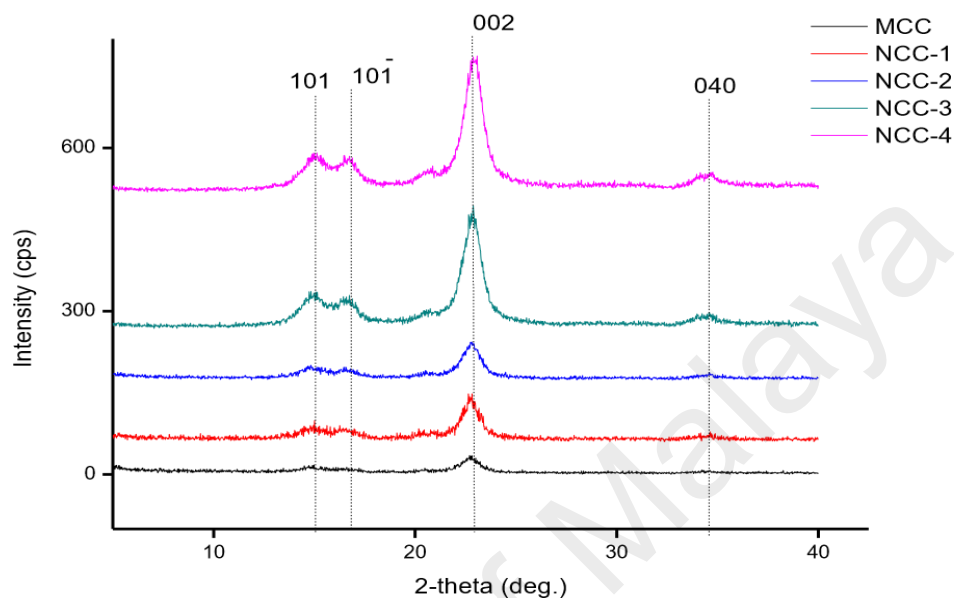

Figure 4.13: XRD diffractograms of NCC at increased dissolution time (NCC-1=30 minutes, NCC-2=60 minutes, NCC-3=90 minutes and NCC-4=120 minutes)

The XRD of NCC-4 exhibits the most intense 002 peak and the most resolved 101 and 10ī peaks indicating higher crystallinity. Meanwhile, NCC-2 had the widest and least defined XRD peaks among the four samples (NCC-1, NCC-2, NCC-3, and NCC-4), which is a clear hint of low crystallinity. The CrI and crystallite size were verified for all samples and the results are summarized in Table 4.14. The increased crystallinity following 30 minutes dissolution time compared to the raw material (MCC) was a clear indication of the progressive elimination of the amorphous materials.

Table 4.15: Crystallinity index of NCC at increased dissolution time (NCC-1=30 minutes, NCC-2=60 minutes, NCC-3=90 minutes and NCC-4=120 minutes)

Sample	Crystallinity index (%)	Crystallite size (nm)
MCC	60 ± 0.2	12.5
NCC-1	73 ± 0.2	9.9
NCC-2	71 ± 0.1	8.4
NCC-3	75 ± 0.1	6.2
NCC-4	76 ± 0.2	5.0

The CrI and crystallite size calculated from XRD pattern of all samples were 73, 71, 75, 76% and 9.9, 8.4, 6.2, 5.0 nm (Table 4.14). The CrI slightly decreased from 73 to 71% as the reaction time increases to 60 minutes and this data is supported by a previous study (Fahma et al. 2010). This reducing CrI was probably due to the destructuring of the crystalline structure at longer reaction time. As the reaction time increased to 90 and 120 minutes, the CrI increased to 75 and 76% most probably due to the realignment of the crystalline structure at longer reaction time. The XRD results together with the FTIR data confirmed that the NCC retained the cellulose I crystalline structure at different dissolution times while becoming more crystalline than the MCC as the dissolution times increases. These results indicated that the CrI was positively correlated with the dissolution times as supported by the previous study (Rosa, M. F. et al., 2010). However, no significant correlation between crystallinity index and yield of NCC was obtained.

To give more detailed information about the effect of the chemical hydrolysis of the MCC with different reaction temperature (40, 60, 80, 100 °C), an x-ray diffractometry (XRD) analysis was used to determine the CrI obtained from NCC. The XRD results of MCC, NCC-1, NCC-5, NCC-9, and NCC-13 were shown in Figure 4.12, which exhibits similar diffraction peaks with four diffraction peaks at 2Θ=14.0, 16.0, 22.0, and 34.0°.
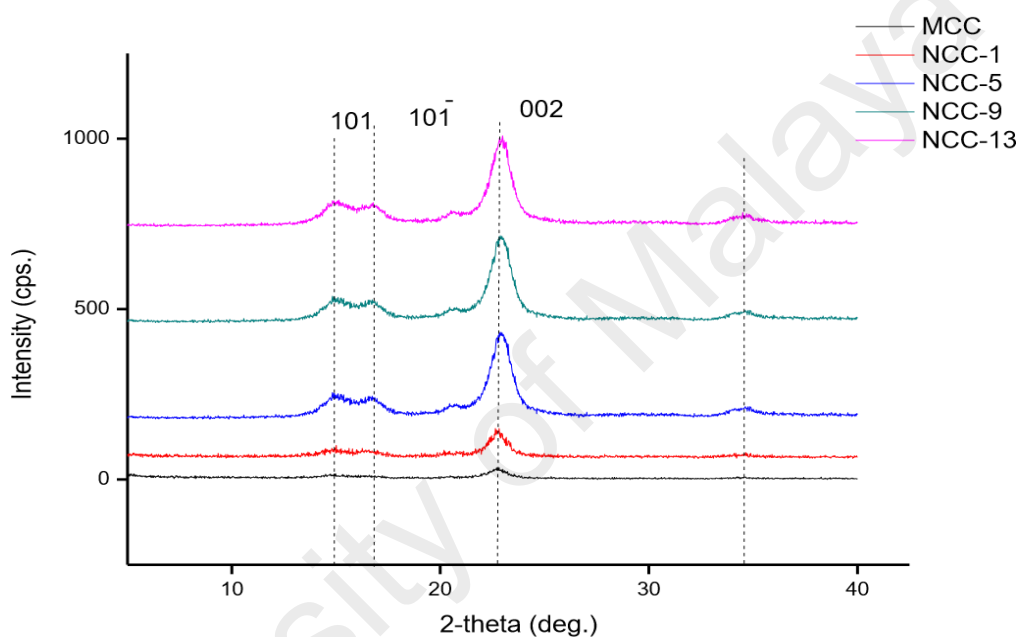

Figure 4.14: XRD diffractograms of NCC at increasing temperature (NCC-1=40 °C, NCC-5=60 °C, NCC-9=80 °C and NCC-13=100 °C)

After treatment at four different temperatures, cellulose I structure remains in all four samples. For untreated and treated samples, the (200) peak position and peak width stay essentially the same. An investigation on the effect of the temperature on CrI of the NCC shows an increasing trend as observed in Table 4.15.

Table 4.16: Crystallinity index of NCC at increasing temperature (NCC-1=40 °C, NCC-5=60 °C, NCC-9=80 °C and NCC-13=100 °C)

Sample	Crystallinity index (%)	Crystallite size (nm)
MCC	60 ± 0.2	12.5
NCC-1	73 ± 0.2	9.9
NCC-5	75 ± 0.1	10.1
NCC-9	75 ± 0.1	4.5
NCC-13	76 ± 0.1	10.1

A similar observation has been reported for ILs treated sample (Man, Zakaria et al., 2011). The CrI obtained from X-ray Diffractograms for MCC and extracted NCC at 40, 60, 80, and 100 °C was found to be 60, 73, 75, 75, and 76%, respectively. Increased CrI of NCC synthesized at 40 °C from MCC was probably due to the realignment of the crystalline structure, after removing the amorphous regions as supported by the previous study (Maheswari et al., 2012). Further temperature increases at 60 °C enhance more realignments to occur, thus increasing the CrI of the NCC. As the crystallinity index increased, the yield of the respective NCC sample also increases due to the removal of the amorphous structure at a higher temperature. [14]However, there was no significant relationship between crystallite size and crystalline or yield properties.

---

[14] Reaction condition 1: NCC-1=30 minutes, NCC-2=60 minutes, NCC-3=90 minutes, NCC-4=120 minutes reaction time 2: NCC-1=40 ℃, NCC-5=60 ℃, NCC-9=80 ℃ and NCC-13=100 ℃, 3: NCC-9C=1:4, NCC-9B=1:6, NCC-9A=1:8 and NCC-9=1:10 MCC/ionic liquids' ratio.

Cellulose samples treated under different MCC/ionic liquids ratio were characterized by XRD as shown in Figure 4.13. MCC and NCC exhibit three main reflection peaks at 2Θ= 14.0, 16.0, and 22.0° relative to the cellulose I crystalline structure. Table 4.16 shows the CrI of the synthesized MCC and NCC.

Table 4.17: Crystallinity index of NCC at increasing MCC/ionic liquids' ratio (NCC-9C=1;4, NCC-9B=1:6, NCC-9A=1:8 and NCC-9=1:10)

Sample	Crystallinity index (%)	Crystallite size (nm)
MCC	60 ± 0.2	12.5
NCC-9C	76 ± 0.1	10.1
NCC-9B	74 ± 0.2	4.7
NCC-9A	73 ± 1.1	9.9
NCC-9	75 ± 0.1	4.5

From Table 4.16, the CrI of the synthesized NCC was higher than the untreated MCC. This shows that treated material have more crystalline regions as compared to the non-treated material, which confirmed the particular elimination of the amorphous portion during ILs treatment. Figure shows the structure of the cellulose, linked by hydrogen bond and Van der Waals forces.
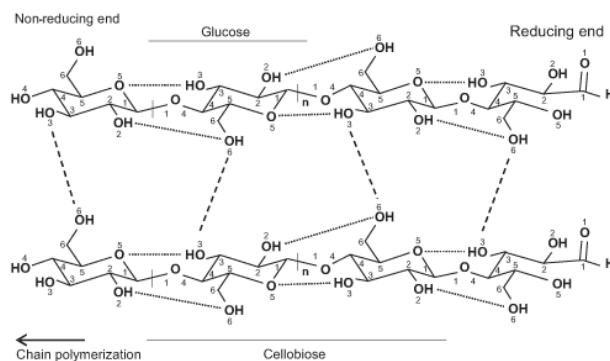
Figure 4.15: Structure of cellulose dashed line; inter-hydrogen bonding and dotted line; intra-hydrogen bonding

Crystalline regions are formed due to the inter and intra-chain hydrogen bonding between the glucose molecule. This was supported by the previous study which stated that the CrI will increase with the transformation of the MCC to NCC (Jahan et al., 2011).
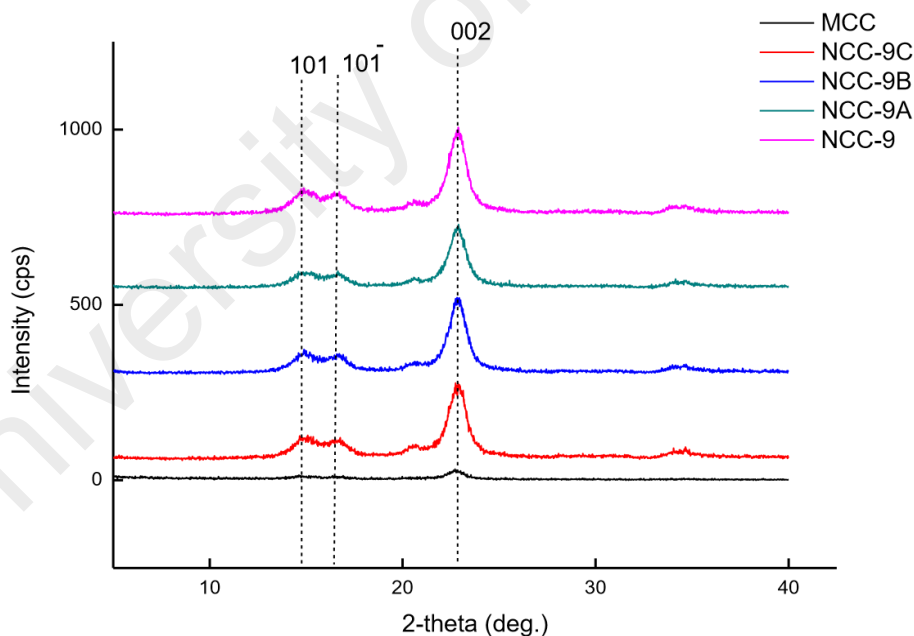

Figure 4.16: XRD diffractograms of NCC at increasing MCC/ionic liquids' ratio (NCC-9C=1;4, NCC-9B=1:6, NCC-9A=1:8 and NCC-9=1:10)

The CrI sample treated at 1:6 and 1:8 MCC/ionic liquids ratio was noticed to be lower than the sample treated at 1:4, with the CrI of 74 and 73%, respectively (Table

4.16). From the previous study, pretreating corn stover in [C$_2$mim][OAc] at increasing solid loading from 5 to 41 and 50wt % led to a decrease in the CrI of cellulose I (Zhang, J. et al., 2014). Further increasing the ratio to 1:10, the CrI increases to 75% probably due to the rearrangement of the crystalline structure. From this study, there was no significant correlation between crystallinity index and yield of NCC.

4.4.4 Thermogravimetric Analysis (TGA)

TGA was measured to assess the thermal stability of NCC-1, NCC-2, NCC-3, and NCC-4 and the thermographs are presented in Figure 4.13. They resemble the mass loss of the sample upon continuous heating up to 700 °C. Initial mass loss of all samples occur below 100 °C irrespective of their treatment. The initial change is attributed to the vaporisation of the water because of the hydrophilic character of the samples. The mass loss was reliant on the initial moisture content of the analysed samples. Meanwhile, the second peak corresponded to the thermal disintegration of the cellulose (Deepa et al., 2011).

Table 4.18: Thermal stability of NCC at increasing dissolution time (NCC-1=30 minutes, NCC-2=60 minutes, NCC-3=90 minutes, NCC-4=120 minutes)

Sample	25-150°C		150-700°C			Residue
	Mass loss (%)	T_1 (°C)	Onset (°C)	Mass loss (%)	T_{max} (°C)	mass (%)
NCC-1	1.5	60	330	90	350	8
NCC-2	2.1	60	342	90	375	8
NCC-3	1.8	60	344	83	375	15
NCC-4	1.6	60	280	85	375	13

As shown in Table 4.17, the onset temperature of NCC-1, NCC-2, and NCC-3, which indicates the thermal stability increased as the dissolution time increases. In details, the DTG curve of the sample hydrolysed at 60 and 90 minutes showed a minor increase in the degradation temperature of 342 and 344 °C, respectively. The initial mass loss is the result of the presence of trace quantity of impurities in the NCC during chemical treatment. However, no specific trend was observed from the mass loss as shown in Table 4.17. Many studies were carried out to assess the decomposition of the lignocellulosic materials. For instance, Yang et al., (2007) reported that in the thermal analysis, cellulose decomposition started at 315 °C and persisted until 400 °C. Maximum mass loss rate was reached at 355 °C, while at 400 °C, almost all cellulose was pyrolyzed, leaving small (6.5wt %) solid residuals (Morán et al., 2008). The fibre residue that remains after heating all the samples at 700 °C is a product of carbonization of the cellulosic materials in the inert atmosphere. As shown in Table 4.17, the residue at temperature around 700 °C in NCC-1, NCC-2, NCC-3, and NCC-4 were remarkably low which is in the range of 8-15 °C. It can be seen in Figure 4.14 that no other degradation peaks were present except that of the cellulose, which verified the conclusion that the prepared NCC samples were very pure. The DTG and TGA results proved that the developed NCC have enhanced thermal properties (330, 342, 344 °C) for NCC-1, NCC-2, and NCC-3 making them less inclined to degradation and therefore can be processed at elevated temperatures. However, no significant relationship between the thermal stability and CrI of NCC-1, NCC-2, NCC-3, and NCC-4 can be concluded.
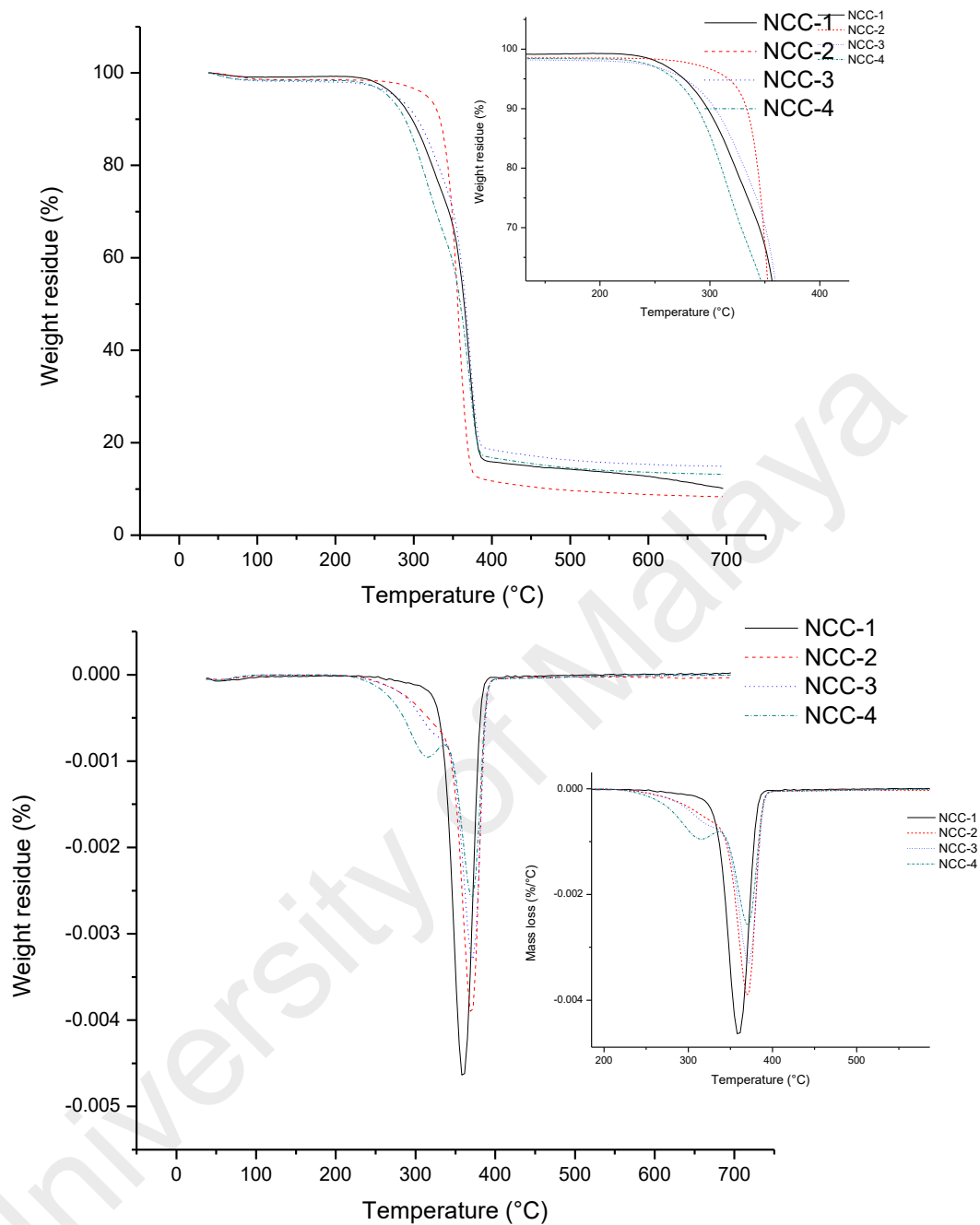
Figure 4.17: TGA and DTG curve of NCC at increasing temperature (NCC-1=30 minutes, NCC-2=60 minutes, NCC-3=90 minutes, NCC-4=120 minutes)[15]

---

[15] Reaction condition 1: NCC-1=30 minutes, NCC-2=60 minutes, NCC-3=90 minutes, NCC-4=120 minutes reaction time 2: NCC-1=40 ℃, NCC-5=60 ℃, NCC-9=80 ℃ and NCC-13=100 ℃, 3: NCC-9C=1:4, NCC-9B=1:6, NCC-9A=1:8 and NCC-9=1:10 MCC/ionic liquids' ratio.

Thermogravimetric (TG) and derivative thermogravimetric (DTG) curves of NCC synthesized at different MCC/ionic liquids' ratio; 1:4, 1:6, 1:8, 1:10 were shown in Figure 4.15.
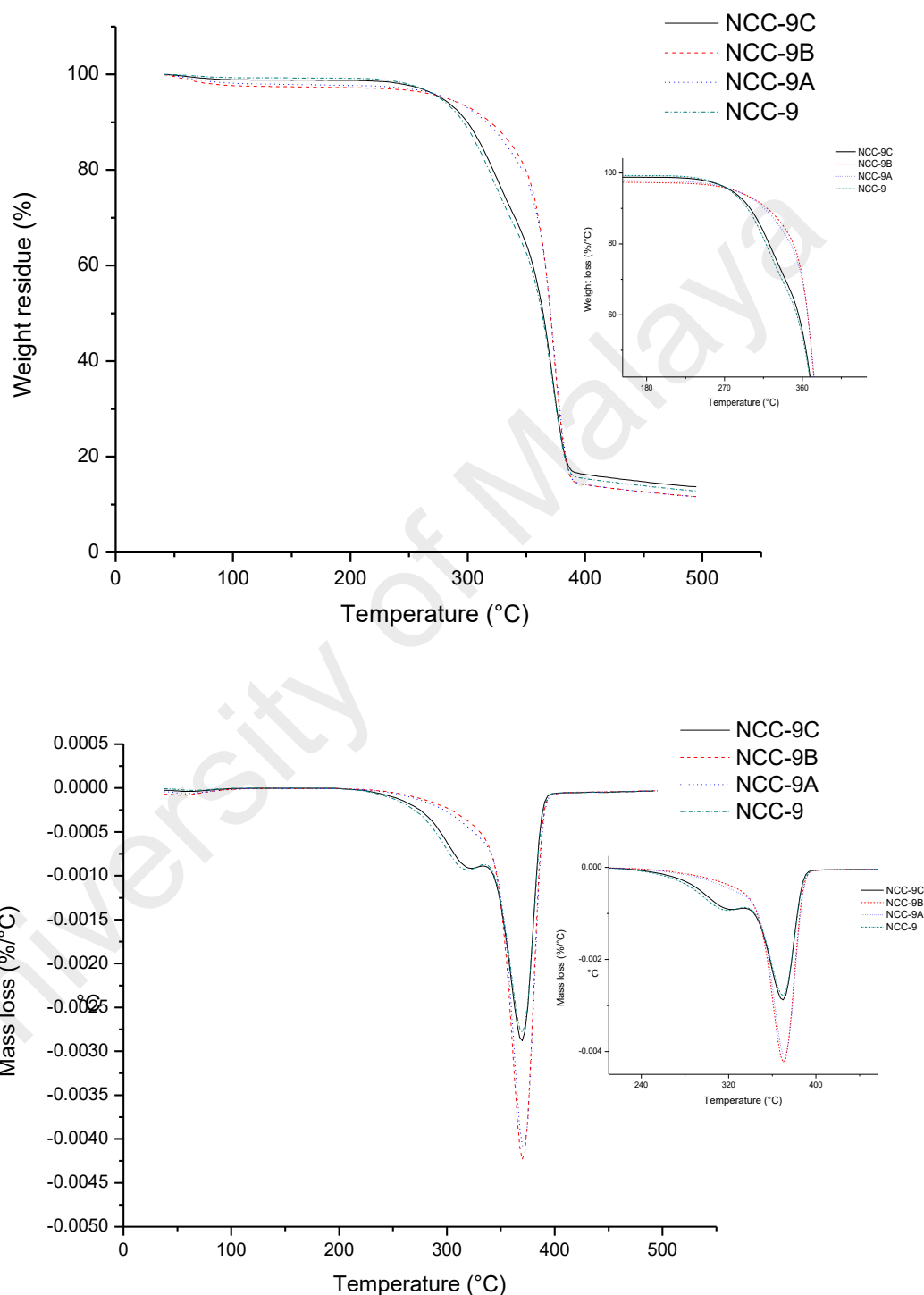

Figure 4.18: TGA and DTG curve of NCC at increasing cellulose/ionic liquids' ratio (NCC-9C=1;4, NCC-9B=1:6, NCC-9A=1:8 and NCC-9=1:10)

Characterization of the thermal decomposition process was conducted by extrapolating the onset and maximum degradation temperatures of the main loss regions. Two mass-loss regions were observed from the curve. In the low temperature range (≤150 °C), all the NCC have a mass loss of 1.7, 2.5, 2.0, and 0.8%. This mass loss corresponded to the evaporation of the water. However, the NCC samples behaved differently in a high temperature range between (150 °C – 700 °C), whereby the mass loss occurred due to the thermal degradation of the NCC. Similar with DSC study, the thermal stability decreases as the MCC/ ionic liquids ratio increases from 1:4 to 1:6 and 1:8 as can be observed in Table 4.18.

Table 4.19: Thermal stability of NCC at increasing MCC/ionic liquids' ratio

(NCC-9C=1;4, NCC-9B=1:6, NCC-9A=1:8 and NCC-9=1:10)

Sample	25-150°C		150-700°C			Residue
	Mass loss (%)	T_1 (°C)	Onset (°C)	Mass loss (%)	Tmax (°C)	mass (%)
NCC-9C	1.7	60	350	85	370	18
NCC-9B	2.5	60	345	86	370	12
NCC-9A	2.0	60	343	87	370	11
NCC-9	0.8	60	350	84	380	15

The thermal stability was gradually increased from 343 to 350 °C at maximum MCC/ ionic liquids ratio (1:10). The increased thermal stability was probably due to the more compact structure of the NCC as the structures with higher crystallinity generally need a higher degradation temperature. Likewise, the degradation temperature of the NCC was proportionally related to the crystallinity of the NCC. In the case of NCC-9C, NCC-9B, NCC-9A, and NCC-9, the maximum temperature of the peak appears at 370, 370, 370, and 380 °C, respectively. The residual mass

94

remaining after heating to 700 °C stems from the carbonization of the cellulosic materials in the inert atmosphere (Deepa et al., 2011). Results of the thermal behaviour of the NCC-1, NCC-5, NCC-9, and NCC-13 are presented in Table 4.19. The initial mass loss can be ascribed to the evaporation of the moisture from the cellulose materials. The chemisorbed water was found to be given off at a temperature of 60 °C for all four samples.

Table 4.20: Thermal stability of NCC at increasing temperature (NCC-1=40 °C, NCC-5=60 °C, NCC-9=80 °C and NCC-13=100 °C)[16]

Sample	25-150°C		150-700°C			Residue
	Mass loss (%)	T_1 (°C)	Onset (°C)	Mass loss (%)	T_{max} (°C)	mass (%)
NCC-1	1.5	60	330	90	350	8
NCC-5	2.0	60	340	87	370	11
NCC-9	0.8	60	350	84	380	15
NCC-13	2.6	60	352	85	384	12

In the thermal analysis for NCC-1, NCC-5, NCC-9, and NCC-13, cellulose decomposition started at 330, 340, 350, and 352 °C, respectively. At 700 °C almost all cellulose were pyrolyzed, and the residue mass were relatively small (8, 11, 15, 12%) for NCC-1, NCC-5, NCC-9, and NCC-13, respectively. Based on the TGA and DTG curves in Figure 4.16, the thermal decomposition peaks of the maximum mass loss appeared at 350, 370, 380 and 384 °C for NCC-1, NCC-5, NCC-9 and NCC-13,

---

[16] Reaction condition 1: NCC-1=30 minutes, NCC-2=60 minutes, NCC-3=90 minutes, NCC-4=120 minutes reaction time 2: NCC-1=40 ºC, NCC-5=60 ºC, NCC-9=80 ºC and NCC-13=100 ºC, 3: NCC-9C=1:4, NCC-9B=1:6, NCC-9A=1:8 and NCC-9=1:10 MCC/ionic liquids' ratio.

respectively. The increase of the temperature was found to increase the thermal properties of the NCC.
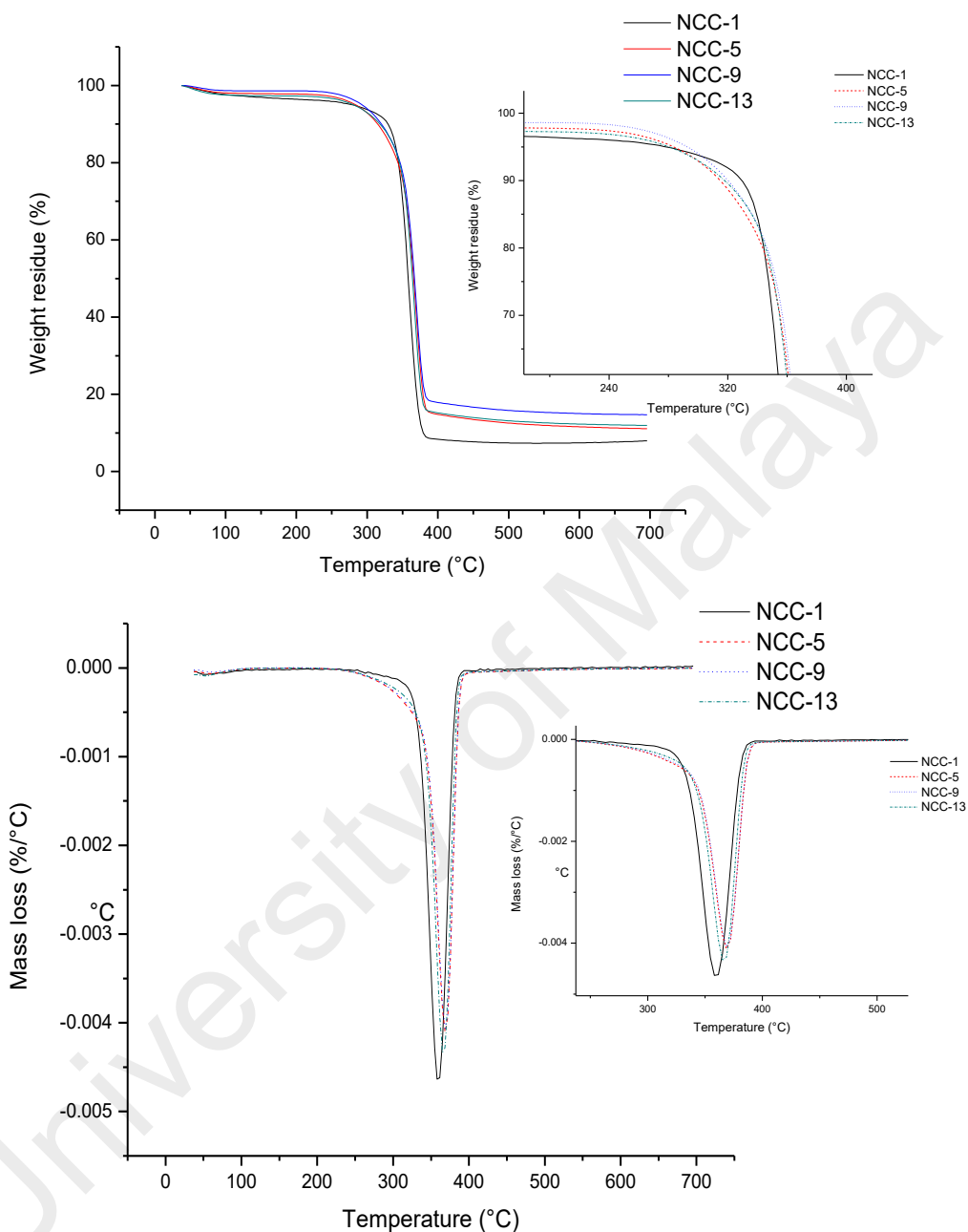

Figure 4.19: TGA and DTG curve of NCC at increasing temperature (NCC-1=40 °C, NCC-5=60 °C, NCC-9=80 °C and NCC-13=100 °C)[17]

---

[17] Reaction condition 1: NCC-1=30 minutes, NCC-2=60 minutes, NCC-3=90 minutes, NCC-4=120 minutes reaction time 2: NCC-1=40 °C, NCC-5=60 °C, NCC-9=80 °C and NCC-13=100 °C, 3: NCC-9C=1:4, NCC-9B=1:6, NCC-9A=1:8 and NCC-9=1:10 MCC/ionic liquids' ratio.

4.4.5 Differential Scanning Calorimetry (DSC)

DSC was measured to access the thermal stability of NCC-1, NCC-2, NCC-3 and NCC-4. Figure 4.17 shows the thermograms obtained for all samples. In all thermograms, an endothermic peak appeared within the ranges of 27 °C – 34 °C due to water evaporation.
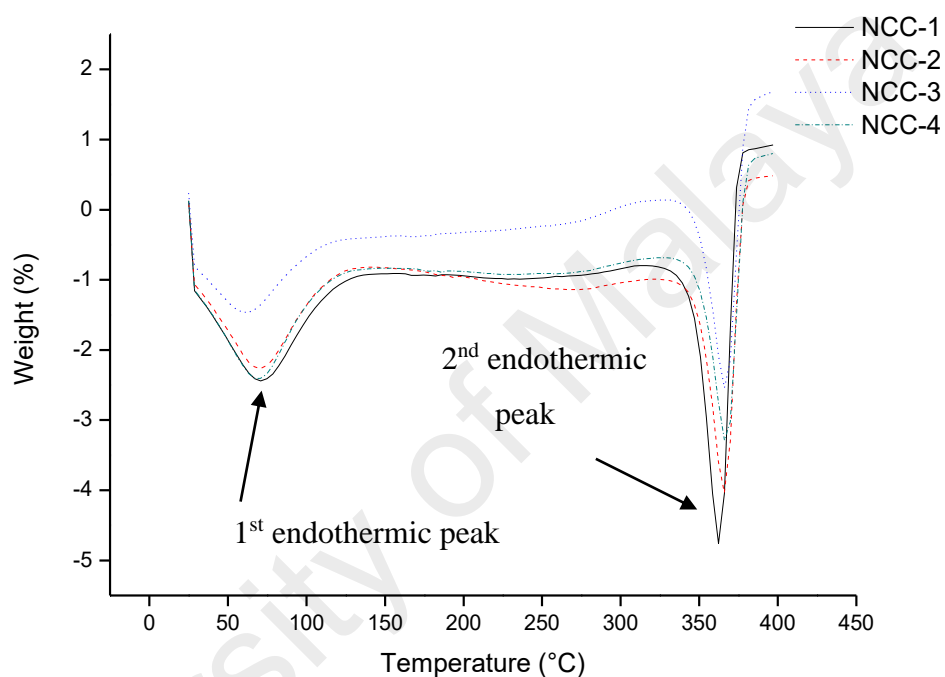

Figure 4.20: Thermograms of NCC at increased dissolution time (NCC-1=30 minutes, NCC-2=60 minutes, NCC-3=90 minutes and NCC-4=120 minutes)[18]

Table 4.20 shows the thermal behaviour of NCC-1, NCC-2, NCC-3, and NCC-4. In the thermal analysis for NCC-1, NCC-2, NCC-3, and NCC-4, cellulose decomposition started at 328, 334, 352, and 351 °C, respectively. The rate of the degradation reaches its peaks at 350, 351, 368, and 373 °C for NCC-1, NCC-2, NCC-3, and NCC-4,

---

[18] Reaction condition 1: NCC-1=30 minutes, NCC-2=60 minutes, NCC-3=90 minutes, NCC-4=120 minutes reaction time 2: NCC-1=40 ºC, NCC-5=60 ºC, NCC-9=80 ºC and NCC-13=100 ºC, 3: NCC-9C=1:4, NCC-9B=1:6, NCC-9A=1:8 and NCC-9=1:10 MCC/ionic liquids' ratio.

respectively. Higher degradation temperature of the NCC could be due to the large fibre dimensions (9, 10, 21, 31 nm) obtained from AFM analysis, which leads to higher surface areas exposed to heat.

Table 4.21: Thermal stability of NCC at increased dissolution time (NCC-1=30 minutes, NCC-2=60 minutes, NCC-3=90 minutes and NCC-4=120 minutes)

Sample	Onset (°C)	Max (°C)	Enthalphy (kJ/mol)
NCC-1	34	76	103
	328	350	267
NCC-2	33	79	143
	334	351	240
NCC-3	27	73	143
	352	368	56
NCC-4	27	70	139
	351	373	113

Table 4.21 shows the DSC analysis of the NCC synthesized at different MCC/ionic liquids ratio. From table 4.21, the initial endotherm occurs between 28-38 °C, indicating the moisture removal due to evaporation. The moisture loss is also confirmed by the TGA studies (Mandal et al., 2011). As for the second endotherm, the decomposition temperature decreased as the MCC/ionic liquids ratio increases from 1:4 to 1:6. However, the decomposition temperature was then gradually increased to 346 and 352 °C at 1:8 and 1:10, respectively. Meanwhile, the maximum degradation peak was 381, 365, 372, and 384 °C, respectively.

Table 4.22: Thermal stability of NCC at increasing MCC/ionic liquids' ratio

(NCC-9C=1;4, NCC-9B=1:6, NCC-9A=1:8 and NCC-9=1:10)

Sample	Onset (°C)	Max (°C)	Enthalpy (kJ/mol)
NCC-9	30	111	109
	352	381	67
NCC-9A	28	97	139
	340	365	287
NCC-9B	34	109	120
	342	372	174
NCC-9C	38	110	135
	352	384	60

In detail, the second endotherm is a suggestion of the course of fusion or melting, which provides an idea of the nature of the decomposition of the NCC. The increase in degradation and maximum decomposition temperature of the NCC occurs due to the increase in the crystalline value of the NCC itself. A greater crystalline structure needs a higher degradation temperature since the rigidity of the crystalline structure enables the NCC to tolerate drastic heat and processing conditions. The DSC results proved that the developed NCC have heightened thermal properties, making them less inclined to degradation and therefore, can be processed at elevated temperatures over their non-treated counterparts. In addition, these results proved that there is a significant relationship between crystallinity index and thermal properties of the NCC. The heating DSC curves were expressed in terms of heat flow (Figure 4.18). All DSC thermograms revealed two distinct endothermic changes within the range of the studied temperatures.
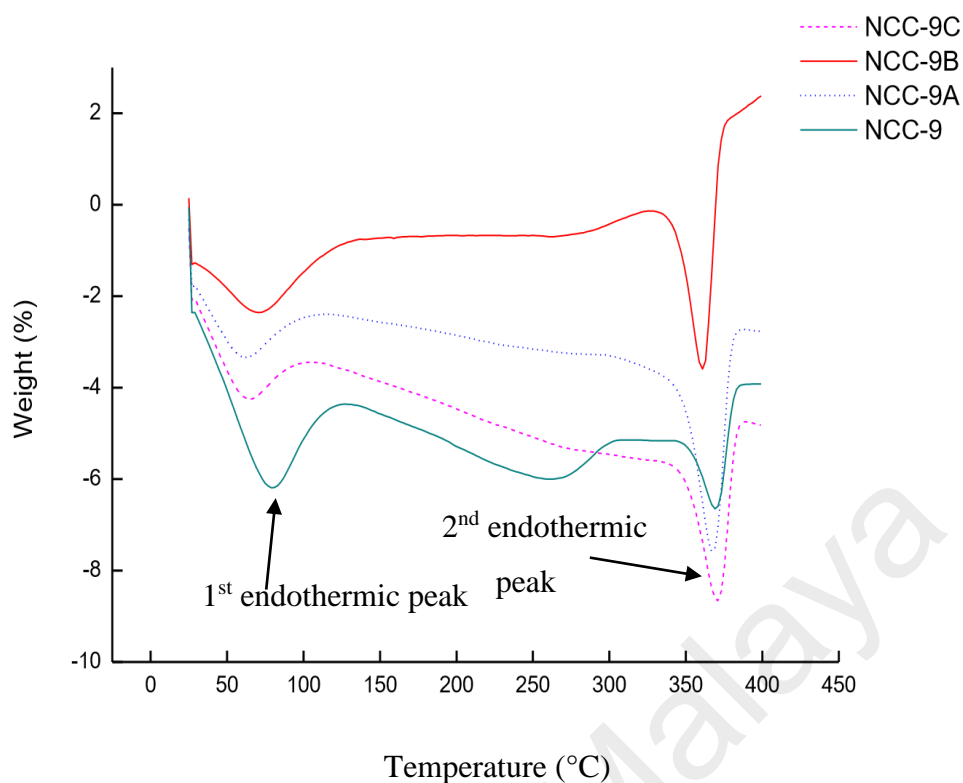
Figure 4.21: Thermograms of NCC at increasing MCC/ionic liquids' ratio (NCC-9C=1;4, NCC-9B=1:6, NCC-9A=1:8 and NCC-9=1:10)

Table 4.22 clearly illustrates the high stability of the NCC-1, NCC-5, NCC-9, and NCC-13. The increase in the degradation temperature in all samples occurred due to the higher crystallinity of the NCC-1, NCC-5, NCC-9, and NCC-13 during the treatment, which enables them to withstand drastic heat and processing conditions.

Table 4.23: Thermal stability of NCC at increasing temperature (NCC-1=40 °C, NCC-5=60 °C, NCC-9=80 °C and NCC-13=100 °C)

Sample	Onset (°C)	Max (°C)	Enthalphy (kJ/mol)
NCC-1	34	76	103
	328	350	267
NCC-5	32	70	125
	351	366	282

Table 4.23, continued

NCC-9	30	72	109
	352	371	67
NCC-13	33	70	113
	354	373	131

Figure 4.19 shows the thermograms obtained from all samples. The DSC curves of all samples demonstrate evaporation of water around 32-34 °C trailed by decomposition of the cellulose around 328, 351, 352, and 354 °C and has been confirmed from the TGA result. The DSC and TGA results proved that the developed NCC have indeed heightened thermal properties, making them less prone to degradation and therefore can be processed at a higher temperature.
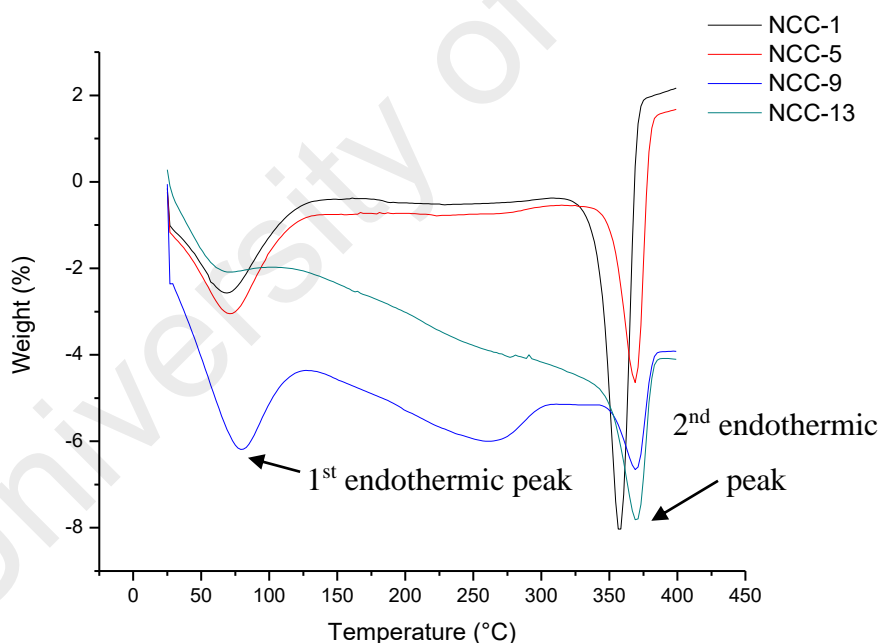
Figure 4.22: Thermograms of NCC at increasing temperature (NCC-1=40 °C, NCC-5=60 °C, NCC-9=80 °C and NCC-13=100 °C)

4.4.6 Atomic Force Microscopy (AFM)

The isolations of the NCC were depicted by means of an AFM image, which is presented in Figure 4.20. The NCC was observed as having a rod-like feature, individualized or agglomerated due to their high specific area and the presence of strong hydrogen bonds between the crystallites.
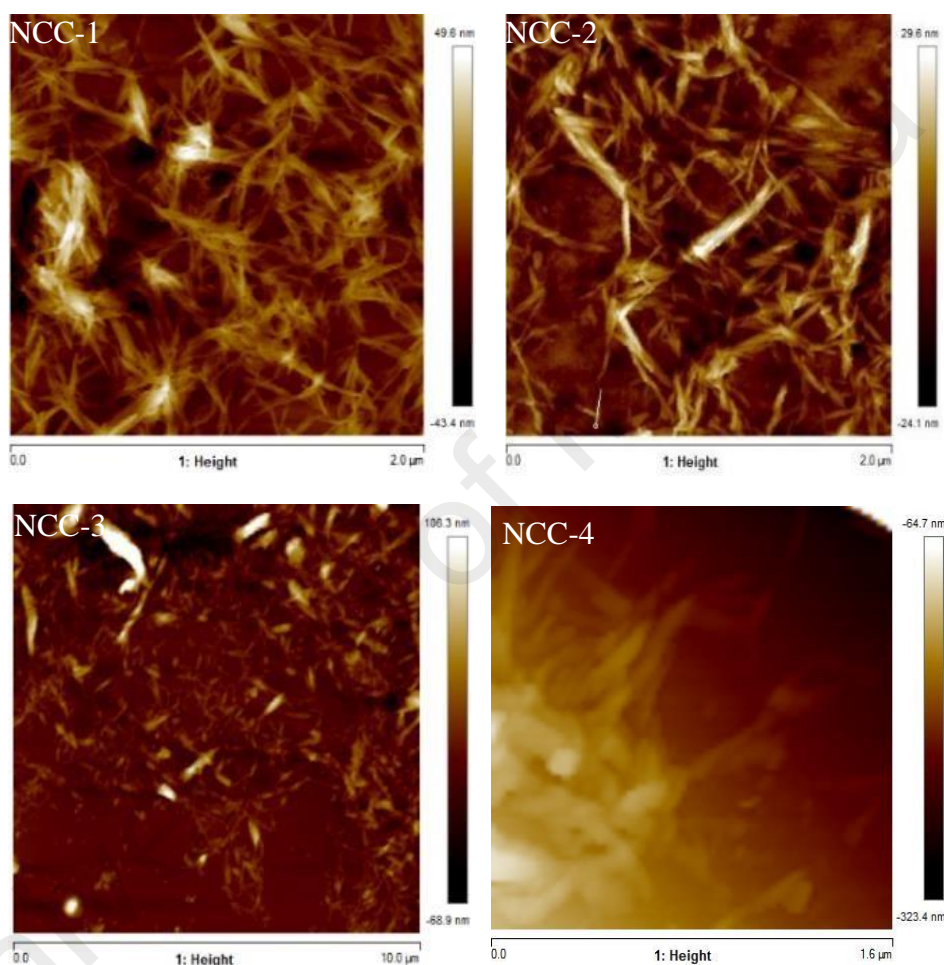
Figure 4.23: AFM images of NCC at increased dissolution time (NCC- 1=30 minutes, NCC-2=60 minutes, NCC-3=90 minutes and NCC-4=120 minutes)[19]

---

[19] Reaction condition 1: NCC-1=30 minutes, NCC-2=60 minutes, NCC-3=90 minutes, NCC-4=120 minutes reaction time 2: NCC-1=40 ℃, NCC-5=60 ℃, NCC-9=80 ℃ and NCC-13=100 ℃, 3: NCC-9C=1:4, NCC-9B=1:6, NCC-9A=1:8 and NCC-9=1:10 MCC/ionic liquids' ratio.

The average diameter, length, and aspect ratio of the NCC obtained is shown in Table 4.23. The NCC exhibited increased widths (9, 10, 21, 31 nm), decreased lengths (155, 146, 123, 80 nm), and aspect ratio (17, 15, 6,3) with increasing dissolution time. Most results show that longer hydrolysis time induces shorter NCC (Pla, 2013).

Table 4.24: Diameter (nm), length (nm) and aspect ratio of NCC at increased dissolution time (NCC-1=30 minutes, NCC-2=60 minutes, NCC-3=90 minutes and NCC-4=120 minutes)

Sample	Diameter (nm)	Length (nm)	Aspect ratio
NCC-1	9 ± 0.05	155 ± 0.78	17
NCC-2	10 ± 0.16	146 ± 0.44	15
NCC-3	21 ± 0.03	123 ± 0.44	6
NCC-4	31 ± 2.6	80 ± 4.9	3

The increasing trend of NCC diameter can be explained by the re-aggregation phenomenon. NCC tends to aggregate easily, forming a branch of cellulose or network-like cellulose. As longer time was introduced during the dissolution process, more aggregations will occur, resulting in bigger dimensions of the NCC. Figure 4.20 shows the AFM images of the maximum aggregations at longer dissolution time. In contrast, the length of the NCC decreased from 155 nm to 146, 123, and 80 nm at longer dissolution time. The decreasing length could be attributed to the efficiency of the longer dissolution time in breaking the cellulose chains. Introducing longer time will cause more cleavage resulting in shorter NCC, as supported by the previous study (Fahma et al., 2010). Although longer dissolution time was proven to be efficient in breaking the cellulose chains, it will also enhance the agglomeration, thus explained

the decreased length of the NCC even though the particle diameter increases. A similar trend was also observed for the aspect ratio, whereby it decreased from 17 to 15, 6, and 3, respectively. Overall, the production of NCC was most efficient at minimum dissolution time. Figure 4.21 shows the AFM images of the NCC synthesized at different temperature (40, 60, 80, and 100 °C). On average, the NCC are 155, 290, 451, 769 nm long, 9, 20, 30, 33 nm wide, and have an aspect ratio (L/D) of 17, 14, 15, 23 for NCC-1, NCC-5, NCC-9, and NCC-13, respectively (Table 4.24). In the previous study, it was mentioned that the NCC with 30 to 120 nm diameter is very useful in tissue engineering and filtration applications (Zhao, H.-P. et al., 2007). Analysis of the result revealed a relation between regeneration yield and the morphological properties of the NCC.
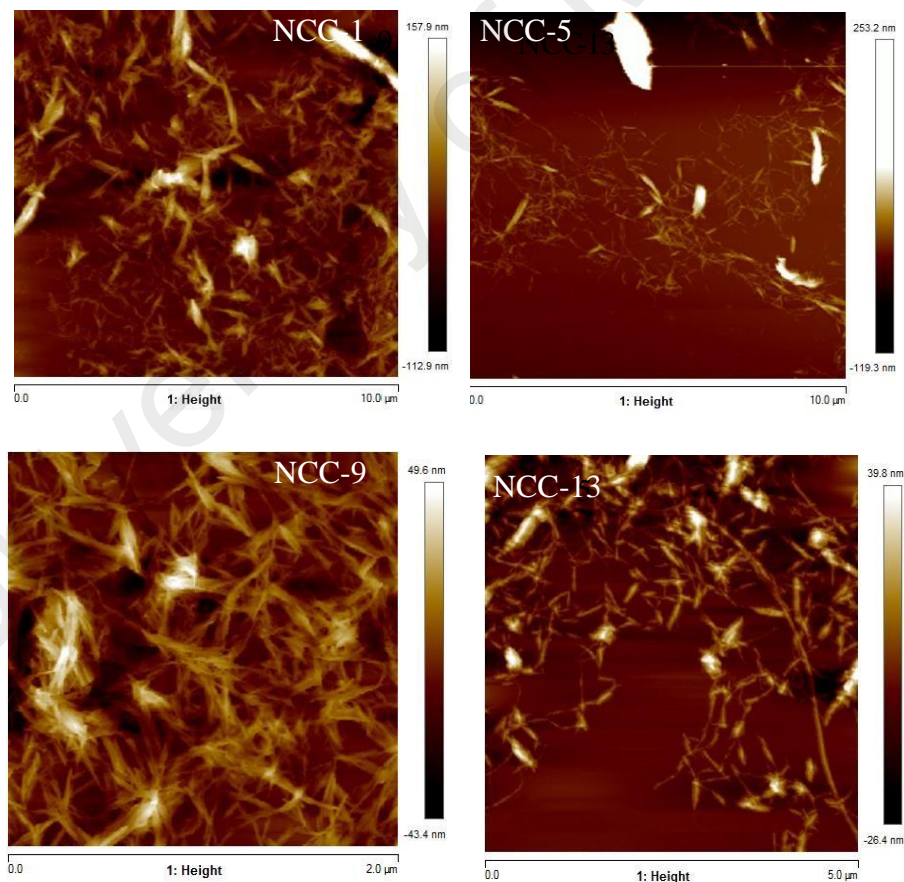
Figure 4.24: AFM images of NCC at increasing temperature (NCC-1=40 °C, NCC-5=60 °C, NCC-9=80 °C and NCC-13=100 °C)

The sample with the smallest size of NCC aggregates was 9 nm, obtained with lowest reaction temperature (40 °C). The low standard deviation acquired confirmed the accuracy and the precision of the method employed to chemically characterize all samples.

Table 4.25: Diameter (nm), Length (nm) and aspect ratio of NCC at increasing temperature (NCC-1=40 °C, NCC-5=60 °C, NCC-9=80 °C and NCC-13=100 °C)

Sample	Diameter (nm)	Length (nm)	Aspect ratio
NCC-1	9 ±0.05	155 ± 0.78	17
NCC-5	20 ± 0.37	290 ± 0.46	14
NCC-9	30 ± 0.5	451 ± 0.54	15
NCC-13	33 ± 0.28	769 ± 0.32	23

Figure 4.22 shows the optical micrograph of the NCC obtained after the chemical treatment at different MCC/ionic liquids ratio. It is worth to note that in contrast to high-molecular cellulose fibres such as cotton, flax and wood cellulose that are required to hydrolyse mandatory up to level-off DP in order to prepare NCC, the initial MCC sample is already a hydrolysed cellulose comprises the NCC aggregates. Therefore, the main aim of MCC treatment with sufficient MCC/ionic liquids ratio is corrosion of contacts between NCC aggregates and the introduction of the chloride anion that contributed to the breakdown of these aggregates at subsequent mechanical disintegration by ultrasonication.
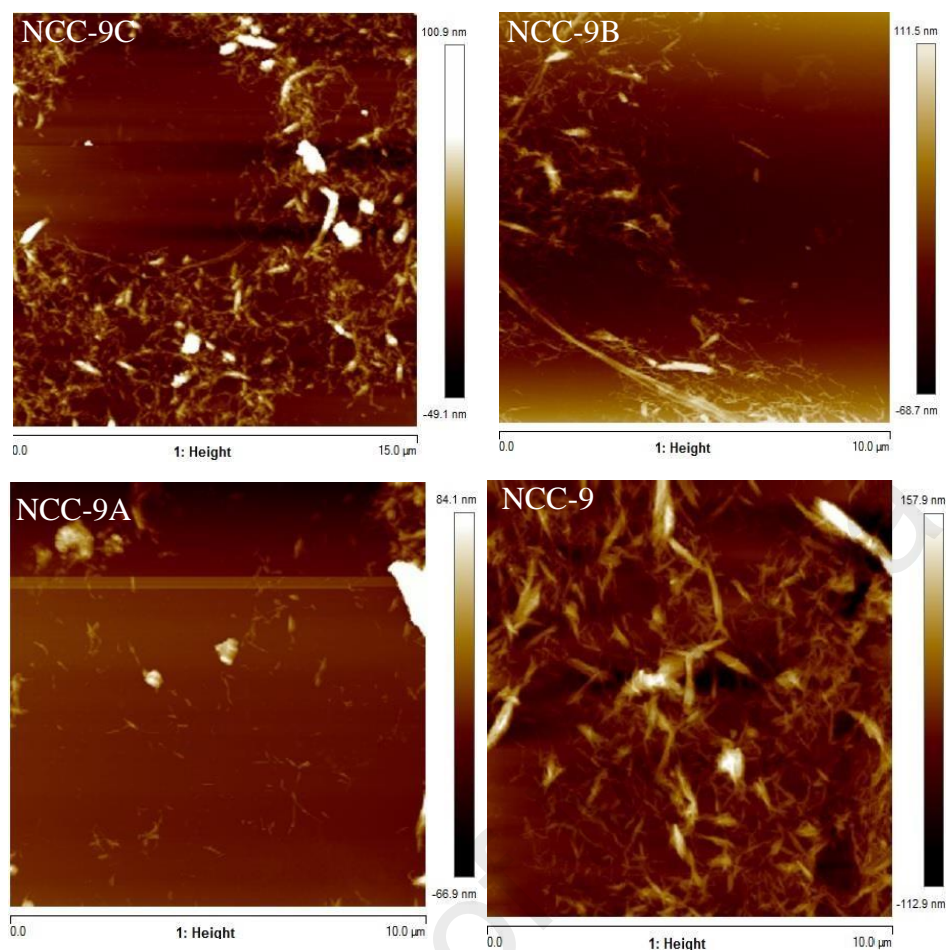
Figure 4.25: AFM images of NCC at increasing MCC/ionic liquids' ratio (NCC-9C=1;4, NCC-9B=1:6, NCC-9A=1:8 and NCC-9=1:10) [20]

Table 4.25 shows the diameter (nm), length (nm), and aspect ratio of the NCC at increasing MCC/ ionic liquids ratio. If the MCC/ ionic liquids ratio is too low (1:4), then the NCC aggregates remained intact resulting in wider dimension (54 nm) and maximum length (490 nm) of the NCC. As the MCC/ ionic liquids ratio increased to 1:6 and 1:8, the diameter and length of the NCC decreases to (27, 13 nm) and (400, 131) nm, respectively. The rate of erosion between cellulose and ILs probably increased as the ratio increases, promoting disaggregation of the NCC. However, maximum MCC/ ionic liquids ratio (1:10) causes opposite effect with increased

---

[20] Reaction condition 1: NCC-1=30 minutes, NCC-2=60 minutes, NCC-3=90 minutes, NCC-4=120 minutes reaction time 2: NCC-1=40 ºC, NCC-5=60 ºC, NCC-9=80 ºC and NCC-13=100 ºC, 3: NCC-9C=1:4, NCC-9B=1:6, NCC-9A=1:8 and NCC-9=1:10 MCC/ionic liquids' ratio.

diameter and length of the NCC (30, 451 nm), respectively. Meanwhile, the aspect ratio shows no specific trend. The high aspect ratio of the NCC provides an improved mechanical function beneficial in nanocomposite approach.

Table 4.26: Diameter (nm), Length (nm) and aspect ratio of NCC at increasing MCC/ionic liquids' ratio (NCC-9C=1;4, NCC-9B=1:6, NCC-9A=1:8 and NCC-9=1:10)

Sample	Diameter (nm)	Length (nm)	Aspect ratio
NCC-9C	54 ±0.63	490 ±2.94	9
NCC-9B	27 ±3.59	400 ± 0.24	15
NCC-9A	13 ± 0.2	131 ± 0.63	10
NCC-9	30 ± 0.5	451 ± 0.54	15

Under organized conditions, the chemical treatment was predicted to cleave the amorphous regions of the cellulose while diagonally keeping the straight crystalline domains intact. The treatment should ultimately reduce the size of the fibres from micron to the nanometre scale. This result is supported by the previous research conducted by Ioelovich, M (Ioelovich, 2012a). Thus, as the MCC/ ionic liquids ratio increased, the MCC will fully dissolve accompanied by a smaller dimension of the NCC as shown in Table 4.25. However, opposite effect was observed at maximum MCC/ ionic liquids ratio (1:10) probably due to the agglomeration of the NCC. In comparison with the previous studies, Bondeson et al. (2006) managed to successfully obtain larger NCC from MCC derived from Norway spruce, with a length between 200-400 nm and a width less than 10nm. On the other hand, the NCC separated from black spruce exhibited smaller and wider crystals, with a length of 120 nm and a diameter of 4.9 nm, giving an aspect ratio of 24 (Beck-Candanedo et al., 2005).

Nevertheless, another group isolated NCC from the bark of Norway spruce having the average aspect ratio (L/D) of about 63, showing a better result as compared to the NCC isolated from wood (Normand et al., 2014). The aspect ratio of extracted NCC is also different from those extracted from coconut husks (35-44) (Rosa, M. F. et al., 2010), sugarcane bagasse (32-64) (Teixeira et al., 2010), sisal (43-60) (Rodriguez et al., 2006), regular cotton fibre (1014) (Teixeira et al., 2010), microcrystalline cellulose (11-13) (Capadona et al., 2009; hanmuganathan et al., 2010), and flax (Linum usitatissimum) (15) (Cao et al., 2007) (Morais et al., 2013). However, the dimensions, length and aspect ratio of the NCC synthesized was within the accepted value, referring to all previous data in these studies. However, improvements on the current method should be planned in order to increase the aspect ratio of the NCC. Considering that, optimization is a well-suited step to be taken in this study.

4.4.7 Field Emission Scanning Electron Microscopy (FESEM)

The morphology of the original fibres (MCC) and after subsequent treatments at a different dissolution time, temperature, and MCC/ionic liquids ratio was investigated by SEM. Figure 4.23 (a, b, c) shows the SEM images of the NCC under various magnifications as compared to the initial source (MCC). Figure 4.23 (a,b,c) shows aggregated fibrils of the MCC and a rough surface morphology. According to the previous study, the roughness of the MCC favours the production of the NCC via hydrolysis. Similar morphologies have been observed during isolation of the MCC from OPEFB α-cellulose (Ioelovich, 2012b). It is reported that these aggregated MCC are composed of strong hydrogen bonding between hundreds of individual NCC (Haafiz, M.K.M. et al., 2014). Meanwhile, NCC images showed that the aggregation has been broken down after the treatment by the separation of the MCC bundles into

individual fibres. The length and diameter of the NCC were not measured because it is

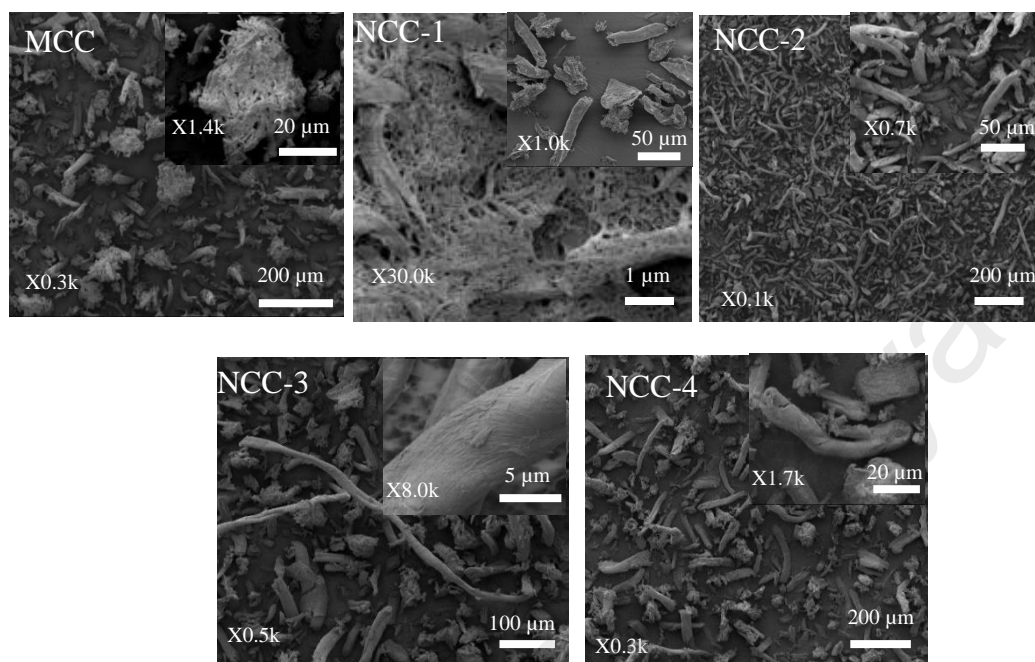challenging to clearly distinguish individual NCC from the agglomerated structures.

Figure 4.26(a): FESEM images of MCC and NCC at increased dissolution time

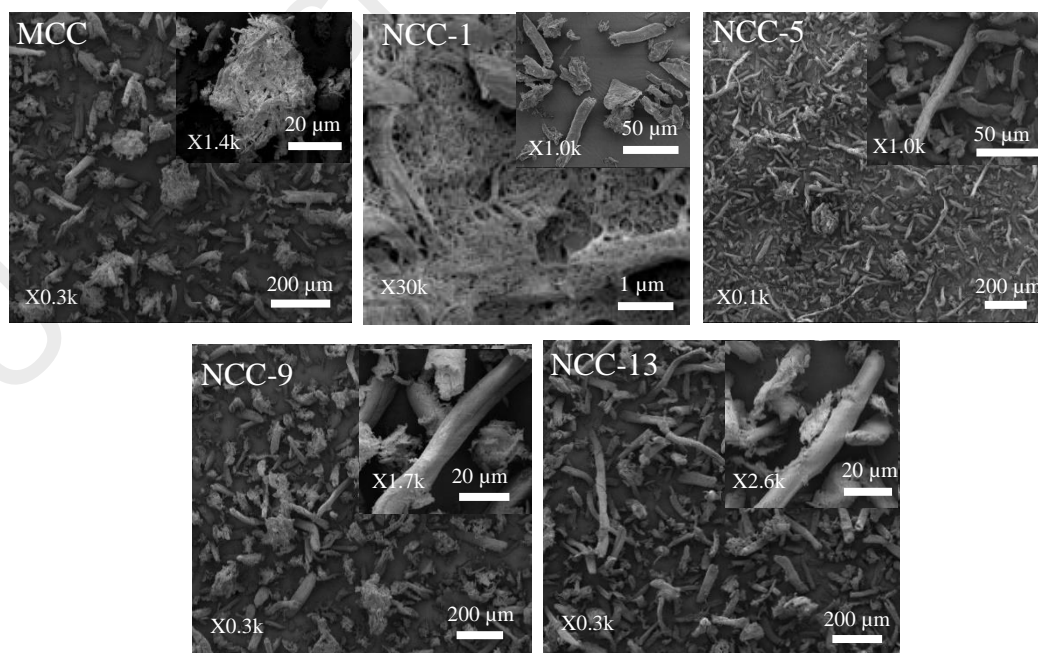**(NCC- 1=30 minutes, NCC-2=60 minutes, NCC-3=90 minutes and NCC-4=120**

minutes)

Figure 4.26(b): FESEM images of NCC at increasing temperature (NCC-1=40
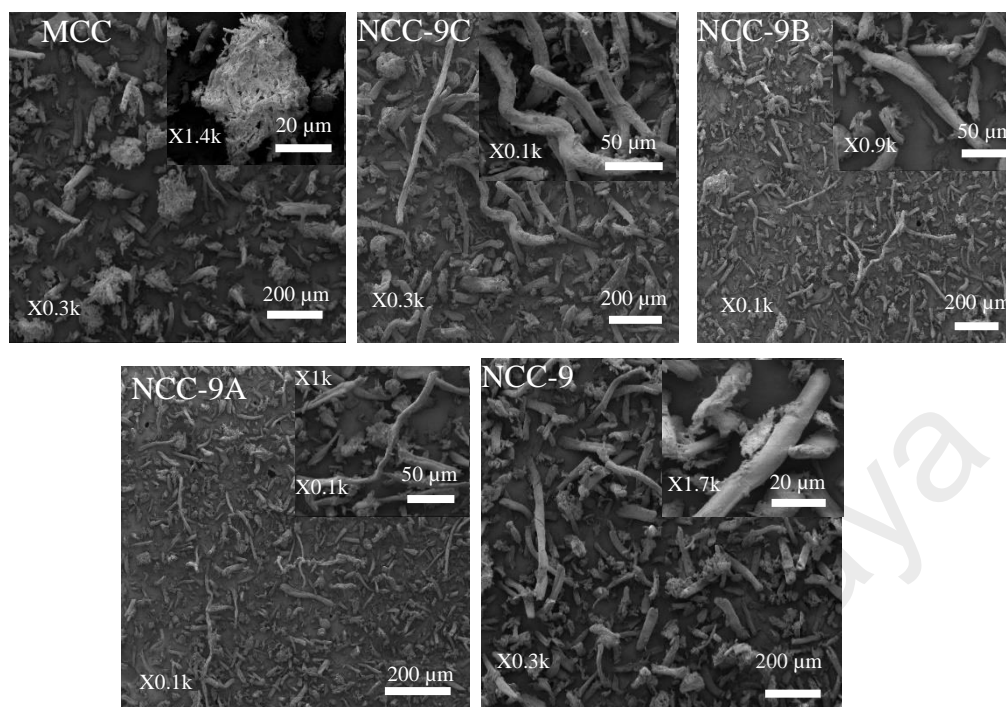
°C, NCC-5=60 °C, NCC-9=80 °C and NCC-13=100 °C)

Figure 4.26(c): FESEM images of MCC and NCC at increasing MCC/ionic liquids' ratio (NCC-9C=1;4, NCC-9B=1:6, NCC-9A=1:8 and NCC-9=1:10) [21]

FESEM and AFM images proved the effectiveness of the chemical treatment by confirming that the NCC in the aqueous suspensions consists mostly of individual crystals and some aggregates.

4.4.8 Dynamic Light Scattering (DLS)

The DLS technique has been employed to seek out the statistical distribution of the particles exist in the NCC. DLS analysis data revealed features of the defibrillation process of the MCC, which transpired with different intensities in all four samples. The statistical distribution as shown in Table 4.26 clearly depicts that majority of the NCC particles lie in the nanorange. The sample with the smallest size of NCC aggregates was 18 nm, which was obtained from the shortest dissolution time (30

---

[21] Reaction condition 1: NCC-1=30 minutes, NCC-2=60 minutes, NCC-3=90 minutes, NCC-4=120 minutes reaction time 2: NCC-1=40 ºC, NCC-5=60 ºC, NCC-9=80 ºC and NCC-13=100 ºC, 3: NCC-9C=1:4, NCC-9B=1:6, NCC-9A=1:8 and NCC-9=1:10 MCC/ionic liquids' ratio.

minutes). There has been a gradual increase in the sizes of the particles as dissolution time was extended, which reached a peak at 58 nm under 2 hours of the dissolution time.

Table 4.27: Particle distribution size of NCC at increased dissolution time (NCC-1=30 minutes, NCC-2=60 minutes, NCC-3=90 minutes and NCC-4=120 minutes)

Sample	Particle distribution size (nm)
NCC-1	18
NCC-2	25
NCC-3	48
NCC-4	58

A similar trend was observed for the NCC diameter measured by AFM technique with aggregations are the possible reasons. DLS analysis results showed various sizes of the NCC aggregates identified by light scattering when different reaction temperature being applied (Table 4.27). Figure shows the particle distribution profile for NCC-1, NCC-2, NCC-3 and NCC-4.
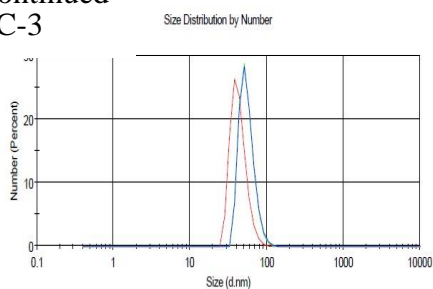
NCC-1
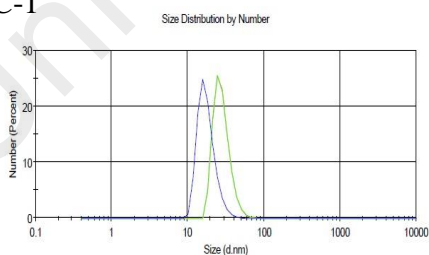
NCC-2
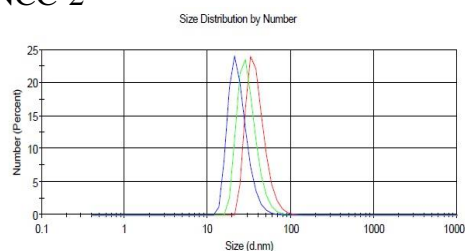
Figure 4.27, continued
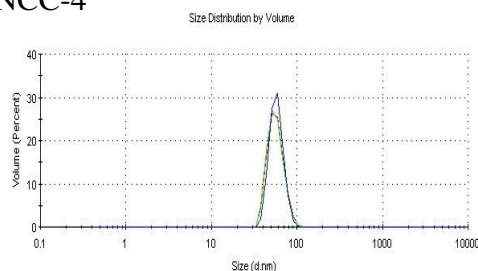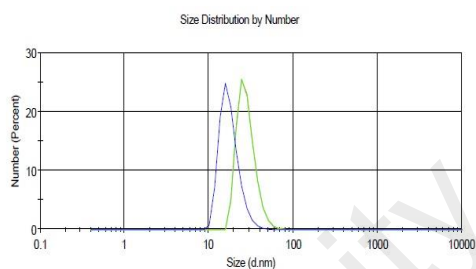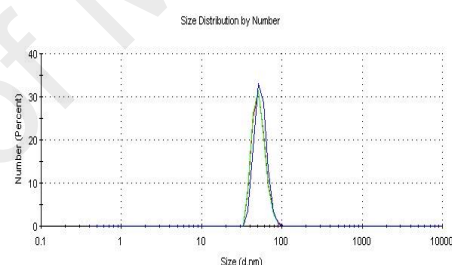
Figure 4.27, continued

NCC-3

NCC-4

Figure 4.27: Size distribution profile of NCC at increased dissolution time (NCC-1=30 minutes, NCC-2=60 minutes, NCC-3=90 minutes and NCC-4=120 minutes)

Figure 4.28 shows the size distribution profile of NCC-1, NCC-5, NCC-9 and NCC-13. The minimum particle size was found to be only 18 nm which accounted for the sample under 40 °C reaction temperature.
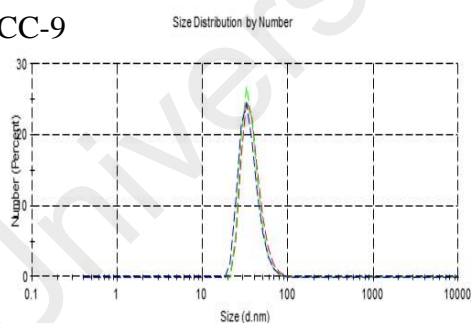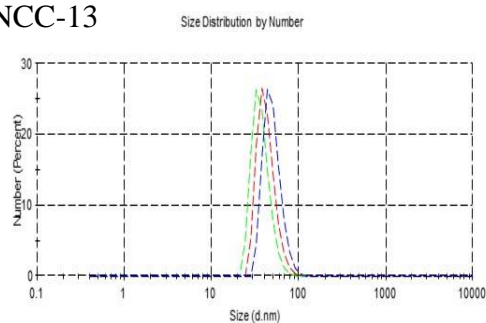
NCC-1

NCC-5

NCC-9

NCC-13

Figure 4.28: Size distribution profile of NCC at increasing temperature (NCC-1=40 °C, NCC-5=60 °C, NCC-9=80 °C and NCC-13=100 °C)[22]

---

[22] Reaction condition 1: NCC-1=30 minutes, NCC-2=60 minutes, NCC-3=90 minutes, NCC-4=120 minutes reaction time 2: NCC-1=40 ºC, NCC-5=60 ºC, NCC-9=80 ºC and NCC-13=100 ºC, 3: NCC-9C=1:4, NCC-9B=1:6, NCC-9A=1:8 and NCC-9=1:10 MCC/ionic liquids' ratio.

The minimum particle size was found to be only 18 nm which accounted for the sample under 40 °C reaction temperature. There has been an increase in the sizes of the particles as the reaction temperature was increased to 60 °C. However, the particle size gradually decreases to 36 and 32 nm as the reaction temperature increased to 80 and 100 °C, respectively.

Table 4.28: Particle distribution size of NCC at increasing temperature (NCC1=40 °C, NCC-5=60 °C, NCC-9=80 °C and NCC-13=100 °C)[23]

Sample	Particle distribution size (nm)
NCC-1	18
NCC-5	55
NCC-9	36
NCC-13	32

These results show that the minimum temperature as low as 40 °C was efficient in breaking the aggregations nature of the NCC. Since overestimation and inaccuracy can always happen when measuring the particle size by using DLS, no significant relationship can be observed between the particle sizes measured by DLS and AFM. The PSD and the average size of the NCC-9C, NCC-9B, NCC-9A, and NCC-9 were determined and the results are shown in Table 4.28.

---

[23] Reaction condition 1: NCC-1=30 minutes, NCC-2=60 minutes, NCC-3=90 minutes, NCC-4=120 minutes reaction time 2: NCC-1=40 ºC, NCC-5=60 ºC, NCC-9=80 ºC and NCC-13=100 ºC, 3: NCC-9C=1:4, NCC-9B=1:6, NCC-9A=1:8 and NCC-9=1:10 MCC/ionic liquids' ratio.

Table 4.29: Particle distribution size of NCC at increasing MCC/ionic liquids' ratio (NCC-9C=1;4, NCC-9B=1:6, NCC-9A=1:8 and NCC-9=1:10)
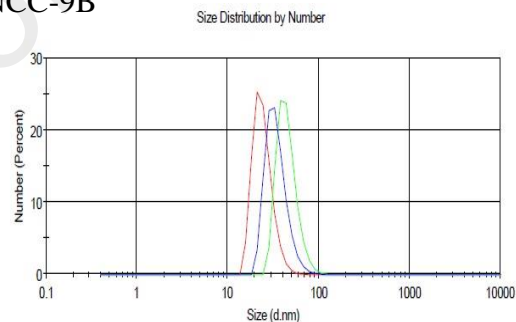
Sample	Particle distribution size (nm)
NCC-9C	48
NCC-9B	39
NCC-9A	30
NCC-9	36

Similar trend was observed for the diameter of NCC measured by AFM technique with re-aggregations of NCC-9 sample as the most possible reasons. Figure shows the size distribution profile of NCC-9C, NCC-9B, NCC-9A and NCC-9.
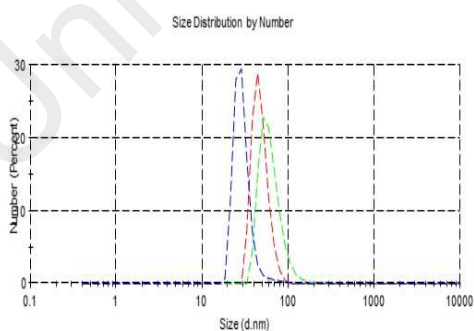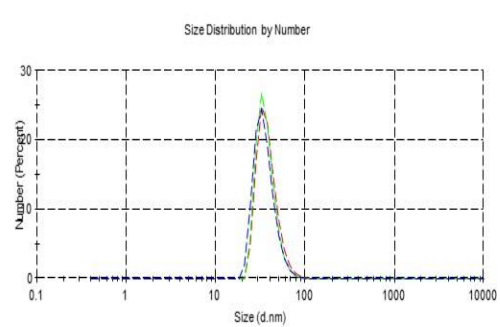
NCC-9C
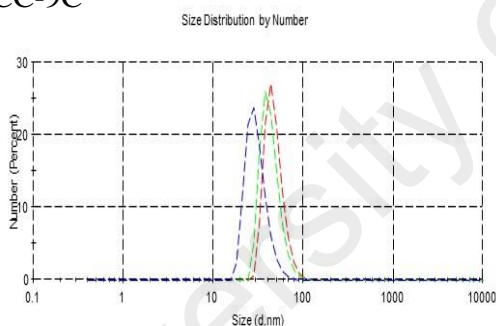
NCC-9B

NCC-9A

NCC-9

Figure 4.29: Size distribution profile of at increasing MCC/ionic liquids' ratio (NCC-9C=1;4, NCC-9B=1:6, NCC-9A=1:8 and NCC-9=1:10)

Even though DLS measurements tend to overestimate the actual sample particle size, all the NCC showed a relatively narrow range of the size distribution. In the previous study, overestimation of the particle size by DLS technique could happen since NCC were not ideal spheres (Chang, 2010).

4.5 Mechanism

The ability of [Bmim][Cl] to cleave the extensive hydrogen bonding network of the complex macromolecules and polymers, and promoting dissolution of the complexes with high efficiency deem it as a suitable candidate of solvent. The presence of small chloride anion and large cation accounts for its efficacy in the cellulose disintegration process. Oxygen atoms of the cellulose hydroxyl group act as an electron acceptors while ILs cations serve as electron donors (Tan, H. T. et al., 2012). The chloride anions interact with hydrogen atoms while the formation of inter- and intra- molecular hydrogen bonds is easily developed between the 1-butyl-3-methylimidazolium cation and oxygen. For this to occur, the original hydrogen bonds were broken, and the new hydrogen bonds enable the cellulose to dissolve in [Bmim][Cl]. On the contrary, ILs could not extract hemicelluloses even though it contains inter- and intra-molecular hydrogen bonds because hemicelluloses are linked to lignin by covalent bonds, such as the α-aryl ether bond, which proves to be stronger than hydrogen bonds (Li et al., 2013). Conversely, the electron rich aromatic π system cation interacts weakly with the hydroxyl oxygen atom through nonbonding or л electrons, whereas anion interacts with the cellulose via the hydrogen bond to the hydroxyl proton (Tan, H. T. et al., 2012). Regeneration of the dissolved cellulose can easily take place by precipitation from ILs via the addition of anti-solvent such as water, methanol, ethanol, and acetone. The ions of the ILs form hydrogen bonds with water molecules during the addition of the anti-solvent such as water to the ILs and biomass mixture and are displaced into the aqueous phase. Hydrodynamic shells built up by water molecules

115

around the ions of ILs shielded the interactions between ILs and cellulose. Accordingly, cellulose, which was expelled during the interaction with ILs rebuilt its intra and intermolecular hydrogen bonds and then was precipitated. Eventually, the precipitate is separated from ILs by centrifugation (Tan, H. T. et al., 2012). Based on the aspect ratio value, the following optimal conditions of the ionic liquids treatment were recorded at 40 °C reaction temperature, 120 minutes dissolution time, and MCC/ionic liquids ratio of 1:10.

CHAPTER 5: CONCLUSIONS

- Increasing the vibration amplitude of ultrasonication had increased the yield, crystallinity index and thermal stability of nanocrystalline cellulose.

- At 90% vibration amplitude, 90% yield of nanocrystalline cellulose was obtained, with 70% crystallinity index and 330-350 °C degradation temperature.

- Decreasing the ultrasonication time had improved the crystallinity index, thermal properties and particle size of nanocrystalline cellulose

- At 5 minutes ultrasonication time, 73% crystallinity index with degradation temperature between 328-350 °C and 9 nm of nanocrystalline cellulose was obtained.

- Increasing the temperature, dissolution time and MCC to ionic liquids' ratio had enhances the yield, crystalline and thermal properties of nanocrystalline cellulose.

- No changes in the crystalline structure (Cellulose I) was shown, as observed by XRD and FTIR.

- From this study, a significant relationship can be observed between crystalline value and thermal stability of nanocrystalline cellulose when the vibration amplitude, ultrasonication time, dissolution time and MCC/ionic liquids' ratio were varied.

- Correlation between particle distribution size measured by DLS and AFM was also observed.

- Optimized conditions were finally determined to be as follows: vibration amplitude (70%), ultrasonication time (5 minutes), temperature (100 °C), dissolution time (30 minutes) and MCC/ionic liquids' ratio (1:10).

REFERENCES

Abe, K., Iwamoto, S., & Yano, H. (2007). Obtaining cellulose nanofibers with a uniform width of 15 nm from wood. Biomacromolecules, 8(10), 3276-3278.

Abnisa, F., Arami-Niya, A., Daud, W. W., Sahu, J. N., & Noor, I. M. (2013). Utilization of oil palm tree residues to produce bio-oil and bio-char via pyrolysis. Energy Conversion and Management, 76, 1073-1082.

Abraham, E., Deepa, B., Pothan, L. A., Jacob, M., Thomas, S., Cvelbar, U., & Anandjiwala, R. (2011). Extraction of nanocellulose fibrils from lignocellulosic fibres: a novel approach. Carbohydrate Polymers, 86(4), 1468-1475.

Araki, J., Wada, M., & Kuga, S. (2001). Steric stabilization of a cellulose microcrystal suspension by poly (ethylene glycol) grafting. Langmuir, 17(1), 21-27.

Azizi Samir, M. A. S., Alloin, F., & Dufresne, A. (2005). Review of recent research into cellulosic whiskers, their properties and their application in nanocomposite field. Biomacromolecules, 6(2), 612-626.

Bai, W., Holbery, J., & Li, K. (2009). A technique for production of nanocrystalline cellulose with a narrow size distribution. Cellulose, 16(3), 455-465.

Beck-Candanedo, S., Roman, M., & Gray, D. G. (2005). Effect of reaction conditions on the properties and behavior of wood cellulose nanocrystal suspensions. Biomacromolecules, 6(2), 1048-1054.

Beck, S., Bouchard, J., & Berry, R. (2016). U.S. Patent No. 9,394,481. Washington, DC: U.S. Patent and Trademark Office.

Belbekhouche, S., Bras, J., Siqueira, G., Chappey, C., Lebrun, L., Khelifi, B., ... & Dufresne, A. (2011). Water sorption behavior and gas barrier properties of cellulose whiskers and microfibrils films. Carbohydrate Polymers, 83(4), 1740-1748.

Bian, J., Peng, F., Peng, X. P., Xiao, X., Peng, P., Xu, F., & Sun, R. C. (2014). Effect of [Emim] Ac pretreatment on the structure and enzymatic hydrolysis of sugarcane bagasse cellulose. Carbohydrate polymers, 100, 211-217.

Bondeson, D., Mathew, A., & Oksman, K. (2006). Optimization of the isolation of nanocrystals from microcrystalline cellulose by acid hydrolysis. Cellulose, 13(2), 171-180.

Börjesson, M., & Westman, G. (2015). Crystalline Nanocellulose—Preparation, Modification, and Properties. In Cellulose-Fundamental Aspects and Current Trends. InTech.

Brinchi, L., Cotana, F., Fortunati, E., & Kenny, J. M. (2013). Production of nanocrystalline cellulose from lignocellulosic biomass: technology and applications. Carbohydrate Polymers, 94(1), 154-169.

118

Camacho, F., Gonzalez-Tello, P., Jurado, E., & Robles, A. (1996). Microcrystalline-cellulose hydrolysis with concentrated sulphuric acid. Journal of chemical technology and biotechnology, 67(4), 350-356.

Cao, X., Dong, H., & Li, C. M. (2007). New nanocomposite materials reinforced with flax cellulose nanocrystals in waterborne polyurethane. *Biomacromolecules*, *8*(3), 899-904.

Cao, Y., Wu, J., Zhang, J., Li, H., Zhang, Y., & He, J. (2009). Room temperature ionic liquids (RTILs): a new and versatile platform for cellulose processing and derivatization. Chemical Engineering Journal, 147(1), 13-21.

Chang, C. P., Wang, I. C., Hung, K. J., & Perng, Y. S. (2010). Preparation and characterization of nanocrystalline cellulose by acid hydrolysis of cotton linter. Taiwan J For Sci, 25(3), 251-264.

Chen, Y., Liu, C., Chang, P. R., Cao, X., & Anderson, D. P. (2009). Bionanocomposites based on pea starch and cellulose nanowhiskers hydrolyzed from pea hull fibre: effect of hydrolysis time. Carbohydrate Polymers, 76(4), 607-615.

Chen, W., Yu, H., Liu, Y., Chen, P., Zhang, M., & Hai, Y. (2011). Individualization of cellulose nanofibers from wood using high-intensity ultrasonication combined with chemical pretreatments. Carbohydrate Polymers, 83(4), 1804-1811

Chen, W., Yu, H., Liu, Y., Hai, Y., Zhang, M., & Chen, P. (2011). Isolation and characterization of cellulose nanofibers from four plant cellulose fibers using a chemical-ultrasonic process. Cellulose, 18(2), 433-442.

Chenampulli, S., Unnikrishnan, G., Sujith, A., Thomas, S., & Francis, T. (2013). Cellulose nano-particles from Pandanus: viscometric and crystallographic studies. Cellulose, 20(1), 429-438.

Cheng, J. Y., & Chu, Y. H. (2006). 1-Butyl-2, 3-trimethyleneimidazolium bis (trifluoromethylsulfonyl) imide ([b-3C-im][NTf 2]): a new, stable ionic liquid. Tetrahedron letters, 47(10), 1575-1579.

Cherian, B. M., Leão, A. L., de Souza, S. F., Thomas, S., Pothan, L. A., & Kottaisamy, M. (2010). Isolation of nanocellulose from pineapple leaf fibres by steam explosion. Carbohydrate Polymers, 81(3), 720-725.

D'Arrigo, P., Allegretti, C., Tamborini, S., Formantici, C., Galante, Y., Pollegioni, L., & Mele, A. (2014). Single-batch, homogeneous phase depolymerization of cellulose catalyzed by a monocomponent endocellulase in ionic liquid [BMIM][Cl]. Journal of Molecular Catalysis B: Enzymatic, 106, 76-80.

De Souza Lima, M. M., Wong, J. T., Paillet, M., Borsali, R., & Pecora, R. (2003). Translational and rotational dynamics of rodlike cellulose whiskers. Langmuir, 19(1), 24-29.

Deepa, B., Abraham, E., Cherian, B. M., Bismarck, A., Blaker, J. J., Pothan, L. A., ... & Kottaisamy, M. (2011). Structure, morphology and thermal characteristics of

banana nano fibers obtained by steam explosion. Bioresource Technology, 102(2), 1988-1997.

Dharaskar, S. A., Varma, M. N., Shende, D. Z., Yoo, C. K., & Wasewar, K. L. (2013). Synthesis, characterization and application of 1-butyl-3 methylimidazolium chloride as green material for extractive desulfurization of liquid fuel. The Scientific World Journal, 2013.

Dufresne, A., Cavaillé, J. Y., & Helbert, W. (1997). Thermoplastic nanocomposites filled with wheat straw cellulose whiskers. Part II: effect of processing and modeling. Polymer composites, 18(2), 198-210.

Dufresne, A., Dupeyre, D., & Vignon, M. R. (2000). Cellulose microfibrils from potato tuber cells: processing and characterization of starch–cellulose microfibril composites. Journal of Applied Polymer Science, 76(14), 2080-2092.

Elazzouzi-Hafraoui, S., Nishiyama, Y., Putaux, J. L., Heux, L., Dubreuil, F., & Rochas, C. (2007). The shape and size distribution of crystalline nanoparticles prepared by acid hydrolysis of native cellulose. Biomacromolecules, 9(1), 57-65.

Elmabrouk, A. B., Wim, T., Dufresne, A., & Boufi, S. (2009). Preparation of poly (styrene-co-hexylacrylate)/cellulose whiskers nanocomposites via miniemulsion polymerization. Journal of applied polymer science, 114(5), 2946-2955.

Fahma, F., Iwamoto, S., Hori, N., Iwata, T., & Takemura, A. (2010). Isolation, preparation, and characterization of nanofibers from oil palm empty-fruit-bunch (OPEFB). Cellulose, 17(5), 977-985.

Feng, L., & Chen, Z. L. (2008). Research progress on dissolution and functional modification of cellulose in ionic liquids. Journal of Molecular Liquids, 142(1), 1-5

FitzPatrick, M., Champagne, P., Cunningham, M. F., & Whitney, R. A. (2010). A biorefinery processing perspective: treatment of lignocellulosic materials for the production of value-added products. Bioresource technology, 101(23), 8915-8922.

Fortunati, E., Puglia, D., Monti, M., Peponi, L., Santulli, C., Kenny, J. M., & Torre, L. (2013). Extraction of cellulose nanocrystals from Phormium tenax fibres. Journal of Polymers and the Environment, 21(2), 319-328.

Frone, A. N., Panaitescu, D. M., Donescu, D., Spataru, C. I., Radovici, C., Trusca, R., & Somoghi, R. (2011). Preparation and characterization of PVA composites with cellulose nanofibers obtained by ultrasonication. BioResources, 6(1), 487-512.

Fukaya, Y., Sugimoto, A., & Ohno, H. (2006). Superior solubility of polysaccharides in low viscosity, polar, and halogen-free 1, 3-dialkylimidazolium formates. Biomacromolecules, 7(12), 3295-3297.

Guo, H., Qi, X., Li, L., & Smith, R. L. (2012). Hydrolysis of cellulose over functionalized glucose-derived carbon catalyst in ionic liquid. Bioresource technology, 116, 355-359.

Guo, Y. H., Xiao, L., & Cao, F. (2015). Theoretical study on the activity of hydrogen atom of imidazolium ring in ionic liquids. Computational and Theoretical Chemistry, 1067, 7-12.

Gupta, K. M., & Jiang, J. (2015). Cellulose dissolution and regeneration in ionic liquids: A computational perspective. Chemical Engineering Science, 121, 180-189.

Haafiz, M. M., Hassan, A., Zakaria, Z., & Inuwa, I. M. (2014). Isolation and characterization of cellulose nanowhiskers from oil palm biomass microcrystalline cellulose. Carbohydrate Polymers, 103, 119-125.

Haafiz, M. M., Hassan, A., Zakaria, Z., Inuwa, I. M., & Islam, M. S. (2013). Physicochemical characterization of cellulose nanowhiskers extracted from oil palm biomass microcrystalline cellulose. Materials Letters, 113, 87-89.

Habibi, Y., Lucia, L. A., & Rojas, O. J. (2010). Cellulose nanocrystals: chemistry, self-assembly, and applications. Chemical reviews, 110(6), 3479-3500.

Habibi, Y., Mahrouz, M., & Vignon, M. R. (2009). Microfibrillated cellulose from the peel of prickly pear fruits. Food Chemistry, 115(2), 423-429.

Hao, Y., Peng, J., Ao, Y., Li, J., & Zhai, M. (2012). Radiation effects on microcrystalline cellulose in 1-butyl-3-methylimidazolium chloride ionic liquid. Carbohydrate polymers, 90(4), 1629-1633.

Heinze, T., Schwikal, K., & Barthel, S. (2005). Ionic liquids as reaction medium in cellulose functionalization. Macromolecular bioscience, 5(6), 520-525.

Hernoux-Villière, A., Lévêque, J. M., Kärkkäinen, J., Papaiconomou, N., Lajunen, M., & Lassi, U. (2014). Task-specific ionic liquid for the depolymerisation of starch-based industrial waste into high reducing sugars. Catalysis Today, 223, 11-17.

Hu, X., Xiao, Y., Niu, K., Zhao, Y., Zhang, B., & Hu, B. (2013). Functional ionic liquids for hydrolysis of lignocellulose. Carbohydrate polymers, 97(1), 172-176.

Ibrahim, M. M., El-Zawawy, W. K., Jüttke, Y., Koschella, A., & Heinze, T. (2013). Cellulose and microcrystalline cellulose from rice straw and banana plant waste: preparation and characterization. Cellulose, 20(5), 2403-2416.

Ioelovich, M. (2012). Study of cellulose interaction with concentrated solutions of sulfuric acid. ISRN Chemical Engineering, 2012.

Isik, M., Sardon, H., & Mecerreyes, D. (2014). Ionic liquids and cellulose: Dissolution, chemical modification and preparation of new cellulosic materials. International journal of molecular sciences, 15(7), 11922-11940.

121

Jahan, M. S., Saeed, A., He, Z., & Ni, Y. (2011). Jute as raw material for the preparation of microcrystalline cellulose. Cellulose, 18(2), 451-459.

Jiang, F., & Hsieh, Y. L. (2013). Chemically and mechanically isolated nanocellulose and their self-assembled structures. Carbohydrate Polymers, 95(1), 32-40.

Jiang, M., Zhao, M., Zhou, Z., Huang, T., Chen, X., & Wang, Y. (2011). Isolation of cellulose with ionic liquid from steam exploded rice straw. Industrial Crops and Products, 33(3), 734-738.

Johar, N., Ahmad, I., & Dufresne, A. (2012). Extraction, preparation and characterization of cellulose fibres and nanocrystals from rice husk. Industrial Crops and Products, 37(1), 93-99.

Khalil, H. A., Bhat, A. H., & Yusra, A. I. (2012). Green composites from sustainable cellulose nanofibrils: a review. Carbohydrate Polymers, 87(2), 963-979.

Khalil, H. A., Davoudpour, Y., Islam, M. N., Mustapha, A., Sudesh, K., Dungani, R., & Jawaid, M. (2014). Production and modification of nanofibrillated cellulose using various mechanical processes: a review. Carbohydrate Polymers, 99, 649-665.

Kim, H. Y., Han, J. A., Kweon, D. K., Park, J. D., & Lim, S. T. (2013). Effect of ultrasonic treatments on nanoparticle preparation of acid-hydrolyzed waxy maize starch. Carbohydrate polymers, 93(2), 582-588.

Kimura, F., Kimura, T., Tamura, M., Hirai, A., Ikuno, M., & Horii, F. (2005). Magnetic alignment of the chiral nematic phase of a cellulose microfibril suspension. Langmuir, 21(5), 2034-2037.

Komanoya, T., Kobayashi, H., Hara, K., Chun, W. J., & Fukuoka, A. (2011). Catalysis and characterization of carbon-supported ruthenium for cellulose hydrolysis. Applied Catalysis A: General, 407(1), 188-194.

Kosan, B., Michels, C., & Meister, F. (2008). Dissolution and forming of cellulose with ionic liquids. Cellulose, 15(1), 59-66.

Lai, D. M., Deng, L., Guo, Q. X., & Fu, Y. (2011). Hydrolysis of biomass by magnetic solid acid. Energy & Environmental Science, 4(9), 3552-3557.

Lamaming, J., Hashim, R., Leh, C. P., & Sulaiman, O. (2017). Properties of cellulose nanocrystals from oil palm trunk isolated by total chlorine free method. Carbohydrate Polymers, 156, 409-416.

Lavoine, N., Desloges, I., Dufresne, A., & Bras, J. (2012). Microfibrillated cellulose– Its barrier properties and applications in cellulosic materials: A review. Carbohydrate polymers, 90(2), 735-764.

Lazko, J., Sénéchal, T., Landercy, N., Dangreau, L., Raquez, J. M., & Dubois, P. (2014). Well defined thermostable cellulose nanocrystals via two-step ionic liquid swelling-hydrolysis extraction. Cellulose, 21(6), 4195-4207

Le Normand, M., Moriana, R., & Ek, M. (2014). Isolation and characterization of cellulose nanocrystals from spruce bark in a biorefinery perspective. Carbohydrate polymers, 111, 979-987.

Lee, S. H., Doherty, T. V., Linhardt, R. J., & Dordick, J. S. (2009). Ionic liquid-mediated selective extraction of lignin from wood leading to enhanced enzymatic cellulose hydrolysis. Biotechnology and Bioengineering, 102(5), 1368-1376.

Li, R., Fei, J., Cai, Y., Li, Y., Feng, J., & Yao, J. (2009). Cellulose whiskers extracted from mulberry: A novel biomass production. Carbohydrate Polymers, 76(1), 94-99.

Liu, C. F., Ren, J. L., Xu, F., Liu, J. J., Sun, J. X., & Sun, R. C. (2006). Isolation and characterization of cellulose obtained from ultrasonic irradiated sugarcane bagasse. Journal of agricultural and food chemistry, 54(16), 5742-5748.

Liu, L., Ju, M., Li, W., & Hou, Q. (2013). Dissolution of cellulose from AFEX-pretreated Zoysia japonica in AMIMCl with ultrasonic vibration. Carbohydrate polymers, 98(1), 412-420.

Liu, Y., Xiao, W., Xia, S., & Ma, P. (2013). SO 3 H-functionalized acidic ionic liquids as catalysts for the hydrolysis of cellulose. Carbohydrate polymers, 92(1), 218-222.

Lu, P., & Hsieh, Y. L. (2012). Preparation and characterization of cellulose nanocrystals from rice straw. Carbohydrate Polymers, 87(1), 564-573.

Maheswari, C. U., Reddy, K. O., Muzenda, E., Guduri, B. R., & Rajulu, A. V. (2012). Extraction and characterization of cellulose microfibrils from agricultural residue–Cocos nucifera L. Biomass and bioenergy, 46, 555-563.

Man, Z., Muhammad, N., Sarwono, A., Bustam, M. A., Kumar, M. V., & Rafiq, S. (2011). Preparation of cellulose nanocrystals using an ionic liquid. Journal of Polymers and the Environment, 19(3), 726-731.

Mandal, A., & Chakrabarty, D. (2011). Isolation of nanocellulose from waste sugarcane bagasse (SCB) and its characterization. Carbohydrate Polymers, 86(3), 1291-1299.

Mao, J., Heck, B., Reiter, G., & Laborie, M. P. (2015). Cellulose nanocrystals' production in near theoretical yields by 1-butyl-3-methylimidazolium hydrogen sulfate ([Bmim] HSO 4)–mediated hydrolysis. Carbohydrate polymers, 117, 443-451.

Mishra, S. P., Manent, A. S., Chabot, B., & Daneault, C. (2011). Production of nanocellulose from native cellulose–various options utilizing ultrasound. BioResources, 7(1), 0422-0436.

Mohd Basyaruddin, A. R., Ishak, Z. I., Abdullah, D. K., Aziz, A. A., Basri, M., & Salleh, A. B. (2012). Swelling and dissolution of oil palm biomass in ionic liquids. Journal of Oil Palm Research, 24(April), 1267-1276.

Montalbo-Lomboy, M., & Grewell, D. (2015). Rapid dissolution of switchgrass in 1-butyl-3-methylimidazolium chloride by ultrasonication. Ultrasonics sonochemistry, 22, 588-599.

Moon, R. J., Martini, A., Nairn, J., Simonsen, J., & Youngblood, J. (2011). Cellulose nanomaterials review: structure, properties and nanocomposites. Chemical Society Reviews, 40(7), 3941-3994

Morais, J. P. S., de Freitas Rosa, M., Nascimento, L. D., do Nascimento, D. M., & Cassales, A. R. (2013). Extraction and characterization of nanocellulose structures from raw cotton linter. Carbohydrate polymers, 91(1), 229-235.

Morán, J. I., Alvarez, V. A., Cyras, V. P., & Vázquez, A. (2008). Extraction of cellulose and preparation of nanocellulose from sisal fibers. Cellulose, 15(1), 149-159.

Ohno, H., & Fukaya, Y. (2008). Task specific ionic liquids for cellulose technology. Chemistry Letters, 38(1), 2-7.

Olivier-Bourbigou, H., Magna, L., & Morvan, D. (2010). Ionic liquids and catalysis: Recent progress from knowledge to applications. Applied Catalysis A: General, 373(1), 1-56.

Paul, S. A., Oommen, C., Joseph, K., Mathew, G., & Thomas, S. (2010). The role of interface modification on thermal degradation and crystallization behavior of composites from commingled polypropylene fiber and banana fiber. Polymer Composites, 31(6), 1113-1123.

Peng, B. L., Dhar, N., Liu, H. L., & Tam, K. C. (2011). Chemistry and applications of nanocrystalline cellulose and its derivatives: a nanotechnology perspective. The Canadian Journal of Chemical Engineering, 89(5), 1191-1206.

Pranger, L., & Tannenbaum, R. (2008). Biobased nanocomposites prepared by in situ polymerization of furfuryl alcohol with cellulose whiskers or montmorillonite clay. Macromolecules, 41(22), 8682-8687.

Qing, Y., Sabob, R., Zhub, J. Y., Cai, Z., & Wu, Y. (2013). Comparative study of cellulose nanofibrils Disintegrated from different Approaches. Bioresource Technology, 130, 783-788.

Qiu, Z., Aita, G. M., & Walker, M. S. (2012). Effect of ionic liquid pretreatment on the chemical composition, structure and enzymatic hydrolysis of energy cane bagasse. Bioresource Technology, 117, 251-256.

Qua, E. H., Hornsby, P. R., Sharma, H. S. S., & Lyons, G. (2011). Preparation and characterisation of cellulose nanofibres. Journal of Materials Science, 46(18), 6029-6045.

Rebouillat, S., & Pla, F. (2013). State of the art manufacturing and engineering of nanocellulose: a review of available data and industrial applications. Journal of Biomaterials and Nanobiotechnology, 4(2), 165.

Rondeau-Mouro, C., Bouchet, B., Pontoire, B., Robert, P., Mazoyer, J., & Buléon, A. (2003). Structural features and potential texturising properties of lemon and maize cellulose microfibrils. Carbohydrate Polymers, 53(3), 241-252.

Remsing, R. C., Swatloski, R. P., Rogers, R. D., & Moyna, G. (2006). Mechanism of cellulose dissolution in the ionic liquid 1-n-butyl-3-methylimidazolium chloride: a 13 C and 35/37 Cl NMR relaxation study on model systems. Chemical Communications, (12), 1271-1273.

Revol, J. F. (1982). On the cross-sectional shape of cellulose crystallites in Valonia ventricosa. Carbohydrate Polymers, 2(2), 123-134.

Rinaldi, R., & Schüth, F. (2009). Design of solid catalysts for the conversion of biomass. Energy & Environmental Science, 2(6), 610-626.

Rosa, M. F., Medeiros, E. S., Malmonge, J. A., Gregorski, K. S., Wood, D. F., Mattoso, L. H. C., ... & Imam, S. H. (2010). Cellulose nanowhiskers from coconut husk fibers: Effect of preparation conditions on their thermal and morphological behavior. Carbohydrate Polymers, 81(1), 83-92.

Schlufter, K., Schmauder, H. P., Dorn, S., & Heinze, T. (2006). Efficient Homogeneous Chemical Modification of Bacterial Cellulose in the Ionic Liquid 1-N-Butyl-3-methylimidazolium Chloride. Macromolecular rapid communications, 27(19), 1670-1676.

Segal, L. G. J. M. A., Creely, J. J., Martin Jr, A. E., & Conrad, C. M. (1959). An empirical method for estimating the degree of crystallinity of native cellulose using the X-ray diffractometer. Textile Research Journal, 29(10), 786-794.

Sheltami, R. M., Abdullah, I., Ahmad, I., Dufresne, A., & Kargarzadeh, H. (2012). Extraction of cellulose nanocrystals from mengkuang leaves (Pandanus tectorius). Carbohydrate Polymers, 88(2), 772-779.

Silvério, H. A., Neto, W. P. F., Dantas, N. O., & Pasquini, D. (2013). Extraction and characterization of cellulose nanocrystals from corncob for application as reinforcing agent in nanocomposites. Industrial Crops and Products, 44, 427-436.

Singh, S., Varanasi, P., Singh, P., Adams, P. D., Auer, M., & Simmons, B. A. (2013). Understanding the impact of ionic liquid pretreatment on cellulose and lignin via thermochemical analysis. Biomass and Bioenergy, 54, 276-283.

Siró, I., & Plackett, D. (2010). Microfibrillated cellulose and new nanocomposite materials: a review. Cellulose, 17(3), 459-494.

Soom, R. M., Aziz, A. A., & Wan Hasamudin, W. H. (2009). Solid-state characteristics of microcrystalline cellulose from oil palm empty fruit bunch fibre. Journal of oil palm research, 21(June), 613-620.

Spence, K. L., Venditti, R. A., Rojas, O. J., Habibi, Y., & Pawlak, J. J. (2011). A comparative study of energy consumption and physical properties of

microfibrillated cellulose produced by different processing methods. Cellulose, 18(4), 1097-1111.

Sun, Y., Lin, L., Deng, H., Li, J., He, B., Sun, R., & Ouyang, P. (2008). Structural changes of bamboo cellulose in formic acid. BioResources, 3(2), 297-315.

Suzuki, T., Kono, K., Shimomura, K., & Minami, H. (2014). Preparation of cellulose particles using an ionic liquid. Journal of colloid and interface science, 418, 126-131.

Swatloski, R. P., Spear, S. K., Holbrey, J. D., & Rogers, R. D. (2002). Dissolution of cellose with ionic liquids. Journal of the American Chemical Society, 124(18), 4974-4975.

Tan, H. T., & Lee, K. T. (2012). Understanding the impact of ionic liquid pretreatment on biomass and enzymatic hydrolysis. Chemical Engineering Journal, 183, 448-458.

Tan, X. Y., Hamid, S. B. A., & Lai, C. W. (2015). Preparation of high crystallinity cellulose nanocrystals (CNCs) by ionic liquid solvolysis. Biomass and Bioenergy, 81, 584-591.

Tang, Y., Yang, S., Zhang, N., & Zhang, J. (2014). Preparation and characterization of nanocrystalline cellulose via low-intensity ultrasonic-assisted sulfuric acid hydrolysis. Cellulose, 21(1), 335-346.

Tian, J., Wang, J., Zhao, S., Jiang, C., Zhang, X., & Wang, X. (2010). Hydrolysis of cellulose by the heteropoly acid $H_3PW_{12}O_{40}$. Cellulose, 17(3), 587-594.

Tingaut, P., Zimmermann, T., & Sèbe, G. (2012). Cellulose nanocrystals and microfibrillated cellulose as building blocks for the design of hierarchical functional materials. Journal of Materials Chemistry, 22(38), 20105-20111.

Torres, F. G., Commeaux, S., & Troncoso, O. P. (2012). Biocompatibility of bacterial cellulose based biomaterials. Journal of functional biomaterials, 3(4), 864-878.

Vitz, J., Erdmenger, T., Haensch, C., & Schubert, U. S. (2009). Extended dissolution studies of cellulose in imidazolium based ionic liquids. Green chemistry, 11(3), 417-424.

Wang, S., & Cheng, Q. (2009). A novel process to isolate fibrils from cellulose fibers by high-intensity ultrasonication, Part 1: Process optimization. Journal of Applied Polymer Science, 113(2), 1270-1275.

Wang, Y., Wei, X., Li, J., Wang, Q., Wang, F., & Kong, L. (2013). Homogeneous isolation of nanocellulose from cotton cellulose by high pressure homogenization. Journal of Materials Science and Chemical Engineering, 1(05), 49.

Wang, B., & Sain, M. (2007). Isolation of nanofibers from soybean source and their reinforcing capability on synthetic polymers. Composites Science and Technology, 67(11), 2521-2527.

Warner, J. C., et al. (2004). Green chemistry. Environmental Impact Assessment Review, 24(7–8), 775-799. doi:http://dx.doi.org/10.1016/j.eiar.2004.06.006

Wei, H., Rodriguez, K., Renneckar, S., & Vikesland, P. J. (2014). Environmental science and engineering applications of nanocellulose-based nanocomposites. Environmental Science: Nano, 1(4), 302-316.

Welton, T. (2004). Ionic liquids in catalysis. Coordination Chemistry Reviews, 248(21), 2459-2477.

Wendler, F., Todi, L. N., & Meister, F. (2012). Thermostability of imidazolium ionic liquids as direct solvents for cellulose. Thermochimica acta, 528, 76-84.

Wu, Q., Meng, Y., Wang, S., Li, Y., Fu, S., Ma, L., & Harper, D. (2014). Rheological behavior of cellulose nanocrystal suspension: influence of concentration and aspect ratio. Journal of Applied Polymer Science, 131(15).

Xie, J., Hse, C. Y., Cornelis, F., Hu, T., Qi, J., & Shupe, T. F. (2016). Isolation and characterization of cellulose nanofibers from bamboo using microwave liquefaction combined with chemical treatment and ultrasonication. Carbohydrate Polymers, 151, 725-734.

Xin, D., Yang, M., Zhang, Y., Hou, X., Wu, J., Fan, X., ... & Zhang, J. (2016). Physicochemical characterization and enzymatic digestibility of Chinese pennisetum pretreated with 1-ethyl-3-methylimidazolium acetate at moderate temperatures. Renewable Energy, 91, 409-416.

Yang, C. Y., & Fang, T. J. (2014). Combination of ultrasonic irradiation with ionic liquid pretreatment for enzymatic hydrolysis of rice straw. Bioresource technology, 164, 198-202.

Yang, H., Yan, R., Chen, H., Lee, D. H., & Zheng, C. (2007). Characteristics of hemicellulose, cellulose and lignin pyrolysis. Fuel, 86(12), 1781-1788.

Yassin, F. A., El Kady, F. Y., Ahmed, H. S., Mohamed, L. K., Shaban, S. A., & Elfadaly, A. K. (2015). Highly effective ionic liquids for biodiesel production from waste vegetable oils. Egyptian Journal of Petroleum, 24(1), 103-111.

Zavrel, M., Bross, D., Funke, M., Büchs, J., & Spiess, A. C. (2009). High-throughput screening for ionic liquids dissolving (ligno-) cellulose. Bioresource technology, 100(9), 2580-2587.

Zhang, H., Wu, J., Zhang, J., & He, J. (2005). 1-Allyl-3-methylimidazolium chloride room temperature ionic liquid: a new and powerful nonderivatizing solvent for cellulose. Macromolecules, 38(20), 8272-8277.

Zhang, J., Wang, Y., Zhang, L., Zhang, R., Liu, G., & Cheng, G. (2014). Understanding changes in cellulose crystalline structure of lignocellulosic

biomass during ionic liquid pretreatment by XRD. Bioresource technology, 151, 402-405.

Zhang, Q., Zhang, S., & Deng, Y. (2011). Recent advances in ionic liquid catalysis. Green Chemistry, 13(10), 2619-2637.

Zhao, H. P., Feng, X. Q., & Gao, H. (2007). Ultrasonic technique for extracting nanofibers from nature materials. Applied physics letters, 90(7), 073112.

Zhao, H., Baker, G. A., Song, Z., Olubajo, O., Crittle, T., & Peters, D. (2008). Designing enzyme-compatible ionic liquids that can dissolve carbohydrates. Green chemistry, 10(6), 696-705.

Zhao, H., Jones, C. L., Baker, G. A., Xia, S., Olubajo, O., & Person, V. N. (2009). Regenerating cellulose from ionic liquids for an accelerated enzymatic hydrolysis. Journal of Biotechnology, 139(1), 47-54.

Zhu, S., Wu, Y., Chen, Q., Yu, Z., Wang, C., Jin, S., ... & Wu, G. (2006). Dissolution of cellulose with ionic liquids and its application: a mini-review. Green Chemistry, 8(4), 325-327.

Zhang, J., Wang, Y., Zhang, L., Zhang, R., Liu, G., & Cheng, G. (2014). Understanding changes in cellulose crystalline structure of lignocellulosic biomass during ionic liquid pretreatment by XRD. Bioresource technology, 151, 402-405.

Zhao, H. P., Feng, X. Q., & Gao, H. (2007). Ultrasonic technique for extracting nanofibers from nature materials. Applied physics letters, 90(7), 073112.

Zuluaga, R., Putaux, J. L., Cruz, J., Vélez, J., Mondragon, I., & Gañán, P. (2009). Cellulose microfibrils from banana rachis: Effect of alkaline treatments on structural and morphological features. Carbohydrate Polymers, 76(1), 51-59.

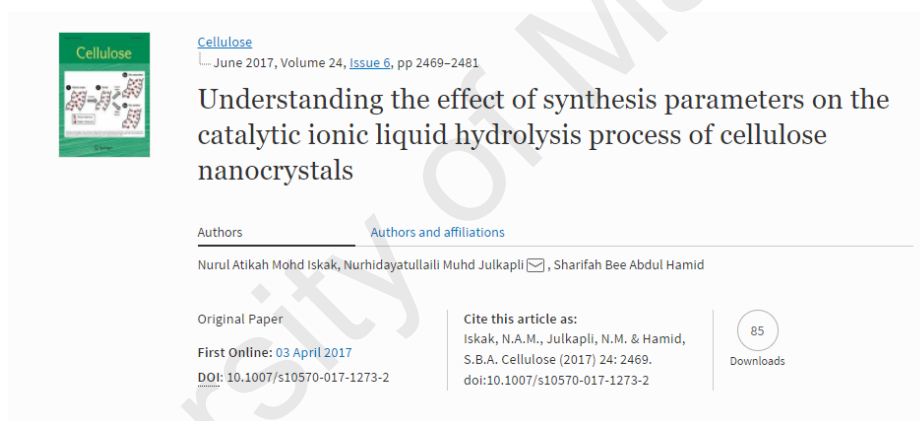# LIST OF PUBLICATIONS AND PAPERS PRESENTED

Conference Proceedings

a) Nurul Atikah Mohd Iskak, Sharifah Bee Abdul Hamid (2016-22 to 24 February). *Effects of Dissolution Time on Nanoparticle Preparation of Cellulose by Task Specific Ionic Liquids.*Paper presented at 4th International Science Postgraduate Conference, ISPC 2016, Universiti Teknologi Malaysia, Skudai, Johor.

Journal Publication

a) Cellulose